Bubble-Chamber Study of Photoproduction by 2.8- and 4.7-GeV Polarized Photons. I. Cross-Section Determinations and Production of ρ^0 and Δ^{++} in the Reaction $\gamma p \to p\pi^+\pi^-$†

J. Ballam, G. B. Chadwick, R. Gearhart, Z. G. T. Guiragossián,* J. J. Murray, P. Seyboth,‡ C. K. Sinclair, I. O. Skillicorn, H. Spitzer,§ and G. Wolf‖
Stanford Linear Accelerator Center, Stanford University, Stanford, California 94305

and

H. H. Bingham, W. B. Fretter, K. C. Moffeit,** W. J. Podolsky,‖ M. S. Rabin, A. H. Rosenfeld, and R. Windmolders††
Department of Physics and Lawrence Radiation Laboratory, University of California, Berkeley, California 94720

and

R. H. Milburn
Tufts University, Medford, Massachusetts 02155
(Received 2 August 1971)

Photoproduction is studied at 2.8 and 4.7 GeV using a linearly polarized monoenergetic photon beam in a hydrogen bubble chamber. We discuss the experimental procedure, the determination of channel cross sections, and the analysis of the channel $\gamma p \to p\pi^+\pi^-$. A model-independent analysis of the ρ^0-decay angular distribution allows us to measure nine independent density-matrix elements. From these we find that the reaction $\gamma p \to p\rho^0$ proceeds almost completely through natural parity exchange for squared momentum transfers $|t| < 1$ GeV^2 and that the ρ production mechanism is consistent with s-channel c.m. helicity conservation for $|t| < 0.4$ GeV^2. A cross section for the production of $\pi^+\pi^-$ pairs in the s-channel c.m. helicity-conserving p-wave state is determined. The ρ mass shape is studied as a function of momentum transfer and is found to be inconsistent with a t-independent Ross-Stodolsky factor. Using a t-dependent parametrization of the ρ^0 mass shape we derive a phenomenological ρ^0 cross section. We compare our phenomenological ρ^0 cross section with other experiments and find good agreement for $0.05 < |t| < 1$ GeV^2. We discuss the discrepancies in the various determinations of the forward differential cross section. We study models for ρ^0 photoproduction and find that the Söding model best describes the data. Using the Söding model we determine a ρ^0 cross section. We determine cross sections and nine density-matrix elements for $\gamma p \to \Delta^{++}\pi^-$. The parity asymmetry for Δ^{++} production is incompatible with simple one-pion exchange. We compare Δ^{++} production with models.

I. INTRODUCTION

This is the first of two final reports on an experiment which used the 82-in. LRL-SLAC hydrogen bubble chamber to study photoproduction of hadrons by a polarized photon beam at 2.8 and 4.7 GeV. This beam yields photons of more than 90% linear polarization at our energies, with an energy resolution of ±(3–4)% between 3 and 5 GeV. We have obtained 92 events/μb (150 events/μb) at 2.8 GeV (4.7 GeV). In this paper we present the general analysis procedure, total and partial hadronic cross sections for the various topological channels, and a detailed study of the three-body reaction $\gamma p \to p\pi^+\pi^-$ with particular emphasis on ρ^0 and Δ^{++} production. We have already published a measurement of the total hadronic photoproduction cross section,[1] and preliminary results on ρ^0 (Refs. 2 and 3), ω (Ref. 4), Δ^{++} (Ref. 5) production and ρ^0-ω interference.[6] These will be treated in this and a forthcoming paper in greater detail and subjected to further analysis.

This experiment, which uses the SLAC Compton backscattered laser beam,[7-9] has the following advantages, not all of which are found in previous studies of multibody photoproduction: a monoenergetic photon spectrum, a 4π detection efficiency, and a polarized beam. By exploiting the narrow energy spectrum and the 4π detection geometry of the bubble chamber we measure the total hadronic photoproduction cross section to an accuracy of ±2.4%. We also determine channel cross sections for reactions with three, five, or seven charged outgoing particles, for those with one additional neutral particle, and the sum of the cross sections for channels with more than one neutral particle.

Photoproduction of ρ^0 mesons in the reaction $\gamma p \to p\pi^+\pi^-$ is known[10-12] to be mainly a diffractive

process. The evidence for this came from the magnitude and the energy dependence of the production cross section above 2 GeV. In addition, there have been indications that the photoproduced ρ^0 mesons are transversely aligned in the helicity system.[11] Knowing the polarization of the photons and using the 4π geometry of the chamber we are able to make a detailed analysis of the ρ^0 production mechanism. The use of polarized photons adds six new independent density-matrix parameters to the three derivable from unpolarized photons. As a direct result, we can separate the cross sections for ρ^0 production into contributions from natural $[P=(-1)^J]$ and unnatural $[P=(-1)^{J+1}]$ parity exchanges in the t channel. We find that ρ^0 photoproduction is dominated by natural parity exchange for momentum transfers squared from target to proton, $|t|$, less than 1 GeV^2, as expected for a diffractive process. We confirm the transverse alignment of the ρ^0's in the helicity system for $|t| < 0.4$ GeV^2 and find that the data are consistent with s-channel helicity conservation in ρ^0 photoproduction. We further determine the cross section for s-channel helicity-conserving p-wave dipion states which dominate the ρ^0 region. We emphasize that the above results are model-independent.

One of the puzzles of ρ^0 photoproduction has been the apparent skewing of the ρ^0 mass shape.[10,11] We confirm the skewing and show that it depends on t. Using an empirical formula which describes this t dependence we determine a phenomenological cross section for ρ^0 production.

We also compare the observed features of dipion production in the ρ^0 region with several theoretical models and find that a modified Söding model is best able to reproduce quantitatively the mass shift, its t dependence, and the decay properties of the dipion system. We also obtain ρ^0 cross sections using the Söding model.

Since there have been substantial discrepancies among the published forward differential cross sections for ρ^0 photoproduction, we compare these cross sections and discuss the differences; we show that there are theoretical as well as experimental problems.

We have determined cross sections for Δ^{++} production in the process $\gamma p \to p\pi^+\pi^-$. Using an analysis similar to that used for ρ^0 production we show that Δ^{++} production proceeds through a mixture of natural and unnatural parity exchanges in the t channel.

The organization of this paper is as follows.

II. EXPERIMENTAL PROCEDURE

A. Beam

In 1962, Milburn,[13] concurrently with Arutyunian *et al.*,[14] pointed out that backward Compton scattering of an intense polarized laser light beam by high-energy electrons would produce useful yields of nearly monoenergetic, polarized photons. Such a beam was used for this experiment.[7-9]

Because the reaction

$$\gamma(k_i)+e^-(E_e)\rightarrow e^-+\gamma(k_f)$$

is a two-body process, for a fixed incident geometry the energy k_f of the scattered photon depends only on its laboratory angle, θ, as measured with respect to the incident electron beam. For a head-on collision and small θ it can be shown that when the energies of the incoming photon, k_i, and electron, E_e, are fixed,

$$k_f \approx \frac{k_{f\max}}{1+E_e^2\theta^2/s}\ , \tag{1}$$

where s is the center-of-mass energy squared,

$$s \approx m_e^2+4k_iE_e\ ,$$

$$k_{f\max} \approx \frac{4E_e^2k_i}{s}\ .$$

By collimating the backscattered photon beam and incident electron beam we select a band of photon energies given by

$$\frac{k_{f\max}-k_{f\min}}{k_{f\max}} \approx \frac{k_{f\max}}{4k_i}\,\theta_c^2\ ,$$

where θ_c is the collimator half-angle ($\approx 10^{-5}$ rad). For this experiment, $k_i = 1.78$ eV. Thus, the energy resolution [full width at half maximum (FWHM)] is expected to vary from about 2% for $k_{f\max} = 1.44$ GeV ($E_e = 8$ GeV) to 6.5% for $k_{f\max} = 4.7$ GeV ($E_e = 16$ GeV). Another feature of the Compton process is that if the incident light is polarized, after backscattering ($\theta \cong 0^0$), it is still almost completely polarized in the same way. [See formula (4) of Ref. 7.]

Figure 1 shows the beam layout. About 3×10^{11} electrons in a 1.5-μsec pulse passed through the 5-m-long interaction region. The electron beam in the interaction region was 1 cm in diameter with a divergence of about 10^{-5} rad [actual beam phase space = $(10^{-6}$ rad cm$)^2$]. The incident linearly polarized light beam was obtained from a Q-switched ruby laser of wavelength 0.6943 μ ($k_i = 1.78$ eV) with a maximum output of 2 J emitted into a phase space of about (0.75 mrad cm)^2. The pulse duration was about 50 nsec. The plane of linearly polarized light could be rotated 90° by inserting a half-wave plate into the laser beam line. After the electron and laser beams clashed at a relative angle of 3 mrad, the electron beam was deflected into a dump. To minimize the synchrotron radiation the electron beam first traversed a weak magnetic field until it was clear of the beam line. The

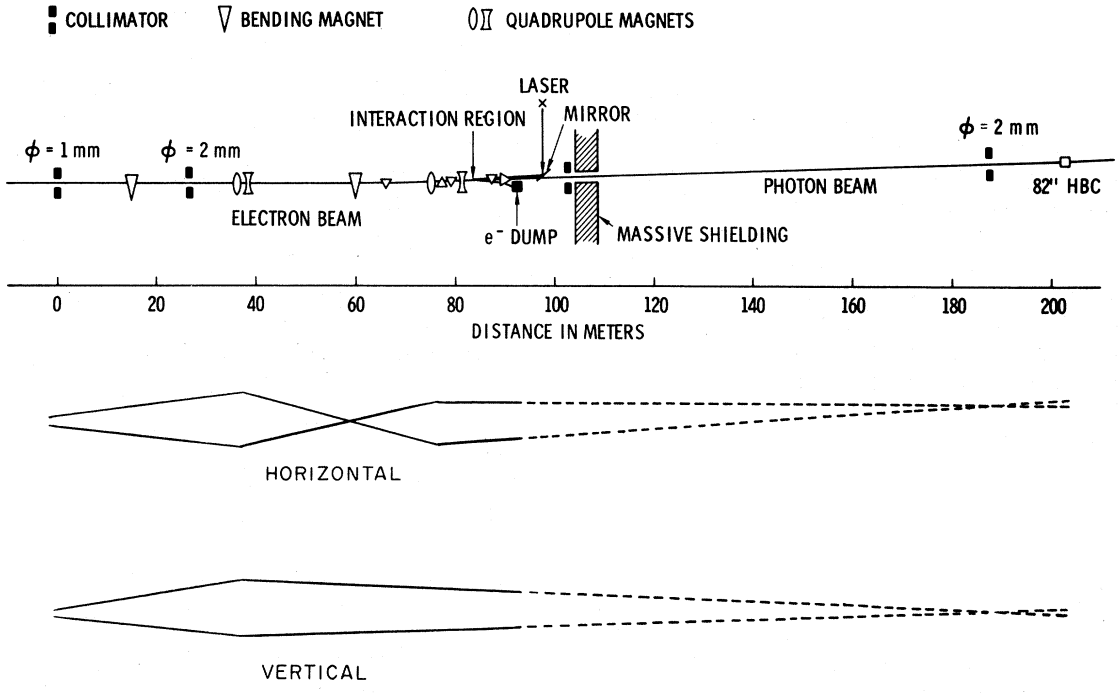

FIG. 1. Layout of the beam. The beam profile is shown in the horizontal and vertical planes (not to scale).

synchrotron radiation resulting from electrons deflected in this weak field had low enough energy to be removed by a high-Z photoelectric absorber (0.16 radiation lengths of uranium) which did not produce any significant deterioration of the high-energy photon spectrum at the bubble chamber. The Compton backscattered photon beam was collimated to $\approx 10^{-5}$ rad by a collimator with a 2-mm-diam hole located 100 m downstream of the interaction region. Four quadrant scintillators surrounded the hole behind 1 in. of Hevimet. The showers in these scintillators allowed us to determine the beam steering to about 10^{-6} rad and to monitor the beam intensity.[9] Our electronics vetoed picture taking if the beam was missteered more than 3×10^{-6} rad or if the intensity was too high or too low. Control of the intensity was accomplished by adjusting the laser output or the electron beam intensity. (For more details see Sec. III of Ref. 15.)

B. Photon Energy Spectrum and Polarization

The energy of the scattered photon depends on the energies of the initial photon and the electron beam. For the ruby laser used, electron energies of 12 and 16 GeV gave mean photon energies of 2.8 and 4.7 GeV, respectively, for the two exposures discussed in this paper. The energy spectra are shown in Fig. 2; the method by which they were obtained is discussed in Sec. III A.

The polarization of the *incident laser light,* which was assumed to be 100%, was measured in the interaction region to be greater than 97%. A half-wave plate was used in 50% of the pictures to rotate the polarization direction by 90°. The degree of linear polarization of the *backscattered photon beam* was calculated, using the formalism of Ref. 7, by averaging over the experimental energy spectrum between the energy limits given in Table I and Fig. 2. The average polarization was 95% (93%) at 2.8 GeV (4.7 GeV). The particular half-wave plate used in 18% of the exposure, when combined with the rest of the run, reduced these values by (2 ± 1)%. We estimate the over-all uncertainty in the polarization to be ±2%.

The alignment and transport of the laser beam introduces an uncertainty in the polarization direction of the high-energy photons at the bubble chamber. Although the polarization direction was measured to an accuracy of 1° at the laser, we estimate the total uncertainty from all effects to be ±3° at the bubble chamber for the polarization state without the half-wave plate. For the half-wave-plate data we estimate a further uncertainty of ±5° in polarization direction. These uncertainties introduce a systematic uncertainty in quantities such as the parity asymmetry P_σ (see Sec. IV B 3) and the total helicity-conserving p-wave $\pi\pi$ intensity Π (see Sec. IV B 6). For the combined data these uncertainties are less than 2%.

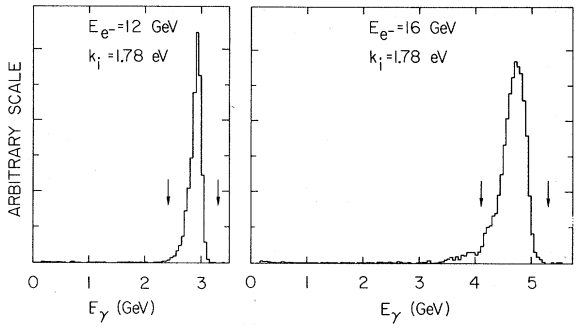

FIG. 2. Photon energy spectra (unnormalized) for the 2.8- and 4.7-GeV runs. The arrows indicate the energy intervals used. The ordinate gives the number of photons.

The average polarization and a summary of the beam and exposure are given in Table I.

C. Bubble Chamber

Approximately 750 000 pictures were taken in the Lawrence Radiation Laboratory (LRL)-SLAC 82-in. hydrogen bubble chamber. The magnetic field at the center of the chamber was 16.6 kG. Most of the pictures were taken with ~50 photons per pulse, corresponding to about seven e^+e^- pairs per picture and about one hadronic event every 25 frames.

D. Scanning Procedures

Both events and pairs were scanned for within a fiducial area of ±4-mm width in the bubble cham-

TABLE I. Beam parameters and exposure statistics.

Average beam energy, E_γ (GeV)	FWHM (MeV)	Number of pictures	E_γ limits accepted (GeV)	Average linear polarization P_γ (%)	Events/μb
2.8	150	294 000	2.4–3.3	93±2	92±4
4.7	450[a]	454 000	4.1–5.3	91±2	150±6

[a] Broadened by electron energy shifts. For a constant electron energy the FWHM was about 350 MeV.

ber along the beam line (the beam has a diameter of 3 mm). The length of the scanning area was chosen to allow a minimum track length of 35 cm for forward going tracks and 8 cm for backward tracks.

Hadronic events could be easily separated from the pair background since hadronic tracks generally have much larger production angles than the e^+e^- tracks, which are produced close to 0°.

The film was double scanned with discrepancies resolved in a third pass. The combined double-scan efficiency was found to be ≥99% for all events except one-prong events, strange-particle decays, and three-prong events with short recoil-proton tracks. The biases in the $p\pi^+\pi^-$ channel will be discussed in Sec. III A. Pairs were counted in both scans on four frames per roll of 660 frames. Discrepancies between the two scans in counting pairs were resolved in a third scan. We estimate uncertainties in the number of pairs counted (as compared to the number of events) to be $(0 \pm 2)\%$.

Equal numbers of pictures were taken with the polarization horizontal and vertical in the bubble chamber in order to check for biases. No detectable differences were found between the two polarizations. Both laboratories scanned a common subset of the film (25%). Comparison of these scan results for the different laboratories was used to

TABLE II. Numbers of events found.

Hypothesis	Channels	Number of constraints	Number of events $E_\gamma = 2.8$ GeV	Number of events $E_\gamma = 4.7$ GeV
1	$\gamma p \to p\pi^+\pi^-$ [c]	3	2936	3281
2	$\to p\pi^+\pi^-\pi^0(m\pi^0)$ [a]	0	3238	4688
3	$\to n\pi^+\pi^+\pi^-(m\pi^0)$ [a]	0	1707	2286
4	$\to pK^+K^-$ [b]	3	83	108
5	$\to pp\bar{p}$	3	0	9
	Hypotheses 2, 3 ambiguous [d]		681	2900
	Hypotheses 1, 4 ambiguous [d]		5	1
	No fit		35	64
	Remeasurable		183	326
	Unmeasurable		387	737
	Total three-prong [c]		9255	14 400
1	$\gamma p \to p\pi^+\pi^+\pi^-\pi^-$	3	354	795
2	$\to p\pi^+\pi^+\pi^-\pi^-\pi^0(m\pi^0)$ [a]	0	260	1194
3	$\to n3\pi^+2\pi^-(m\pi^0)$ [a]	0	64	429
4	$\to pK^+K^-\pi^+\pi^-$ [b]	3	1	45
	Hypotheses 2, 3 ambiguous [d]		40	528
	Hypotheses 1, 4 ambiguous [d]		0	1
	No fit		5	8
	Remeasurable		41	101
	Unmeasurable		65	235
	Total five-prong		830	3336
1	$\gamma p \to p3\pi^+3\pi^-$	3	5	42
2	$\to p3\pi^+3\pi^-\pi^0(m\pi^0)$ [a]	0	0	42
3	$\to n4\pi^+3\pi^-(m\pi^0)$ [a]	0	0	10
	Hypotheses 2, 3 ambiguous [d]		0	17
	No fit		0	1
	Remeasurable		0	13
	Unmeasurable		0	9
	Total seven-prong		5	134
	Total nine-prong		0	1
	Pairs counted		12 294	22 010
	Frames (for pair count)		1808	2784
	Good frames		292 927	452 239

[a] $m \geq 0$.

[b] The number of events for hypothesis 4 does not include those events with a visible K decay (7 at 2.8 GeV and 10 at 4.7 GeV for $\gamma p \to pK^+K^-$).

[c] Includes events with unseen recoil protons.

[d] Hypotheses 2, 3 ambiguous are not included in hypotheses 2 and 3 above (similarly for hypotheses 1, 4 ambiguous).

obtain scanning efficiencies.

The numbers of events found in the scan are shown in Table II.

E. Measuring and Kinematical Reconstruction

Half the events were measured at SLAC and half at LRL. SLAC used conventional measuring machines throughout, while the last two-thirds of the first measurements at LRL were processed by Spiral Reader II: The passing rate and resolution were comparable to conventional measuring machines. When remeasurements were stopped, ≈2% of events remained to be remeasured. The fraction of events that could not be measured due to secondary scatters or track obscuration was ≈5% (see Table II).

At both laboratories the events were analyzed using the geometrical reconstruction program TVGP and the kinematics program SQUAW.[16] The hypotheses attempted in SQUAW are given in Table II. No constraint was placed on the incident photon energy; the beam direction, as determined from measurements of e^+e^- pairs, was assigned errors of ≈±1 mrad in dip and azimuth. Hence, hypotheses 1, 4, and 5 have three constraints in the kinematical fit and 2 and 3 have no constraints. Fits were accepted if they were compatible with the observed bubble density. Three-constraint (3C) fits were required to have kinematic $\chi^2 < 30$ (see also the theses of Moffeit[17] and Podolsky[15]); competing zero-constraint (0C) fits were ignored.

The bubble-chamber magnetic field and the reconstruction procedure were checked by measuring K^0 decays; as shown in Fig. 3, the K^0 mass is correct to 0.2%. The $\pi^+\pi^-$ mass resolution at the K^0 mass is ±5 MeV. The combined data for the two energies are given in Fig. 3; we find no significant differences between the two samples.

In order to compare the measurement and analysis procedures at LRL and SLAC, the 2.8-GeV three-pronged events measured at SLAC were remeasured on Spiral Reader II and processed through the LRL analysis system. A comparison of the two sets of measurements showed that fitted angles and momenta, and such quantities as invariant masses and decay angles, agreed within 1 standard deviation and that kinematic interpretations agreed for >99% of the events.[15,17]

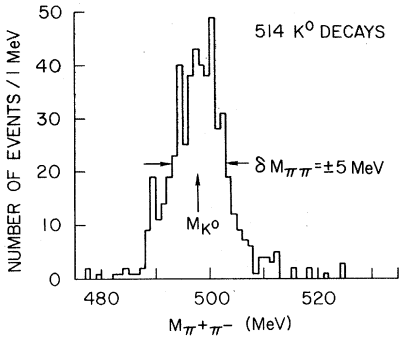

FIG. 3. Dipion mass from 514 K^0 decays (combined data of the two energies).

III. CROSS SECTIONS

A. Procedures

Using the number of e^+e^- pairs together with the known pair-production cross section on hydrogen (σ_{pair}), we obtain hadronic cross sections from

$$\sigma(\gamma p \to \text{hadrons}) = (N_{\text{events}}/N_{\text{pair}})\sigma_{\text{pair}} .$$

The pair cross sections used in this paper are given in Table III. They result from a calculation by Knasel[18] and are 1% higher than the values used in our earlier publications.[1-6] The new values of Knasel are claimed to be accurate to ±0.5% and have been verified to ±1%.[19]

To exclude events and pairs produced by nonbeam photons originating in the bubble-chamber window or hydrogen, the vertices of events and pairs used for the final analysis are required to be within a fiducial volume. This fiducial volume is defined by a cylinder along the beam direction y given by

$$R = \left[[x - x_0(y)]^2 + \left(\frac{z - z_0(y)}{2}\right)^2\right]^{1/2} < 2 \text{ mm},$$

where $x_0(y)$ and $z_0(y)$ were obtained from a straight-line fit to the vertex position of the events and (x, y, z) is the vertex position of the individual event or pair. Note that this expression takes account of the larger errors in the measurement of depth in the bubble chamber (z direction). The fraction of hadronic events outside the fiducial volume was determined directly from the measured vertex distributions. The fraction of pho-

TABLE III. Cross sections for pair production on hydrogen, according to Knasel (Ref. 18), as a function of photon energy, E_γ.

E_γ (GeV)	σ (mb)	E_γ (GeV)	σ (mb)
0.10	11.66	1.0	18.29
0.15	13.15	1.25	18.65
0.175	13.69	1.5	18.91
0.20	14.15	1.75	19.11
0.30	15.45	2.0	19.26
0.40	16.28	3.0	19.65
0.50	16.85	4.0	19.87
0.60	17.28	5.0	20.02
0.70	17.62	8.0	20.25
0.80	17.88	10.0	20.33
0.90	18.10		

tons, and hence of pairs, with $E_\gamma > 0.5$ GeV outside the fiducial volume was calculated from the vertex distribution of events fitting $\gamma p \to p\pi^+\pi^-$ using the known pair and event cross sections. For pairs with $E_\gamma < 0.5$ GeV the correction was found from the vertex distribution of measured pairs. These corrections were applied to the numbers of pairs and hadronic events found in scanning (Table II). Their values are given in Table IV. For more details see Refs. 15 and 17.

The *shape* of the photon energy spectrum, for $E_\gamma > 0.5$ GeV, was found from the E_γ distribution of events, within the fiducial volume, which fit $\gamma p \to p\pi^+\pi^-$ (3C fit). By inversely weighting this spectrum by the previously measured cross sections for this channel[11] and assuming that the cross section is constant in the energy region 2.4–3.3 GeV (4.1–5.3 GeV) for the 2.8-GeV (4.7-GeV) exposures we obtain a more accurate shape of the γ spectrum than can be found using e^+e^- pair measurements, since bremsstrahlung gives rise to large electron energy losses (cf. Fig. 1 of Ref. 1). The error on the photon energy determination for the 3C fit to $\gamma p \to p\pi^+\pi^-$ is small (~1%) and so has a negligible broadening effect on the spectra. For $E_\gamma < 0.5$ GeV the measured pair energy spectrum was used (corrected for the energy dependence of the pair cross section) since this energy range is below the threshold for 3C events. The photon spectra obtained are shown in Fig. 2. The total photon flux in any given energy interval is then determined from the total pair count, the pair-production cross section, and the shape of the photon spectrum. The numbers of events produced by photons outside the energy limits given in Table I were calculated using cross sections measured at lower energies.[11] The resulting corrections, given in Table IV, are smaller than 10%. Thus our cross sections are insensitive to the uncertainties in the low-energy cross sections used.

TABLE IV. Corrections in percent to be applied to the events found in scanning (Table II) in order to obtain topological cross sections. The entries α, β, γ, δ denote corrections for: (α) scanning efficiency and wide-angle pair contamination, (β) events outside the fiducial volume, (γ) events outside the energy selection $2.4 < E_\gamma < 3.3$ GeV and $4.1 < E_\gamma < 5.3$ GeV at $E_\gamma = 2.8$ and 4.7 GeV, (δ) events with undetected Dalitz pairs.

Topology		$E_\gamma = 2.8$ GeV	$E_\gamma = 4.7$ GeV
Three-prong	α	1.3±0.2	2.7±0.2
	β	−0.8±0.1	−1.4±0.1
	γ	−1.5±0.2	−7.7±0.4
	δ		0.0±0.5
Five-prong	α		0.3±0.2
	β	−0.1±0.1	−0.3±0.1
	γ	−0.6±0.3	−4.5±0.4
	δ		−2.3±1.0
Seven-prong	γ		−3.2±0.2
	δ		−17 ±17
Pairs	α	0 ±2	0 ±2
	β	−1.2±0.4	−2.1±0.4
	γ	−1.9±0.4	−7.0±0.6

Both wide-angle pair production (WAP), simulating hadronic events, and a reduced scanning efficiency necessitate corrections to the *channel* $\gamma p \to p\pi^+\pi^-$ for $|t| < 0.02$ GeV^2 for 2.8 GeV (<0.1 GeV^2 for 4.7 GeV). For $|t| > 0.02$ GeV^2 the corrections were determined from the scan efficiency[20] and by calculating the (small) WAP contamination. The combined correction to the channel cross section

TABLE V. Topological cross sections (μb) for events selected in the intervals $2.4 < E_\gamma < 3.3$ GeV and $4.1 < E_\gamma < 5.3$ GeV at 2.8 and 4.7 GeV, respectively. For completeness we include the 1.44-GeV cross sections from Ref. 1.

Topology[a]	$E_\gamma = 1.44$ GeV	$E_\gamma = 2.8$ GeV	$E_\gamma = 4.7$ GeV
Three-prong[b]	85.6±3.7	93.0 ±2.2	82.8 ±1.9
Five-prong	0.2±0.2	8.4 ±0.4	19.1 ±0.7
Seven-prong		0.05±0.03	0.67±0.17
With visible strange-particle decay[c]	4.4±0.9	8.1 ±0.5	8.7 ±0.4
One-prong[d]	54.9±3.2	22.9 ±1.5	15.8 ±1.2
Total	145.1±5.7	132 ±3	127 ±3

[a] An N-prong event has N charged particles without detected strange-particle decay.
[b] Includes two-prong topology.
[c] Based on 50% of total flux.
[d] Based on 10% of the data (Ref. 1) and adjusted to the new values of σ_{pair}.

is $(1\pm1)\%$ at 2.8 GeV $[(3\pm1)\%$ at 4.7 GeV]. For $|t|<0.02$ GeV^2 the scanning and WAP correction were performed by an extrapolation of the measured t distribution for $|t|>0.02$ GeV^2, assuming that the t distribution is of the form e^{At}, with A depending on $M_{\pi\pi}$. The combined correction is $(-0.4\pm0.4)\%$ at 2.8 GeV $[(3.4\pm0.5)\%$ at 4.7 GeV].

Scanning losses were found to be $\lesssim1\%$ for other topologies except for one-prong events and strange-particle decays.

B. Total and Topological Cross Sections

Using the numbers of events in Table II and the corrections of Table IV we obtain the total and topological cross sections given in Table V. The one-prong cross section is based on 10% of the exposure.[1]

Our total cross sections are in excellent agreement with other photoproduction experiments,[19,21,22] but are systematically (~10%) lower than those from electron scattering.[23]

C. Channel Cross Sections

In this section we divide the above topological cross sections into cross sections for various channels (leading to 3C, 0C, and underconstrained fits). In the process the unmeasurable and unmeasured events of Table II are distributed among the different channels in the same proportions as the measurable events.

1. *Three-Constraint Reactions*

The reactions

$\gamma p \to p\pi^+\pi^-$,

$\gamma p \to pK^+K^-$,

$\gamma p \to p\bar{p}$,

$\gamma p \to p\pi^+\pi^+\pi^-\pi^-$,

$\gamma p \to pK^+K^-\pi^+\pi^-$,

$\gamma p \to p\pi^+\pi^+\pi^+\pi^-\pi^-\pi^-$,

have only the beam energy unknown, and they were selected by requiring that the 3C kinematic fit had $\chi^2<30$ and that the mass assignments were consistent with the observed ionization. The application of these selection criteria left only a small number (< 1%) of ambiguities between competing 3C hypotheses. The numbers of 3C fits selected are given in Table II.[24,25] Cross sections were determined using the fiducial volume, energy, and scanning corrections in Table VI. The cross sections for K^+K^- production include visible K^+ or K^- decays. The results are given in Table VII. The cross sections for $p\pi^+\pi^-$, pK^+K^-, and $p\bar{p}p$ are also shown in Fig. 4 together with results from previous bubble-chamber experiments.[11,26-28] Our results agree well with those of other experiments.

TABLE VI. Corrections in percent to be applied to the 3C fits of Table II in order to obtain channel cross sections. The entries α, β, γ, δ denote corrections for: (α) scanning efficiency and wide-angle pair contamination; (β) events outside the fiducial region; (γ) events outside the energy selection; (δ) uncertainty in event selection.

Channel		$E_\gamma=2.8$ GeV	$E_\gamma=4.7$ GeV
$\gamma p \to p\pi^+\pi^-$	α	$+0.7\ \pm0.6$	$+6.4\pm1.1$
	β	-1.3	-2.8
	γ	-2.3	-9.6
	δ	$0\ \ \pm2$	$0\ \ \pm2$
$\gamma p \to p2\pi^+2\pi^-$	α	0.0	0.3 ± 0.2
	β	0.0	-0.5
	γ	-0.60	-5.7
$\gamma p \to p3\pi^+3\pi^-$	γ		-4.5

2. *Zero-Constraint Reactions*

We now discuss the cross-section determination for channels with one or more neutral reaction products, which have zero kinematic constraints

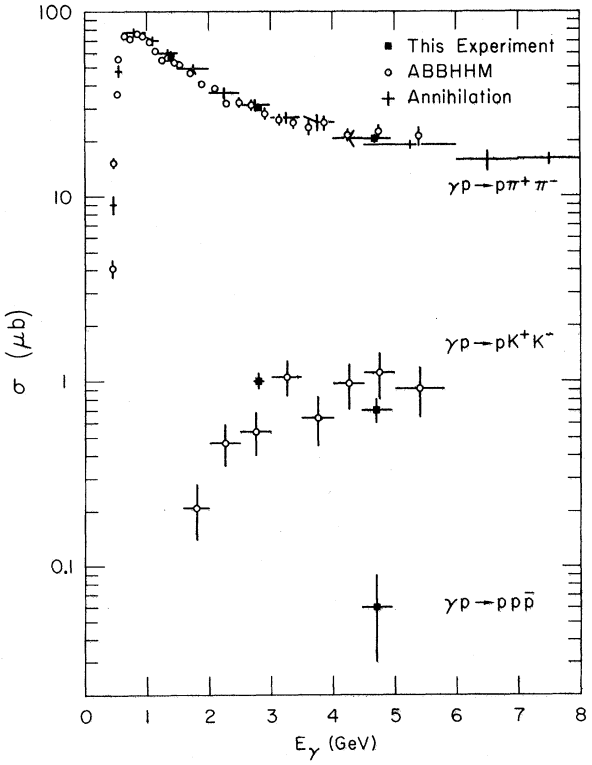

FIG. 4. Three-body cross sections from this experiment, from the ABBHHM collaboration (Ref. 26), and from the annihilation experiment (Ref. 28).

TABLE VII. Channel cross sections (μb).

Channel	E_γ = 1.44 GeV (Ref. 27)	E_γ = 2.8 GeV	E_γ = 4.7 GeV
$\gamma p \to p\pi^+\pi^-$	57.6 ± 3.3	30.9 ± 1.2	20.5 ± 0.8
$\to pK^+K^-$		1.0 ± 0.1	0.7 ± 0.1
$\to p\bar{p}p$			0.06 ± 0.03
$\to p\pi^+\pi^-\pi^0$	20.4 ± 2.0	24.9 ± 1.5	15.1 ± 1.5
$\to p\pi^+\pi^-$(+ neutrals)	1.1 ± 0.6	14.0 ± 2.0	20.8 ± 3.9
$\to n\pi^+\pi^+\pi^-$	5.6 ± 1.0	10.1 ± 1.3	7.2 ± 2.0
$\to n\pi^+\pi^+\pi^-$[+ neutral(s)]	0.9 ± 0.5	11.2 ± 0.9	16.3 ± 2.3
$\gamma p \to p2\pi^+2\pi^-$		4.1 ± 0.3	5.1 ± 0.3
$\to pK^+K^-\pi^+\pi^-$		0.01 ± 0.01	0.3 ± 0.06
$\to p2\pi^+2\pi^-\pi^0$		3.2 ± 0.3	7.0 ± 0.6
$\to p2\pi^+2\pi^-$(+ neutrals)		0.2 ± 0.15	3.2 ± 0.7
$\to n3\pi^+2\pi^-$		0.4 ± 0.07	1.6 ± 0.5
$\to n3\pi^+2\pi^-$[+ neutral(s)]		0.2 ± 0.08	1.6 ± 0.3
$\gamma p \to p3\pi^+3\pi^-$		0.05 ± 0.025	0.3 ± 0.05
$\to p3\pi^+3\pi^-\pi^0$			0.3 ± 0.07
$\to p3\pi^+3\pi^-$(+ neutrals)			0.0 ± 0.05
$\to n4\pi^+3\pi^-$			0.07 ± 0.04
$\to n4\pi^+3\pi^-$[+ neutral(s)]			0.0 ± 0.03

or are underconstrained. The experimental sample consists of all events which did not have an acceptable 3C fit. We describe in detail the technique employed for the three-prong topology. Other topologies were analyzed using a similar technique.

For the three-prong topology we determine the cross sections for the channels

$$\gamma p \to p\pi^+\pi^-\pi^0 \quad \text{(a)}$$
$$\to p\pi^+\pi^-(+\text{neutrals}) \quad \text{(b)}$$
$$\to n\pi^+\pi^+\pi^- \quad \text{(c)}$$
$$\to n\pi^+\pi^+\pi^-[+\text{neutral(s)}]. \quad \text{(d)}$$

In order to separate the channels, events were "fitted" to hypotheses (a) and (c) and, for each hypothesis, a beam momentum was calculated. Channels (b) [(d)] when fitted as (a) [(c)] will yield too low a beam momentum. A "fit" of hypothesis (c) to an event of channel (a) may yield too high a beam momentum; these high-beam-momentum hypotheses were partially eliminated by rejecting interpretations with beam momentum, K_{calc}, such that

$$\frac{K_{\text{calc}} - K_{f\,\max}}{\delta K_{\text{calc}}} > 5 ,$$

where $K_{f\,\max}$ is the maximum beam momentum [~3.0 GeV at 2.8 GeV (~5.0 GeV at 4.7 GeV); see Eq. (1) of Sec. II A] and δK_{calc} is the error in K_{calc}.

Events with acceptable 0C "fits" were subdivided into two classes depending on the observed bubble density: (1) the *unique* class in which either a proton was identified or all tracks were identified as pions, (2) the *ambiguous* class containing all other events. Both the unique and ambiguous classifications include a small number of events with $K^\pm$ tracks which could not be identified by bubble density.

The separation into *single-neutral*-particle and *multiple-neutral*-particle channels was made using missing-mass plots. We used the measured average photon energy to calculate the neutral missing mass (MM) recoiling against the charged particles. The MM distributions for unique and ambiguous three- and five-prong events are shown in Figs. 5 and 6. The distributions for $\gamma p \to p\pi^+\pi^-$MM and $\gamma p \to \pi^+\pi^+\pi^-$MM show clear peaks at $(\text{MM})^2 = M_{\pi^0}{}^2$ and $(\text{MM})^2 = M_n{}^2$, respectively.

In order to obtain cross sections for $\gamma p \to p\pi^+\pi^-\pi^0$ and $\gamma p \to n\pi^+\pi^+\pi^-$, it is necessary to determine the shape and magnitude of the background contributions to the missing-mass plots. The backgrounds fall into two main classes: (1) the contamination of

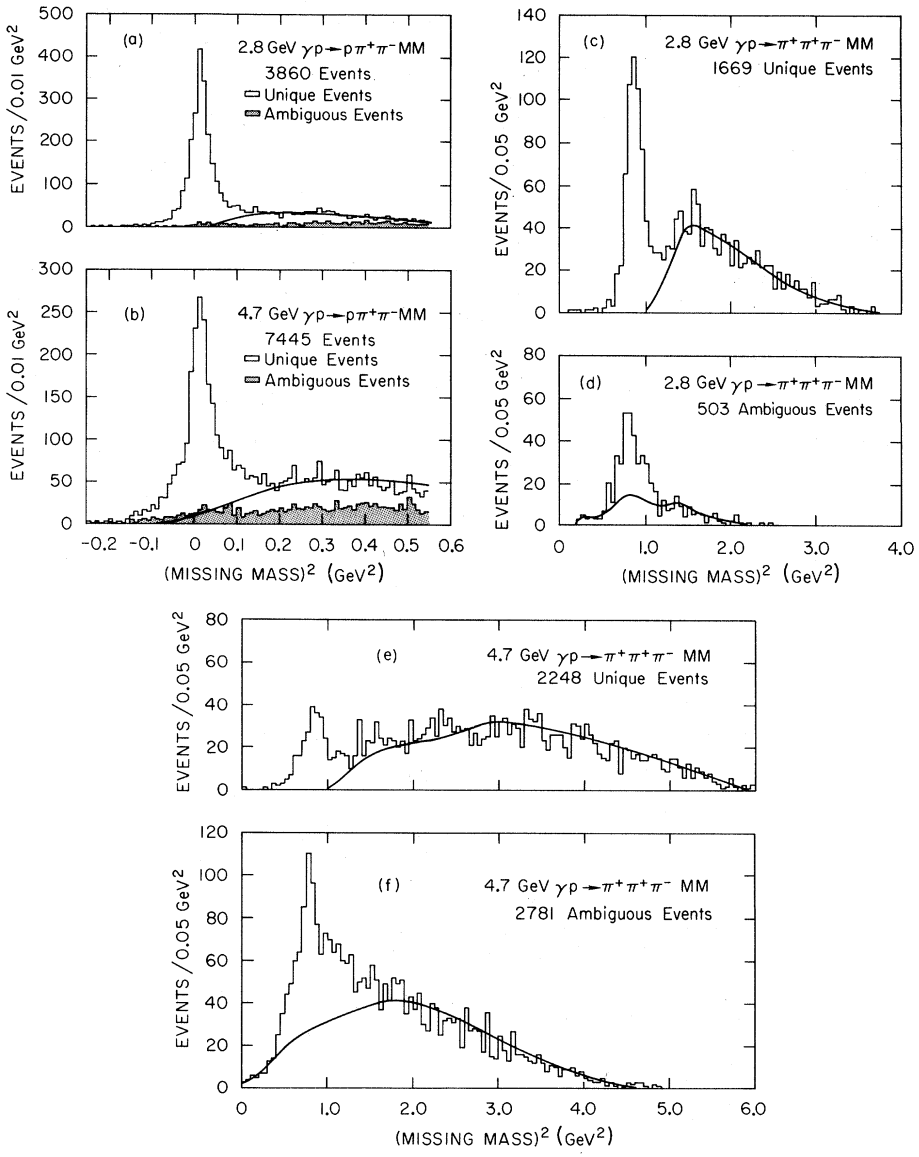

FIG. 5. Missing-mass-squared distributions. Three-prong events: (a) 2.8 GeV $\gamma p \to p\pi^+\pi^-$MM, (b) 4.7 GeV $\gamma p \to p\pi^+\pi^-$MM, (c) 2.8 GeV $\gamma p \to \pi^+\pi^+\pi^-$MM unique, (d) 2.8 GeV $\gamma p \to \pi^+\pi^+\pi^-$MM ambiguous, (e) 4.7 GeV $\gamma p \to \pi^+\pi^+\pi^-$MM unique, (f) 4.7 GeV $\gamma p \to \pi^+\pi^+\pi^-$MM ambiguous. The curves are a sum of model predictions for multineutral production and background from misidentified events normalized to the data as explained in the text.

$n\pi^+\pi^+\pi^-$ by $p\pi^+\pi^-\pi^0$ and vice versa, (2) the contamination of a four-body channel by five- and six-body channels. Backgrounds of type (1) were estimated from scatter plots of missing mass from $p\pi^+\pi^-$MM vs the missing mass from $\pi^+\pi^+\pi^-$MM. In the calculation of type (2) backgrounds we used information from the five-prong channels $p\pi^+\pi^+\pi^-\pi^-$, $p\pi^+\pi^+\pi^-\pi^-\pi^0$, and $n\pi^+\pi^+\pi^+\pi^-\pi^-$. We assumed that a $\pi^+\pi^-$ pair is equivalent to a $\pi^0\pi^0$ pair (ρ^0 production is not important when averaged over all $\pi^+\pi^-$ combinations) and that $\pi^- p$ approximates $\pi^0 n$. Thus omitting in turn each $\pi^+\pi^-$ pair from $p\pi^+\pi^+\pi^-\pi^-$, we recalculated the event as $p\pi^+\pi^-$MM. Similarly, $p\pi^+\pi^-(\pi^+\pi^-)\pi^0$ gives $p\pi^+\pi^-\pi^0\pi^0\pi^0$, $\pi^+\pi^+\pi^-(\pi^- p)$ gives $\pi^+\pi^+\pi^-(\pi^0 n)$, and $(\pi^+\pi^-)\pi^+\pi^+\pi^- n$ gives $\pi^0\pi^0\pi^+\pi^+\pi^- n$ (the parentheses show the omitted particles).

To determine the over-all shape of the combined backgrounds it is necessary to estimate the relative weights of the five- and six-body reactions. We used our five-prong data and a statistical model, the isospin weights for which are given in Table 11 of Ref. 29. The weights were derived assuming that the initial γp state is equivalent to $|\rho^0 p\rangle = (\frac{2}{3})^{1/2}|I=\frac{3}{2}\rangle - (\frac{1}{3})^{1/2}|I=\frac{1}{2}\rangle$ and neglecting reso-

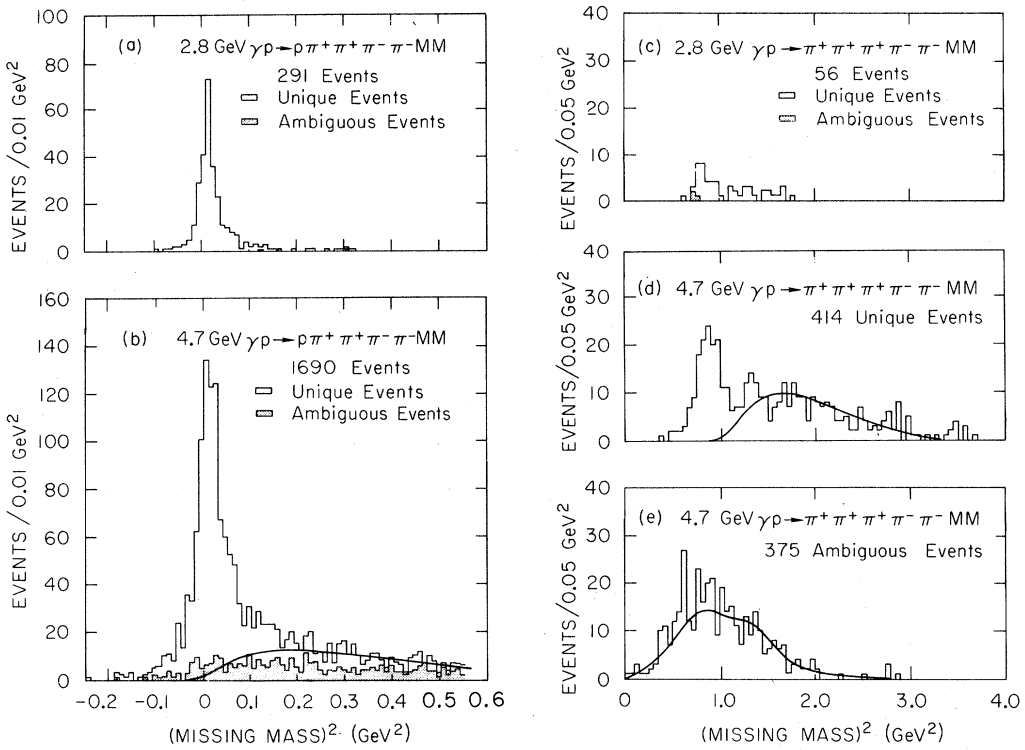

FIG. 6. Missing-mass-squared distributions. Five-prong events: (a) 2.8 GeV $\gamma p \to p\pi^+\pi^+\pi^-\pi^-$MM, (b) 4.7 GeV $\gamma p \to p\pi^+\pi^+\pi^-\pi^-$MM, (c) 2.8 GeV $\gamma p \to \pi^+\pi^+\pi^+\pi^-\pi^-$MM, (d) 4.7 GeV $\gamma p \to \pi^+\pi^+\pi^+\pi^-\pi^-$MM unique, (e) 4.7 GeV $\gamma p \to \pi^+\pi^+\pi^+\pi^-\pi^-$ MM ambiguous. The curves are a sum of model predictions for multineutral production and background from misidentified events normalized to the data as explained in the text.

nance production in the final state. The relative charge distribution among N-body states can then be derived, e.g., the expected ratio of $p\pi^+\pi^+\pi^-\pi^-$: $p\pi^+\pi^-\pi^0\pi^0$: $n\pi^+\pi^+\pi^-\pi^0$ is 20 : 32 : 36. Similar ratios are derived for six-body final states.[29]

We now discuss the characteristics of the backgrounds for each channel, considering the $n\pi^+\pi^+\pi^-$ channel in greatest detail since the background is more important for this channel than for the $p\pi^+\pi^-\pi^0$ channel.

(a) $n\pi^+\pi^+\pi^-$. Figure 5 shows that neutron missing-mass peaks occur in both the unique and ambiguous events. For the *unique* events we used a background of unique $n\pi^+\pi^+\pi^-\pi^0$ and unique $n\pi^+\pi^+\pi^-\pi^0\pi^0$ added in the ratio predicted by the model. We then normalized this background to the number of events with $(\mathrm{MM})^2 > 1.15$ GeV^2. Normalization factors of 1.3 (1.5) relative to the predictions of the model were required at 2.8 GeV (4.7 GeV), i. e., there is apparently more background from these channels than is predicted by the model. As can be seen from Fig. 5 the predicted $(\mathrm{MM})^2$ shape above the neutron peak agrees with the data.

The ambiguous $n\pi^+\pi^+\pi^-$ events present more problems since there are two forms of background, namely, that discussed above for the *unique* channel and that arising from *ambiguous* $p\pi^+\pi^-\pi^0$ and *ambiguous* $p\pi^+\pi^-$ (+neutrals). The ambiguous $p\pi^+\pi^-\pi^0$ background was estimated quantitatively from $(\mathrm{MM})^2$ scatterplots.[15] It yields a small contribution which peaks at missing masses below M_n. The *shape* of the ambiguous $p\pi^+\pi^-$(+neutrals) background was obtained from the five-prong events using the model. The two types of multineutral backgrounds, namely, those with a proton and those with a neutron, can be added either in the ratios predicted by the model or in these ratios multiplied by the normalizations of the corresponding unique multineutral backgrounds. We used a background corresponding to the average of these procedures, although the background shape does not depend strongly on the procedure used. The combined multineutral background thus obtained was normalized to the high-$(\mathrm{MM})^2$ data as before. Figure 5 shows that these backgrounds provide a good description of the $(\mathrm{MM})^2$ shape above the neutron peak. Cross sections for the channel $n\pi^+\pi^+\pi^-$ were obtained by counting the number of events above background up to a $(\mathrm{MM})^2$ of 1.2 GeV^2 (1.4 GeV^2) for 2.8 GeV (4.7 GeV) and using Monte Carlo calculations[30] to estimate the number of

TABLE VIII. Corrections in percent applied to numbers of events in unconstrained reactions.

Energy	2.8 GeV				4.7 GeV			
Channel \ Correction	Low energy[a]	Strange particle	Scanning losses	Dalitz pair	Low energy[a]	Strange particle	Scanning losses	Dalitz pair
$\gamma p \to p\pi^+\pi^-\pi^0$			1.5 ± 0.3		-2.5 ± 1.0		1.3 ± 0.3	0.0 ± 0.5
$\to p\pi^+\pi^-$(+ neutrals)	-1.8 ± 1.0	-2.5 ± 2.5	1.5 ± 0.3	0.0 ± 2.0	-9.7 ± 4.0	-5.5 ± 5.5	1.3 ± 0.3	0.0 ± 1.0
$\to n\pi^+\pi^+\pi^-$			1.5 ± 0.3				1.3 ± 0.3	
$\to n\pi^+\pi^+\pi^-$[+ neutral(s)]	-1.1 ± 0.5	-1.7 ± 1.7	1.5 ± 0.3	0.0 ± 2.0	-9.1 ± 3.0	-3.6 ± 3.6	1.3 ± 0.3	0.0 ± 1.0
$\gamma p \to p2\pi^+2\pi^-\pi^0$				0.0 ± 2.0	-1.5 ± 1.0		0.3 ± 0.2	-1.2 ± 0.7
$\to p2\pi^+2\pi^-$(+ neutrals)				0.0 ± 42.0	-7.8 ± 4.5	-6 ± 6	0.3 ± 0.2	-10.0 ± 4.0
$\to n3\pi^+2\pi^-$					0.0 ± 2.0		0.3 ± 0.2	
$\to n3\pi^+2\pi$[+ neutral(s)]				0.0 ± 25.0	-5.8 ± 4.0	-3 ± 3	0.3 ± 0.2	-9.0 ± 4.0
$\gamma p \to p3\pi^+3\pi^-\pi^0$								-12.5 ± 12.5
$\to p3\pi^+3\pi^-$(+ neutrals)								-100.0 ± 60.0
$\to n4\pi^+3\pi^-$								
$\to n4\pi^+3\pi^-$[+ neutral(s)]								-100.0 ± 200.0

[a] For single-neutral channels the low-energy correction takes account of low-energy events falling within the missing-mass cut. For multineutral channels the correction removes low-energy multineutral events and single-neutral events falling outside the missing-mass cuts.

$n\pi^+\pi^+\pi^-$ events above the limit.

Cross sections for multiple neutral production were obtained from the unique events by subtracting the estimated single neutral production cross section from the total unique cross section. To this cross section was added that corresponding to the ambiguous events divided between the channels in the ratio used in the background calculation described above. Corrections were applied for events produced by low-energy photons, strange-particle contamination, scanning losses, and Dalitz pairs[15]; these corrections are given in Table VIII. The channel cross sections are given in Table VII. The errors given in Table VII include an uncertainty of ±50% in the amount of background.

(b) $p\pi^+\pi^-\pi^0$. From Fig. 5 it can be seen that most of the π^0 peak is in the unique events. Consequently, the background determination is simpler than for the $n\pi^+\pi^+\pi^-$ channel. Background shapes were determined separately for the unique and ambiguous fits and were normalized to the missing-mass distribution for $(\mathrm{MM})^2 \geq 0.2$ GeV^2. Normalization factors of ~3.0 (~2.0) relative to the prediction of the statistical model were required at 2.8 GeV (4.7 GeV) for the unique events. Cross sections for single-π^0 production were obtained from the number of events above background with $(\mathrm{MM})^2 < 0.15$ GeV^2. Corrections for the high-$(\mathrm{MM})^2$ tail and π^0 events from low-energy photons were made using Monte Carlo calculations.[30] These calculations showed that the π^0 peak should be symmetric within statistics. Therefore, the number of π^0 events with $(\mathrm{MM})^2 > 0.15$ GeV^2 was estimated from the number of π^0 events with $(\mathrm{MM})^2 < -0.11$ GeV^2. Cross sections for the $p\pi^+\pi^-$(+neutrals) channel were obtained in the same manner as for the $n\pi^+\pi^+\pi^-$[+neutral(s)] channel. Corrections for low-energy events, strange-particle contamination, scanning losses, and Dalitz pairs are given in Table VIII. Cross sections are given in Table VII; the errors, as before, include an uncertainty of ±50% in the amount of background.

(c) Comparison with other experiments. Figure 7 shows the three-prong 0C cross sections[27] together with cross sections from an experiment using an annihilation beam.[28] We find good agreement between the experiments.[31]

IV. THE REACTION $\gamma p \to p\pi^+\pi^-$: ρ^0 AND Δ^{++} PRODUCTION

A. Introduction and Mass Distributions

In this section we give general characteristics of the channel $\gamma p \to p\pi^+\pi^-$. In Secs. II D and III A it

was shown that event losses for this channel were less than 3% for target to proton four-momentum transfers squared, $|t|$, greater than 0.02 GeV^2. Below $|t|=0.02$ GeV^2 events were lost due to scanning biases; contamination by wide-angle electron pairs also occurred. Consequently, in this section we discuss only events with $|t|>0.02$ GeV^2. In addition, only events within the E_γ intervals given in Table I were used.[32]

In Figs. 8 (a) and (b) we show Dalitz plots for 2.8 GeV and 4.7 GeV, respectively. Chew-Low plots for $\pi^+\pi^-$, $p\pi^+$, and $p\pi^-$ are given in Figs. 9(a)–9(f). Mass projections with momentum-transfer cuts for $\pi^+\pi^-$, $p\pi^+$, and $p\pi^-$ are shown in Figs. 10(a) and 10(b). From these figures it is evident that the channel is dominated by peripheral ρ^0 and Δ^{++} production.[10,11] We discuss in Secs. IV B–IV D the characteristics of ρ^0 photoproduction and in Sec. IV E Δ^{++} production. Upper limits for production of high-mass vector mesons decaying into $\pi^+\pi^-$ are given in Sec. IV F.

B. Model-Independent Study of Dipion and ρ^0 Meson Production

1. *Introduction*

From Fig. 10(a) it can be seen that the ρ^0 does not peak at the commonly accepted ρ^0 mass,[10-12,33] does not have the shape of a p-wave Breit-Wigner distribution,[11] and changes shape as a function of t. Since cross sections for ρ^0 production cannot be deduced without the use of a model which explains this change of ρ^0 shape, we postpone the evaluation of ρ^0 cross sections to Sec. IV C in which models of ρ^0 production are compared with the data.

In this section we make *model-independent* determinations of (a) the differential cross sections for the production of $\pi^+\pi^-$ pairs, (b) the characteristics of the $\pi^+\pi^-$ angular distribution, and (c) the cross section for the production of s-channel helicity-conserving p-wave $\pi^+\pi^-$ pairs.

2. *Double-Differential Cross Sections for Dipion Production in the ρ Region*

In Table IX we give $\Delta\sigma/\Delta t\Delta M$ for the production of *all* pion pairs of mass M, where ΔM is 40 MeV, and for nine t intervals in the range $0.02<|t|<0.4$

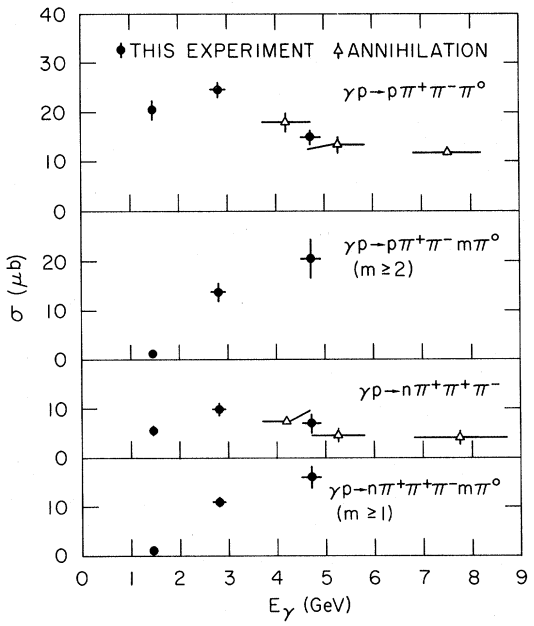

FIG. 7. Cross sections for three-prong events with neutral(s) from this experiment and from the annihilation experiment (Ref. 28).

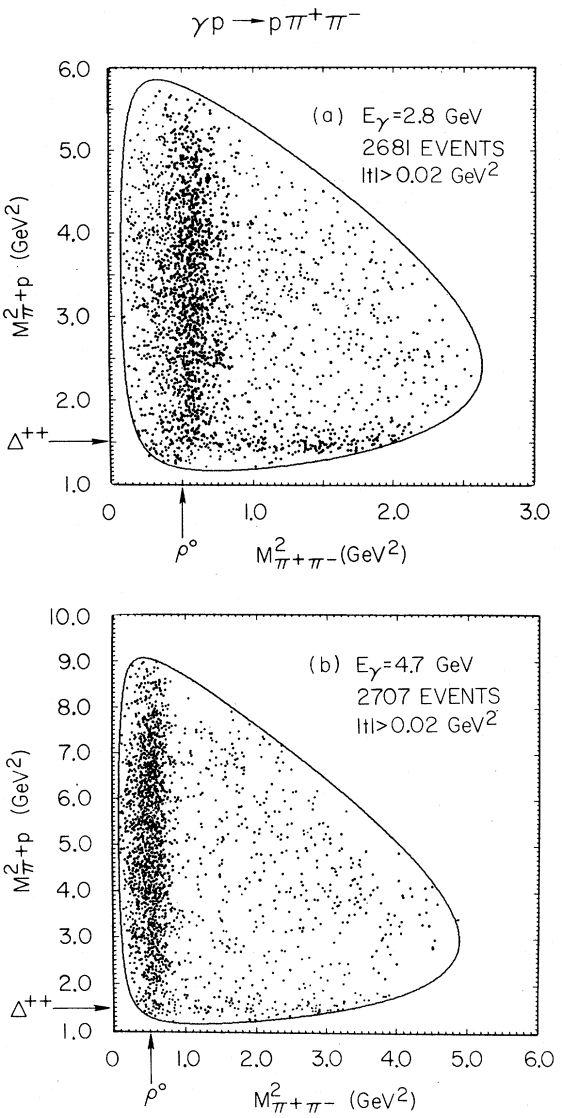

FIG. 8. Reaction $\gamma p \to p\pi^+\pi^-$. Dalitz-plot distribution.

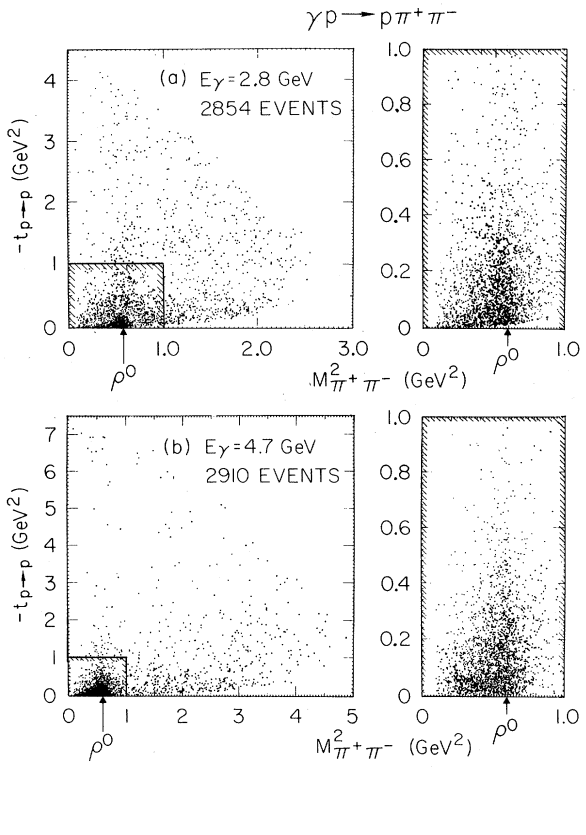

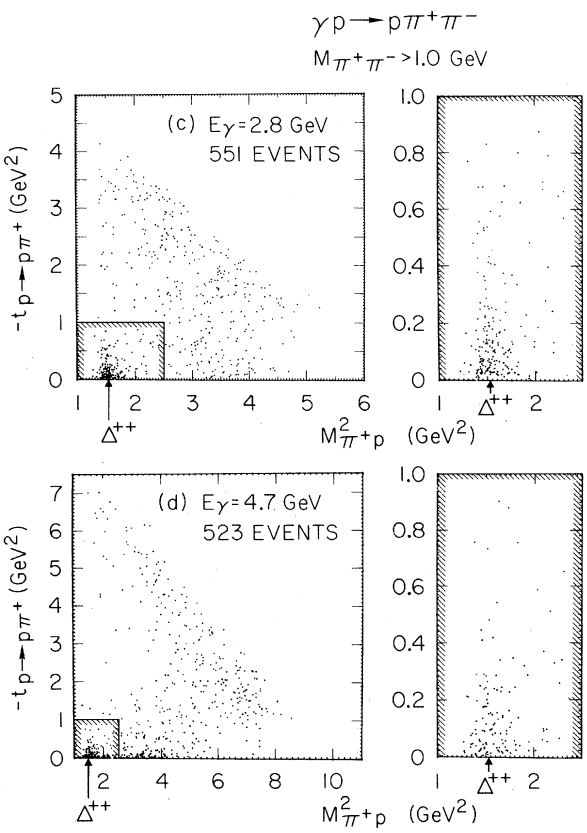

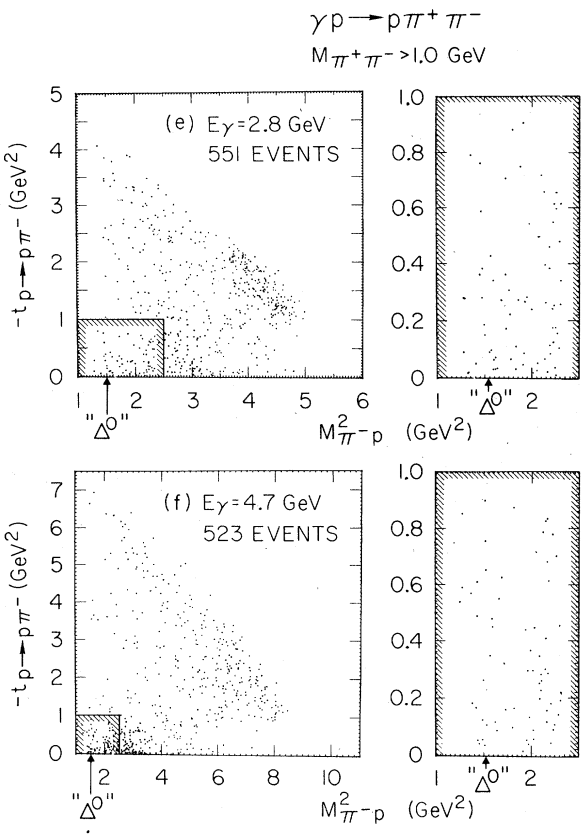

FIG. 9. (a)–(f) Reaction $\gamma p \to p\pi^+\pi^-$. Chew-Low plots for $\pi^+\pi^-$, $\pi^+ p$, and $\pi^- p$. (c)–(f) are for $M_{\pi^+\pi^-} > 1$ GeV. The outlined regions are shown on the right in an expanded scale.

GeV². In this momentum-transfer range the t distribution is well represented by the form Be^{At} where $B = d^2\sigma/dtdM|_{t=0}$ and we present in Fig. 11 the values of A and B, obtained from a maximum-likelihood fit, for intervals of the $\pi\pi$ mass. The value of $\int_{2m_\pi}^{1.08\ \mathrm{GeV}} BdM$, corresponding to the production of *all* dipion pairs in the ρ^0 region, is 159 ±8 μb/GeV² (118 ± 5 μb/GeV²) at 2.8 GeV (4.7 GeV).

3. *Formalism for the Analysis of the Dipion Angular Momentum States*

We now discuss the angular distribution of pion pairs *in the* $\pi^+\pi^-$ *rest system*. As will be shown below the pion pairs are in a predominantly p-wave state, so for *brevity we refer to them as* ρ^0. We use the formalism of Refs. 34 and 35 which describes vector-meson production by polarized photons.

We consider the angular distribution of ρ^0 decay in three reference systems which differ in the choice of the spin-quantization axis (z axis): the *Gottfried-Jackson* system, where the z axis is the

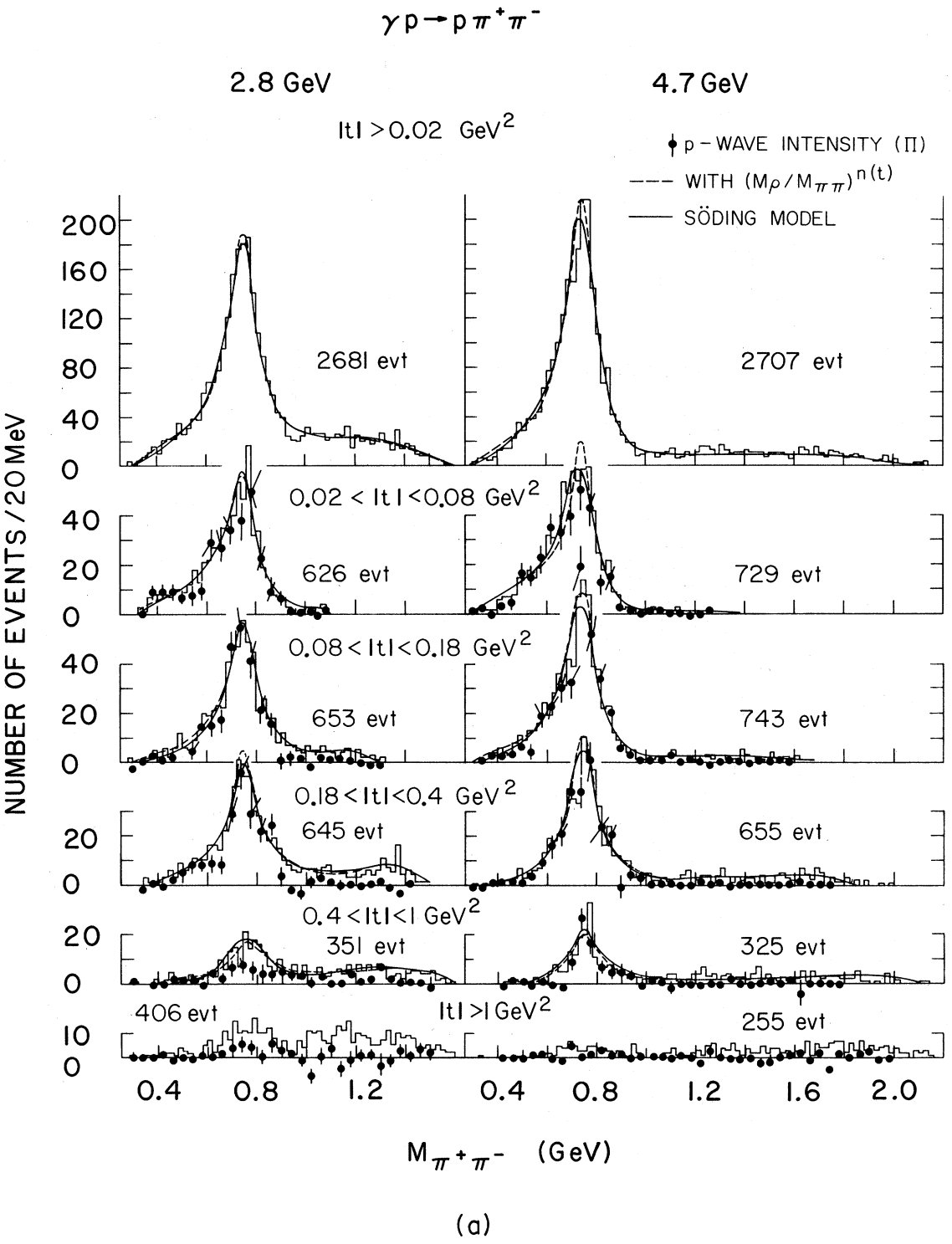

FIG. 10. *(Continued on next page.)*

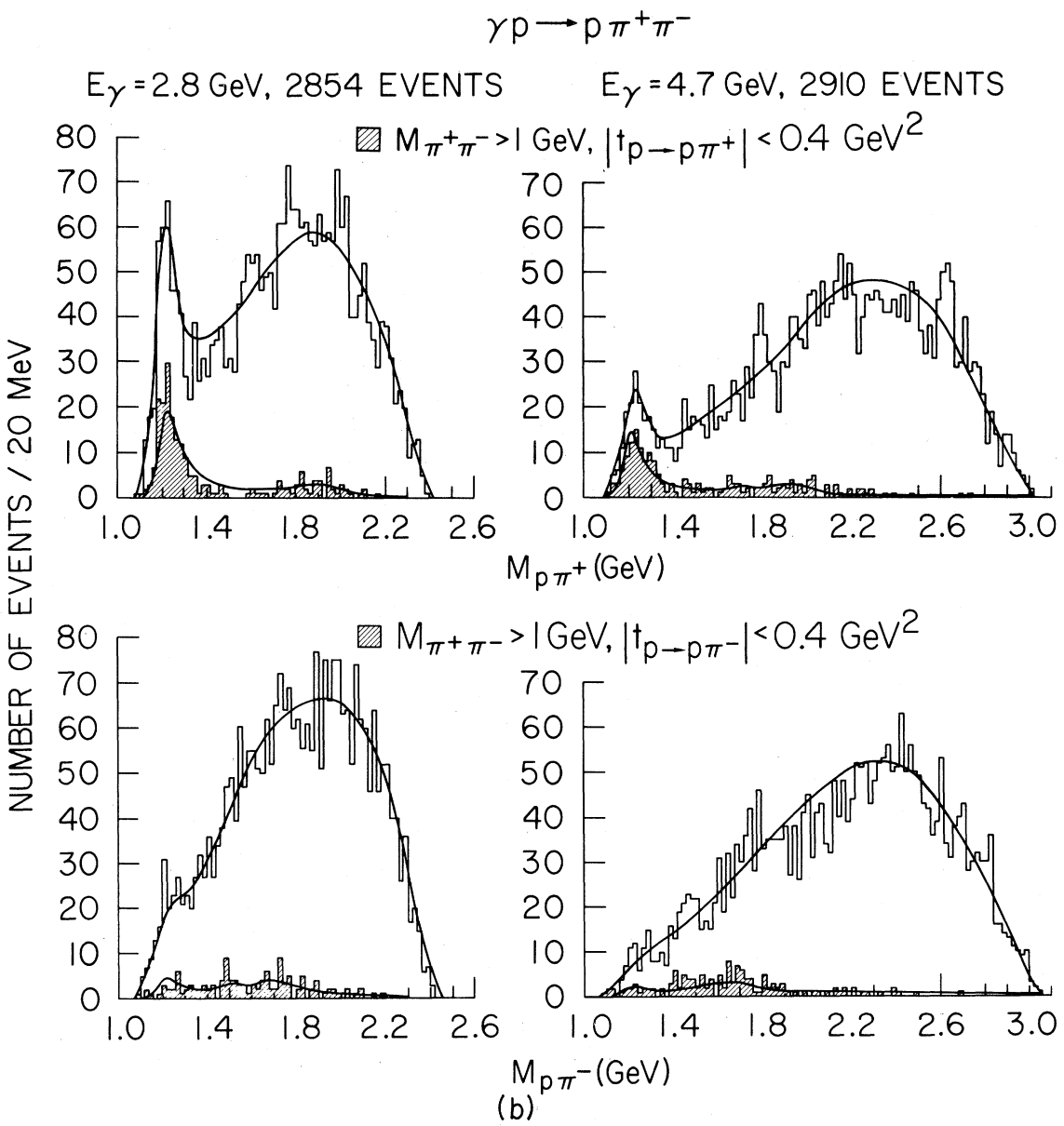

FIG. 10. Reaction $\gamma p \to p\pi^+\pi^-$. (a) $\pi^+\pi^-$ mass distributions for different t intervals. The helicity-conserving p-wave intensity Π is shown by the points ●. The curves give the results of maximum-likelihood fits to the channel using the parametrization method (dashed line) and the Söding model (solid line) described in Appendixes A and B, respectively. (b) $p\pi^+$ and $p\pi^-$ mass distributions. The shaded histograms represent events with $|t_{p\to p\pi^\pm}| < 0.4$ GeV^2 and $M_{\pi^+\pi^-} > 1$ GeV. The curves are from a fit described in Appendix B.

direction of the incident photon in the ρ^0 rest system; the *helicity* system, where the z axis is the direction of the ρ^0 in the over-all (γp) c.m. system, i. e., opposite to the direction of the outgoing proton in the ρ^0 rest system; and the *Adair* system, where the z axis is along the direction of the incident photon in the over-all (γp) c.m. system. The y axis is always normal to the production plane.[36] For forward-produced ρ^0 mesons, all three systems coincide.

Depending upon the production mechanism, the ρ^0 may be aligned in one of these three systems. The system which gives the simplest description of the ρ^0 is then: (1) the Gottfried-Jackson system for t-channel helicity conservation (resulting from, for example, $J^P = 0^+$ exchange with no absorption); (2) the helicity system for s-channel c.m. helicity conservation; (3) the Adair system for "spin independence" in the s-channel c.m. system.[37] One of the objectives of the density-matrix analysis of

Sec IV B is to determine the preferred system for describing ρ^0 photoproduction.

In all three systems the decay angular distribution for ρ mesons produced by linearly polarized photons can be expressed in terms of nine independent measurable spin-density-matrix parameters ρ^{α}_{ik} (Refs. 34 and 35):

$$W(\cos\theta,\phi,\Phi)=\frac{3}{4\pi}\left[\tfrac{1}{2}(1-\rho^0_{00})+\tfrac{1}{2}(3\rho^0_{00}-1)\cos^2\theta-\sqrt{2}\,\mathrm{Re}\rho^0_{10}\sin2\theta\cos\phi-\rho^0_{1-1}\sin^2\theta\cos2\phi\right.$$
$$-P_\gamma\cos2\Phi(\rho^1_{11}\sin^2\theta+\rho^1_{00}\cos^2\theta-\sqrt{2}\,\mathrm{Re}\rho^1_{10}\sin2\theta\cos\phi-\rho^1_{1-1}\sin^2\theta\cos2\phi)$$
$$\left.-P_\gamma\sin2\Phi(\sqrt{2}\,\mathrm{Im}\rho^2_{10}\sin2\theta\sin\phi+\mathrm{Im}\rho^2_{1-1}\sin^2\theta\sin2\phi)\right]. \quad (2)$$

Here, P_γ is the degree of linear polarization of the photon; Φ is the angle of the photon electric polarization vector with respect to the production plane measured in the over-all (γp) c.m. system; θ and ϕ are the polar and azimuthal angles of the π^+ in the ρ^0 rest frame. (See Fig. 12 and Ref. 36.) In terms of helicity amplitudes, $T_{kl,mn}$, the density-matrix parameters are given by[34,35]:

$$\rho^0_{ik}=\frac{1}{A}\sum_{\lambda_\gamma\lambda_{N'},\lambda_N}T_{\lambda_{\rho i}\lambda_{N'},\lambda_\gamma\lambda_N}T^*_{\lambda_{\rho k}\lambda_{N'},\lambda_\gamma\lambda_N},$$
$$\rho^1_{ik}=\frac{1}{A}\sum_{\lambda_\gamma\lambda_{N'},\lambda_N}T_{\lambda_{\rho i}\lambda_{N'},-\lambda_\gamma\lambda_N}T^*_{\lambda_{\rho k}\lambda_{N'},\lambda_\gamma\lambda_N}, \quad (3)$$
$$\rho^2_{ik}=\frac{i}{A}\sum_{\lambda_\gamma\lambda_{N'}\lambda_N}\lambda_\gamma T_{\lambda_{\rho i}\lambda_{N'},-\lambda_\gamma\lambda_N}T^*_{\lambda_{\rho k}\lambda_{N'},\lambda_\gamma\lambda_N},$$

with

$$A=\sum_{\lambda_{\rho i}\lambda_\gamma\lambda_{N'}\lambda_N}T_{\lambda_{\rho i}\lambda_{N'},\lambda_\gamma\lambda_N}T^*_{\lambda_{\rho i}\lambda_{N'},\lambda_\gamma\lambda_N},$$

where $\lambda_{N'}$, λ_γ, λ_N denote the helicity of the outgoing proton, the photon, the target proton, respectively, and λ_{ρ_i}, λ_{ρ_k} the helicity of the produced ρ meson. The matrix elements ρ^0_{ik} describe the ρ decay in the case of an unpolarized beam; the additional terms ρ^1_{ik} and ρ^2_{ik} are measurable with a linearly polarized photon beam. For further details see Appendix C.

It has been shown that to leading order in energy,[38,39] the over-all production cross section (σ) may be split into noninterfering contributions σ^N, σ^U from natural and unnatural parity exchange in the t channel by linear combinations of the density-matrix parameters.[35]

We define P_σ, the parity asymmetry, by

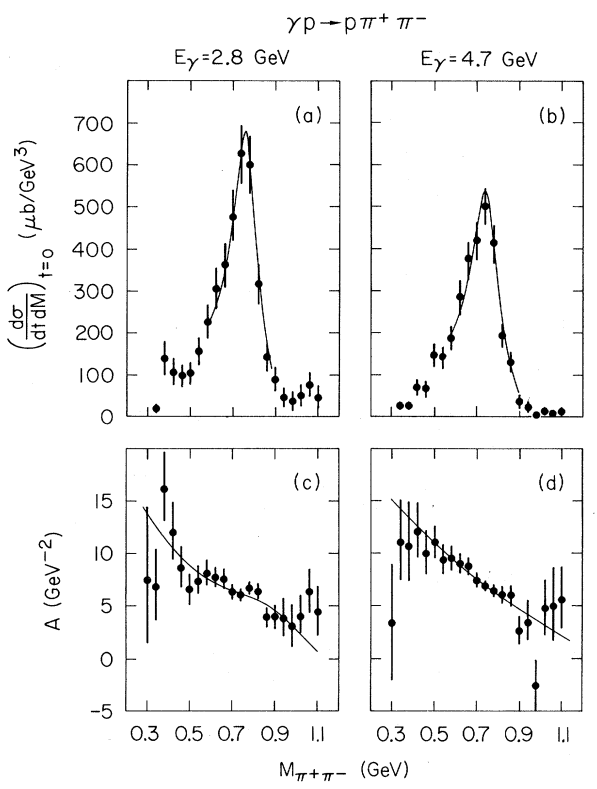

FIG. 11. Reaction $\gamma p \to p\pi^+\pi^-$. (a) and (b) $d^2\sigma/dtdM|_{t=0}$ for dipion production obtained from a maximum-likelihood fit of the form Be^{At} to events in the t interval $0.02<|t|<0.4$ GeV^2. The solid curve is from a fit of the form Breit-Wigner$\times(M_\rho/M_{\pi\pi})^n$ (see Sec. IV C 3) in the interval $0.6<M_{\pi\pi}<0.9$ GeV. (c) and (d) The slope, A, of the invariant-momentum-transfer distribution of dipion pairs as a function of dipion mass. The solid curve is from the Söding model (Sec. IV C 2 and Appendix B).

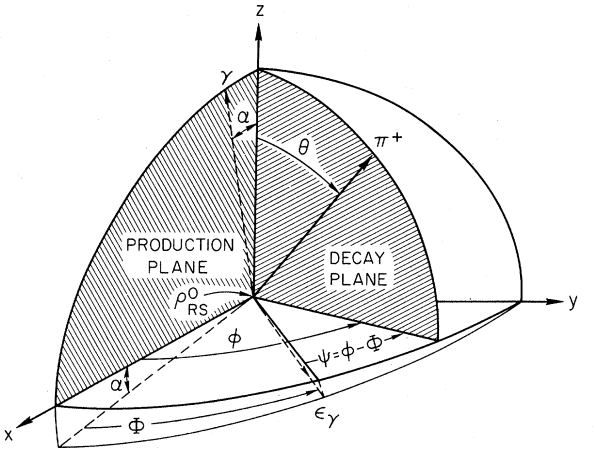

FIG. 12. Angles used in the study of ρ^0 decay. The angle α is zero in the Gottfried-Jackson system.

TABLE IX. $\Delta\sigma/\Delta t\Delta M$ in μb/GeV^3. Here Δt is the interval heading the column (no t_{min} correction has been made) and ΔM is 0.04 GeV^2; the lower limit of the ΔM interval is given in the first column of the table. Also given are B and A from a fit of the form Be^{At} in the interval $t' < |t| < 0.4$ GeV^2, where t' is the larger of $|t|_{min}$ and 0.02 GeV^2.

Mass (GeV) \ $\lvert t\rvert$ (GeV^2)	0.02–0.05	0.05–0.075	0.075–0.10	0.10–0.15	0.15–0.20	0.20–0.25	0.25–0.30	0.30–0.35	0.35–0.40	B (μb/GeV^3) from Be^{At} fit	A (GeV^{-2})
					$\Delta\sigma/\Delta t\Delta M$ (μb/GeV^3); $E_\gamma = 2.8$ GeV						
0.28	0	0	0	11± 8	5± 5	0	0	0	0	8± 8	7.6±6.5
0.32	18±13	11±11	11±11	11± 8	11± 8	0	0	0	5± 5	21±13	6.8±3.5
0.36	72±26	76±29	22±16	16± 9	11± 8	5± 5	0	0	0	141±42	16.3±3.5
0.40	72±26	43±22	54±24	22±11	0	11± 8	11± 8	0	0	110±33	12.5±2.8
0.44	118±33	43±22	11±11	27±12	22±11	11± 8	11± 8	5± 5	11± 8	99±28	8.7±2.0
0.48	99±30	43±22	87±31	43±15	27±12	27±12	16± 9	5± 5	16± 9	107±29	6.6±1.5
0.52	181±41	108±34	43±22	33±14	33±14	43±15	22±11	11± 8	16± 9	157±35	7.4±1.4
0.56	172±40	119±36	130±38	108±25	49±16	38±14	5± 5	16± 9	16± 9	228±42	8.1±1.2
0.60	280±51	163±43	141±40	98±23	98±23	60±18	27±12	43±15	11± 8	309±49	7.6±1.0
0.64	262±50	325±61	206±48	114±25	65±19	54±17	33±14	49±16	33±14	361±53	7.6±0.9
0.68	298±53	347±63	326±61	228±36	190±33	114±25	81±21	65±19	33±14	477±62	6.2±0.7
0.72	461±67	488±75	282±56	336±45	222±36	201±34	92±23	92±23	60±18	627±71	6.0±0.6
0.76	579±76	336±62	304±59	239±37	195±33	125±27	71±20	76±21	71±20	602±69	6.7±0.6
0.80	316±55	152±41	174±44	119±26	114±25	49±16	125±27	38±14	11± 8	318±50	6.3±0.8
0.84	118±33	76±29	195±47	60±18	76±21	43±15	71±20	22±11	38±14	144±39	4.0±1.0
0.88	45±20	65±27	65±27	71±20	38±14	54±17	22±11	22±11	22±11	91±32	4.0±1.3
0.92	27±16	0	54±24	33±14	33±14	22±11	16± 9	16± 9	5± 5	49±24	3.9±1.8
0.96	9± 9	22±16	33±19	27±12	22±11	16± 9	16± 9	16± 9	5± 5	35±24	3.1±2.0
1.0	9± 9	33±19	43±22	22±11	33±14	22±11	16± 9	16± 9	11± 8	52±26	4.0±1.9
1.04	0	65±27	54±24	27±12	11± 8	0	22±11	16± 9	11± 8	75±29	6.3±2.2
1.08	0	11±11	11±11	22±11	27±12	33±14	5± 5	16± 9	0	45±26	4.5±2.4
1.12	0	0	0	16± 9	22±11	5± 5	11± 8	33±14	5± 5	13±50	−0.7±2.6
1.16	0	0	22±16	11± 8	22±11	5± 5	11± 8	11± 8	0	71±38	8.1±3.6
1.20	0	0	0	27±12	16± 9	11± 8	16± 9	5± 5	0	150±70	10.5±4.0
1.24	0	0	0	11± 8	23±11	11± 8	33±14	0	5± 5	77±60	7.6±3.8
1.28	0	0	0	5± 5	11± 8	33±14	38±14	5± 5	16± 9	159±91	7.0±3.6
1.32	0	0	0	0	11± 8	33±14	11± 8	11± 8	0		
1.36	0	0	0	0	11± 8	11± 8	43±15	22±11	22±11		
1.40	0	0	0	0	0	5± 5	5± 5	27±12	16± 9		
1.44								5± 5	5± 5		
1.48									5± 5		

TABLE IX *(Continued)*

Mass (GeV) \ $\lvert t\rvert$ (GeV^2)	0.02–0.05	0.05–0.075	0.075–0.10	0.10–0.15	0.15–0.20	0.20–0.25	0.25–0.30	0.30–0.35	0.35–0.40	B (μb/GeV^3)	A (GeV^{-2})
	$\Delta\sigma/\Delta t\Delta M$ (μb/GeV^3); E_γ = 4.7 GeV									from Be^{At} fit	
0.28	0	7± 7	0	0	3± 3	0	0	3± 3	0	3± 4	3.4±5.5
0.32	20±12	14± 9	7± 7	7± 5	7± 5	0	0	3± 3	0	27±12	11.1±3.8
0.36	20±12	7± 7	21±13	3± 3	7± 5	0	0	3± 3	0	26±12	10.7±3.6
0.40	51±18	35±16	14± 9	20± 8	7± 5	7± 5	3± 3	0	0	71±20	12.1±2.6
0.44	32±15	42±17	48±18	13± 7	17± 8	7± 5	0	7± 5	0	67±19	10.0±2.1
0.48	83±23	119±29	48±18	33±11	20± 8	10± 6	10± 6	3± 3	3± 3	149±29	11.1±1.6
0.52	115±28	98±26	35±16	46±12	30±10	10± 6	7± 5	7± 5	10± 6	143±27	9.4±1.4
0.56	121±28	132±30	63±21	70±16	53±13	3±13	20± 8	10± 6	3± 3	194±31	9.5±1.2
0.60	242±40	126±30	160±35	86±17	46±12	56±14	20± 8	7± 5	17± 8	288±38	9.0±0.9
0.64	299±45	195±38	160±35	113±20	110±20	40±12	40±12	33±11	3± 3	375±43	8.8±0.8
0.68	389±52	300±47	126±30	156±24	103±19	76±16	70±16	60±14	13± 7	420±45	7.4±0.7
0.72	389±52	286±46	293±47	222±29	199±27	76±16	76±16	33±11	53±13	502±49	6.9±0.6
0.76	369±51	279±45	216±40	196±27	100±19	93±18	83±17	56±14	40±12	411±45	6.4±0.6
0.80	153±32	126±30	126±30	93±18	83±17	40±12	33±11	27±10	20± 8	193±31	6.0±0.8
0.84	115±28	84±24	105±27	46±12	50±13	27±10	30±10	23± 9	13± 7	131±25	5.9±1.0
0.88	20±12	42±17	28±15	30±10	20± 8	17± 8	30±10	13± 7	7± 5	36±19	2.7±1.3
0.92	25±13	7± 7	28±15	17± 8	10± 6	7± 5	7± 5	7± 5	10± 6	23±13	3.5±1.8
0.96	0	14±10	0	7± 5	0	3± 3	13± 7	3± 3	10± 6	3± 4	−2.5±2.6
1.0	20±12	7± 7	14±10	0	7± 5	10± 6	10± 6	0	0	15± 9	4.8±2.6
1.04	7± 7	0	7± 7	0	13± 7	7± 5	0	0	0	19± 7	5.0±3.5
1.08	13± 9	0	14±10	10± 6	10± 6	0	3± 3	0	3± 3	15± 9	5.7±2.9
1.12	7± 7	14±10	7± 7	3± 3	7± 5	7± 5	3± 3	3± 3	3± 3	10± 9	3.2±2.7
1.16	0	7± 7	13± 9	3± 3	0	0	3± 3	10± 6	3± 3	4±36	−0.3±3.1
1.20	0	7± 7	20±12	3± 3	7± 5	0	7± 5	7± 5	3± 3	7±15	1.3±2.7
1.24	0	20±12	7± 7	7± 5	7± 5	3± 3	3± 3	0	7± 5	12±10	4.2±2.9
1.28	0	0	13± 9	7± 5	13± 7	0	10± 6	7± 5	10± 6	6±20	−0.8±2.4
1.32	0	0	13± 9	0	7± 5	3± 3	3± 3	3± 3	3± 3	5±12	1.6±3.5
1.36	0	7± 7	20±12	7± 5	7± 5	7± 5	3± 3	0	3± 3	24±13	7.2±3.3
1.40	0	0	13± 9	7± 5	7± 5	0	3± 3	10± 6	3± 3	8±15	1.8±3.1
1.44	0	0	7± 7	0	7± 5	3± 3	7± 5	0	0	8± 9	4.6±4.6
1.48	0	0	7± 7	3± 3	7± 5	3± 3	3± 3	3± 3	0	13±11	5.9±4.6
1.52	0	0	0	3± 3	7± 5	3± 3	7± 5	7± 5	7± 5	3± 7	−1.9±3.6
1.56	0	0	0	10± 6	3± 3	3± 3	3± 3	10± 6	0	14±15	4.3±4.1
1.60	0	0	0	10± 6	3± 3	10± 6	7± 5	7± 5	3± 3	23±20	4.6±3.8
1.64	0	0	0	0	10± 6	7± 5	7± 5	3± 3	10± 6	9±40	0.9±4.1
1.68	0	0	0	0	7± 5	7± 5	10± 6	7± 5	3± 3	13±27	2.3±4.6
1.72	0	0	0	0	0	0	3± 3	3± 3	0		
1.76	0	0	0	0	0	0	7± 5	0	0		
1.80	0	0	0	0	0	0	0	13± 7	0		
1.84	0	0	0	0	0	0	7± 5	0	0		
1.88	0	0	0	0	0	0	0	3± 3	3± 3		
1.92	0	0	0	0	0	0	0	0	0		
1.96	0	0	0	0	0	0	0	3± 3	0		

$$P_\sigma = \frac{\sigma^N - \sigma^U}{\sigma^N + \sigma^U}.$$

At high energies

$$P_\sigma = 2\rho^1_{1\,-1} - \rho^1_{00}. \tag{4}$$

Note that P_σ is invariant under rotations around the normal to the production plane; e.g., it is the same in the three systems described above. We also point out that P_σ is sensitive to possible ρ^0-helicity or spin-flip terms (contributing to ρ^1_{00}) which are not usually measured in counter experiments. Counter experiments of the type of Refs. 40 and 41 measure the asymmetry Σ defined as

$$\Sigma = \frac{\sigma_\parallel - \sigma_\perp}{\sigma_\parallel + \sigma_\perp} = \frac{\rho^1_{11} + \rho^1_{1\,-1}}{\rho^0_{11} + \rho^0_{1\,-1}}. \tag{5}$$

Here $\sigma_\parallel$ and $\sigma_\perp$ are the cross sections for the pions from symmetric ρ decay ($\theta = \frac{1}{2}\pi$, $\phi = \frac{1}{2}\pi$) to emerge in the plane of the photon polarization ($\Phi = \frac{1}{2}\pi$) and perpendicular to it ($\Phi = 0$). When the helicity-flip terms, ρ^1_{00}, ρ^1_{11}, ρ^0_{00}, $\rho^0_{1\,-1}$ are zero, Σ is equal to P_σ.

The ρ^0 decay distribution may be simplified if we use the angle $\Psi = \phi - \Phi$ which, in the forward direction, is the angle between the photon polarization and the ρ^0 decay plane. If the ρ^0 production mechanism conserves s-channel helicity, i.e., the ρ is transverse and linearly polarized like the photon, then in the helicity system

$$\rho^1_{1\,-1} = -\mathrm{Im}\rho^2_{1\,-1} = \tfrac{1}{2} \tag{6}$$

and all other ρ^α_{ik} in *Eq. (2)* are 0. In these circumstances Ψ is the azimuthal angle in the helicity system of the decay π^+ with respect to the ρ^0 polarization plane and the decay angular distribution is proportional to $\sin^2\theta\cos^2\Psi$. The distribution of Ψ is also related to P_σ if the helicity-flip terms are zero: For 100% linear polarization the decay is $\sin^2\theta\cos^2\Psi$ for $P_\sigma = +1$ while for $P_\sigma = -1$ the decay distribution is $\sin^2\theta\sin^2\Psi$.

4. *The Moments, Y^m_l, of the Dipion System*

Figure 13 shows the distributions of the polar angle θ and the angle Ψ in the helicity system for events in the ρ^0 mass region (0.60–0.85 GeV) with $|t| < 0.4$ GeV^2. This figure shows that the ρ^0 decay has a simple description in terms of θ and Ψ in the helicity system, viz., the ρ^0 is well described by a $\sin^2\theta\cos^2\Psi$ angular distribution for $|t| < 0.4$ GeV^2. Consequently, in order to give an over-all description of the characteristics of the decay angular distribution of the $\pi^+\pi^-$ system, we present in Fig. 14 the moment sums, $\sum \mathrm{Re}Y^m_l(\theta,\Psi)$, of the $\pi^+\pi^-$ system in the helicity frame as a function of $\pi^+\pi^-$ mass for $|t| < 0.4$ GeV^2. Only those moments are

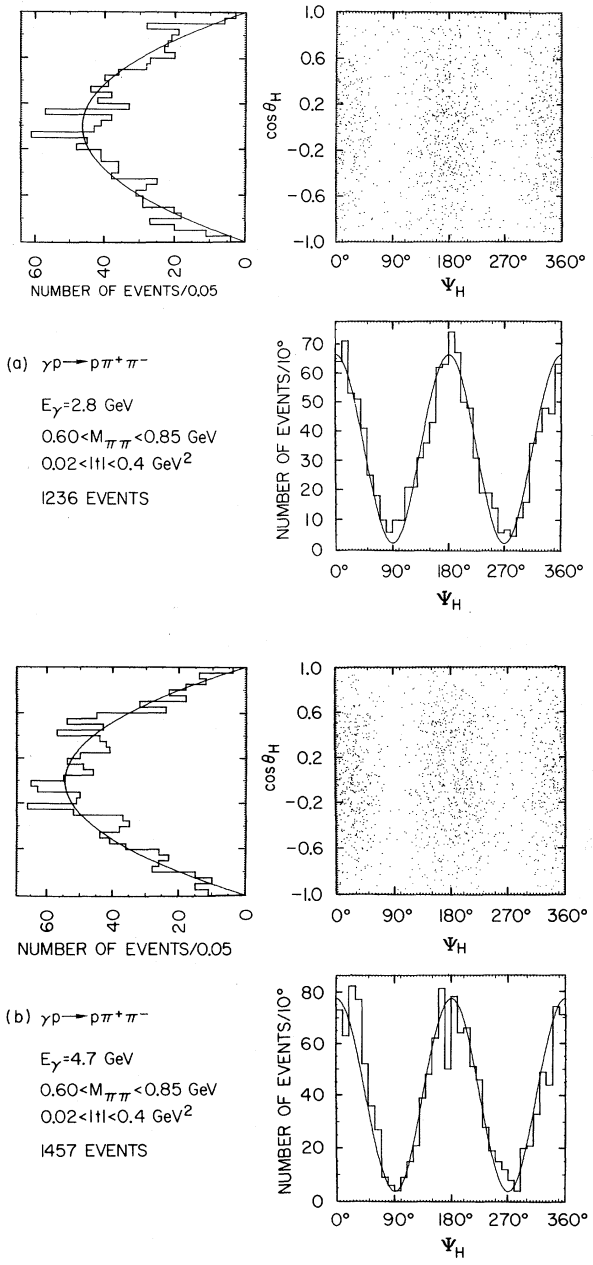

FIG. 13. Reaction $\gamma p \to p\rho^0$ at (a) 2.8 GeV and (b) 4.7 GeV, respectively. ρ-decay angular distributions in the helicity system without background subtraction. The curves are proportional to $\sin^2\theta_H$ and $(1 + P_\gamma \cos 2\Psi_H)$.

shown which have a significant deviation from zero in either the 2.8- or 4.7-GeV data; other moments can be found in Ref. 17. From the moments we conclude that:

(a) Strong Y^0_2 and Y^2_2 moments are present in the ρ^0 region which follow the asymmetric ρ^0 shape. This and the small values of higher even moments demonstrates that *it is the p-wave part of the mass*

spectrum that is skewed.

(b) Odd moments Y_1^0, Y_3^0 are present throughout the dipion mass range. These moments are due to differences in the π^+p and π^-p mass spectra and consequently they result mainly from Δ^{++} production. In addition, Δ^{++} production gives rise to the positive Y_2^0 moment at large $\pi^+\pi^-$ masses.

(c) At 4.7 GeV, evidence exists for a Y_4^0 moment which changes sign through the ρ^0 region. This moment may be interpreted as originating *from the interference of the ρ^0 with angular momentum states*

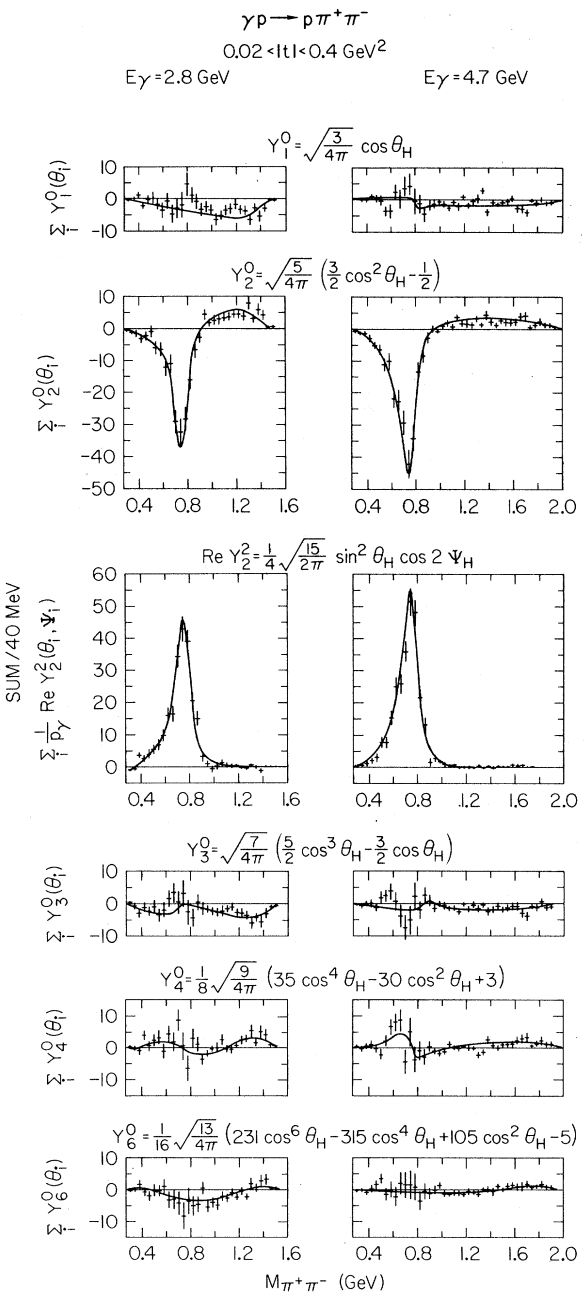

FIG. 14. Reaction $\gamma p \to p\pi^+\pi^-$. The dipion moments $Y_1^0(\theta)$, $Y_2^0(\theta)$, $\mathrm{Re}Y_2^2(\theta,\Psi)$, $Y_3^0(\theta)$, $Y_4^0(\theta)$, $Y_6^0(\theta)$ in the helicity frame as a function of $M_{\pi^+\pi^-}$ for $0.02 < |t| < 0.4$ GeV^2. The curves are obtained from the Söding model (Sec. IV C 2).

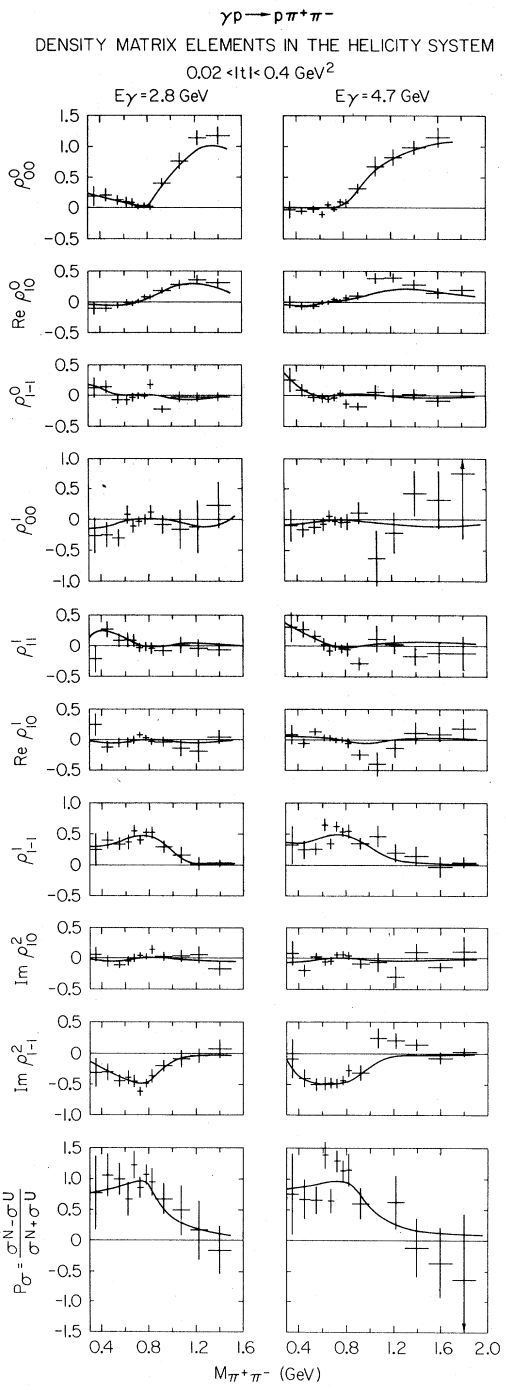

FIG. 15. Reaction $\gamma p \to p\pi^+\pi^-$. Helicity-frame density matrix elements and parity asymmetry as a function of dipion mass for $0.02 < |t| < 0.4$ GeV^2. The curves are obtained from the Söding model.

TABLE X. ρ density-matrix elements for the reaction $\gamma p \to p\rho^0$.

$\lvert t\rvert$ (GeV)^2	0.02–0.05	0.05–0.08	0.08–0.12	0.12–0.18	0.18–0.25	0.25–0.40	0.4–1.0
			(a) E_γ =2.8 GeV, Gottfried-Jackson system				
ρ^0_{00}	0.079 ± 0.030	0.119 ± 0.035	0.298 ± 0.041	0.431 ± 0.047	0.455 ± 0.051	0.525 ± 0.052	0.476 ± 0.071
$\mathrm{Re}\rho^0_{10}$	0.143 ± 0.019	0.195 ± 0.023	0.180 ± 0.020	0.158 ± 0.024	0.146 ± 0.027	−0.002 ± 0.027	−0.089 ± 0.046
ρ^0_{1-1}	0.151 ± 0.037	0.122 ± 0.035	0.111 ± 0.033	0.161 ± 0.035	0.160 ± 0.037	0.267 ± 0.038	0.071 ± 0.057
ρ^1_{00}	−0.140 ± 0.056	−0.057 ± 0.048	−0.231 ± 0.071	−0.328 ± 0.081	−0.390 ± 0.085	−0.359 ± 0.094	−0.483 ± 0.118
ρ^1_{11}	0.091 ± 0.040	0.048 ± 0.045	0.092 ± 0.040	0.114 ± 0.037	0.208 ± 0.042	0.212 ± 0.045	0.134 ± 0.067
$\mathrm{Re}\rho^1_{10}$	−0.085 ± 0.035	−0.170 ± 0.033	−0.167 ± 0.029	−0.113 ± 0.037	−0.111 ± 0.042	−0.059 ± 0.042	0.119 ± 0.067
ρ^1_{1-1}	0.505 ± 0.045	0.414 ± 0.055	0.358 ± 0.039	0.270 ± 0.046	0.258 ± 0.047	0.125 ± 0.060	0.246 ± 0.088
$\mathrm{Im}\rho^2_{10}$	0.136 ± 0.035	0.249 ± 0.040	0.229 ± 0.032	0.274 ± 0.034	0.259 ± 0.042	0.341 ± 0.033	0.094 ± 0.073
$\mathrm{Im}\rho^2_{1-1}$	−0.462 ± 0.036	−0.417 ± 0.053	−0.254 ± 0.058	−0.240 ± 0.054	−0.244 ± 0.058	−0.046 ± 0.040	−0.095 ± 0.091
			(b) E_γ =2.8 GeV, helicity system				
ρ^0_{00}	−0.045 ± 0.030	−0.034 ± 0.033	0.021 ± 0.029	0.026 ± 0.036	0.016 ± 0.042	−0.071 ± 0.042	0.173 ± 0.064
$\mathrm{Re}\rho^0_{10}$	0.013 ± 0.018	−0.032 ± 0.020	0.008 ± 0.023	0.026 ± 0.027	−0.028 ± 0.026	0.112 ± 0.027	0.140 ± 0.043
ρ^0_{1-1}	0.078 ± 0.037	0.027 ± 0.040	−0.024 ± 0.041	−0.045 ± 0.040	−0.052 ± 0.048	−0.001 ± 0.047	−0.079 ± 0.060
ρ^1_{00}	−0.061 ± 0.056	0.018 ± 0.059	−0.036 ± 0.047	−0.015 ± 0.055	0.041 ± 0.059	0.172 ± 0.063	−0.088 ± 0.108
ρ^1_{11}	0.042 ± 0.046	0.001 ± 0.050	−0.008 ± 0.042	−0.049 ± 0.050	−0.011 ± 0.054	−0.050 ± 0.061	−0.073 ± 0.079
$\mathrm{Re}\rho^1_{10}$	0.015 ± 0.030	0.071 ± [illegible]30	0.026 ± 0.037	−0.009 ± 0.039	0.004 ± 0.037	−0.037 ± 0.042	−0.138 ± 0.062
ρ^1_{1-1}	0.539 ± 0.044	0.453 ± 0.052	0.458 ± 0.043	0.427 ± 0.050	0.484 ± 0.064	0.355 ± 0.062	0.457 ± 0.085
$\mathrm{Im}\rho^2_{10}$	−0.050 ± 0.034	0.012 ± 0.040	0.012 ± 0.034	0.016 ± 0.037	−0.073 ± 0.044	0.036 ± 0.031	−0.070 ± 0.064
$\mathrm{Im}\rho^2_{1-1}$	−0.496 ± 0.039	−0.551 ± 0.053	−0.427 ± 0.054	−0.445 ± 0.049	−0.424 ± 0.058	−0.465 ± 0.043	−0.157 ± 0.101
			(c) E_γ =2.8 GeV, Adair system				
ρ^0_{00}	−0.023 ± 0.029	−0.029 ± 0.033	0.066 ± 0.032	0.114 ± 0.043	0.084 ± 0.040	0.238 ± 0.040	0.512 ± 0.073
$\mathrm{Re}\rho^0_{10}$	0.063 ± 0.019	0.060 ± 0.019	0.104 ± 0.022	0.141 ± 0.023	0.129 ± 0.030	0.237 ± 0.030	0.115 ± 0.041
ρ^0_{1-1}	0.088 ± 0.037	0.030 ± 0.040	−0.002 ± 0.039	−0.001 ± 0.039	−0.020 ± 0.045	0.152 ± 0.045	0.091 ± 0.055
ρ^1_{00}	−0.071 ± 0.055	0.039 ± 0.054	−0.052 ± 0.054	−0.084 ± 0.071	−0.054 ± 0.056	−0.027 ± 0.071	−0.442 ± 0.123
ρ^1_{11}	0.048 ± 0.044	−0.009 ± 0.049	0.001 ± 0.042	−0.015 ± 0.049	0.038 ± 0.050	0.051 ± 0.048	0.105 ± 0.066
$\mathrm{Re}\rho^1_{10}$	−0.026 ± 0.033	−0.019 ± 0.031	−0.064 ± 0.034	−0.114 ± 0.034	−0.148 ± 0.044	−0.202 ± 0.046	−0.168 ± 0.062
ρ^1_{1-1}	0.531 ± 0.043	0.464 ± 0.053	0.450 ± 0.043	0.392 ± 0.049	0.438 ± 0.059	0.258 ± 0.063	0.276 ± 0.087
$\mathrm{Im}\rho^2_{10}$	0.008 ± 0.035	0.096 ± 0.041	0.099 ± 0.032	0.132 ± 0.035	0.063 ± 0.044	0.195 ± 0.035	0.007 ± 0.074
$\mathrm{Im}\rho^2_{1-1}$	−0.499 ± 0.038	−0.531 ± 0.051	−0.405 ± 0.056	−0.404 ± 0.051	−0.427 ± 0.058	−0.372 ± 0.035	−0.155 ± 0.086

with spin ≥ 3.

(d) No significant moments, other than those associated with a p-wave system or the Δ^{++}, exist in the ρ^0 region. This indicates *a negligible incoherent background under the* ρ^0.

5. *The Density-Matrix Elements of the Dipion and* ρ^0 *States: Determination of* ρ^0 *Production Properties*

In Sec. IV B 4 we found that, with the exception of Δ^{++} reflections, the $\pi\pi$ angular distributions are p-wave dominated. We therefore use the p-wave formalism of Eq. (2) and show in Fig. 15 the helicity-frame density-matrix elements and P_σ, determined by the method of moments, as a *function of* $\pi\pi$ *mass*. These plots indicate that the ρ^0 region is characterized by $P_\sigma \simeq 1$ and $\rho^1_{1\,-1} \simeq -\mathrm{Im}\rho^2_{1\,-1} \simeq 0.5$ with other ρ^α_{ik} close to zero [see Eq. (6)]. Deviations from these values become apparent at high $\pi\pi$ masses where we observe primarily the Δ^{++} reflection. Deviations at low $\pi\pi$ masses are discussed in Sec. IV C 2.

TABLE X *(Continued)*

$\|t\|$ (GeV)^2	0.02–0.05	0.05–0.08	0.08–0.12	0.12–0.18	0.18–0.25	0.25–0.40	0.4–1.0
			(d) E_γ =4.7 GeV, Gottfried-Jackson system				
ρ^0_{00}	0.143 ± 0.029	0.227 ± 0.036	0.312 ± 0.038	0.357 ± 0.033	0.474 ± 0.047	0.577 ± 0.044	0.476 ± 0.064
$\mathrm{Re}\rho^0_{10}$	0.158 ± 0.016	0.234 ± 0.020	0.148 ± 0.021	0.167 ± 0.019	0.114 ± 0.022	0.017 ± 0.027	−0.029 ± 0.036
ρ^0_{1-1}	0.066 ± 0.029	0.082 ± 0.033	0.133 ± 0.032	0.148 ± 0.030	0.229 ± 0.036	0.199 ± 0.026	0.077 ± 0.048
ρ^1_{00}	−0.172 ± 0.041	−0.187 ± 0.054	−0.245 ± 0.060	−0.315 ± 0.056	−0.554 ± 0.063	−0.338 ± 0.085	−0.377 ± 0.095
ρ^1_{11}	0.061 ± 0.037	0.083 ± 0.038	0.119 ± 0.036	0.147 ± 0.031	0.193 ± 0.035	0.195 ± 0.036	0.157 ± 0.048
$\mathrm{Re}\rho^1_{10}$	−0.117 ± 0.028	−0.179 ± 0.029	−0.159 ± 0.029	−0.196 ± 0.033	−0.186 ± 0.028	−0.111 ± 0.045	0.064 ± 0.051
ρ^1_{1-1}	0.521 ± 0.037	0.302 ± 0.044	0.416 ± 0.038	0.302 ± 0.037	0.259 ± 0.049	0.273 ± 0.041	0.269 ± 0.059
$\mathrm{Im}\rho^2_{10}$	0.152 ± 0.026	0.202 ± 0.029	0.277 ± 0.033	0.301 ± 0.025	0.305 ± 0.036	0.249 ± 0.039	0.256 ± 0.051
$\mathrm{Im}\rho^2_{1-1}$	−0.326 ± 0.044	−0.413 ± 0.042	−0.343 ± 0.043	−0.278 ± 0.037	−0.158 ± 0.047	−0.090 ± 0.051	0.164 ± 0.076
			(e) E_γ =4.7 GeV, helicity system				
ρ^0_{00}	−0.009 ± 0.022	−0.037 ± 0.025	0.027 ± 0.031	0.021 ± 0.029	−0.002 ± 0.035	0.062 ± 0.028	0.208 ± 0.054
$\mathrm{Re}\rho^0_{10}$	0.009 ± 0.018	0.001 ± 0.019	0.010 ± 0.023	−0.024 ± 0.019	0.031 ± 0.023	0.067 ± 0.027	0.043 ± 0.037
ρ^0_{1-1}	−0.001 ± 0.031	−0.064 ± 0.041	−0.003 ± 0.035	−0.031 ± 0.033	−0.006 ± 0.044	−0.052 ± 0.042	−0.048 ± 0.056
ρ^1_{00}	−0.087 ± 0.038	0.052 ± 0.032	−0.051 ± 0.043	−0.001 ± 0.045	0.054 ± 0.045	−0.049 ± 0.057	−0.140 ± 0.078
ρ^1_{11}	0.018 ± 0.039	−0.035 ± 0.041	0.025 ± 0.039	−0.020 ± 0.039	−0.105 ± 0.047	0.048 ± 0.048	0.040 ± 0.055
$\mathrm{Re}\rho^1_{10}$	0.033 ± 0.027	−0.022 ± 0.028	−0.001 ± 0.037	0.008 ± 0.028	−0.007 ± 0.028	0.018 ± 0.046	−0.076 ± 0.053
ρ^1_{1-1}	0.548 ± 0.039	0.420 ± 0.054	0.521 ± 0.036	0.484 ± 0.038	0.563 ± 0.050	0.434 ± 0.051	0.390 ± 0.065
$\mathrm{Im}\rho^2_{10}$	0.014 ± 0.024	−0.023 ± 0.030	−0.002 ± 0.027	−0.028 ± 0.028	0.009 ± 0.031	−0.007 ± 0.039	0.099 ± 0.056
$\mathrm{Im}\rho^2_{1-1}$	−0.388 ± 0.047	−0.475 ± 0.042	−0.508 ± 0.047	−0.510 ± 0.038	−0.470 ± 0.051	−0.344 ± 0.054	−0.366 ± 0.069
			(f) E_γ =4.7 GeV, Adair system				
ρ^0_{00}	0.005 ± 0.023	−0.014 ± 0.028	0.059 ± 0.032	0.044 ± 0.030	0.079 ± 0.038	0.207 ± 0.041	0.320 ± 0.056
$\mathrm{Re}\rho^0_{10}$	0.056 ± 0.017	0.078 ± 0.019	0.081 ± 0.023	0.074 ± 0.018	0.135 ± 0.023	0.170 ± 0.021	0.092 ± 0.035
ρ^0_{1-1}	0.005 ± 0.031	−0.054 ± 0.040	0.014 ± 0.034	−0.022 ± 0.033	0.036 ± 0.042	0.021 ± 0.040	0.002 ± 0.056
ρ^1_{00}	−0.086 ± 0.038	0.017 ± 0.038	−0.073 ± 0.045	−0.032 ± 0.050	−0.030 ± 0.047	−0.072 ± 0.077	−0.296 ± 0.078
ρ^1_{11}	0.017 ± 0.039	−0.019 ± 0.041	0.035 ± 0.038	−0.003 ± 0.039	0.059 ± 0.045	−0.061 ± 0.047	0.120 ± 0.052
$\mathrm{Re}\rho^1_{10}$	−0.008 ± 0.028	−0.085 ± 0.028	−0.067 ± 0.036	−0.084 ± 0.027	−0.162 ± 0.028	−0.072 ± 0.040	−0.105 ± 0.048
ρ^1_{1-1}	0.550 ± 0.038	0.405 ± 0.053	0.507 ± 0.037	0.466 ± 0.038	0.519 ± 0.050	0.419 ± 0.050	0.306 ± 0.072
$\mathrm{Im}\rho^2_{10}$	0.049 ± 0.024	0.036 ± 0.030	0.078 ± 0.029	0.070 ± 0.027	0.114 ± 0.031	0.091 ± 0.040	0.225 ± 0.056
$\mathrm{Im}\rho^2_{1-1}$	−0.382 ± 0.047	−0.472 ± 0.042	−0.498 ± 0.046	−0.499 ± 0.040	−0.441 ± 0.050	−0.320 ± 0.052	−0.233 ± 0.072

We have determined the density-matrix elements for the ρ taking the background into account through a maximum-likelihood fit including ρ^0, Δ^{++}, and phase-space contributions. (See Appendix A.) This method was checked by evaluating the ρ^α_{ik} by the method of moments inside and outside of the ρ region and estimating the contribution of the background from the values outside the ρ^0 region. Within errors, the same results were obtained.[42] Even if all events in the mass region $0.60 < M_{\pi\pi} < 0.85$ GeV are used without background subtraction the values of the ρ^α_{ik} do not change by more than at most 1 standard deviation [from the fit the combined Δ^{++} and phase-space background in the ρ region was found to be $< 5\%$ ($<2\%$) for $|t| < 0.25$ GeV^2 rising to 21% (7%) in the interval $0.4 \leq |t| \leq 1.0$ GeV^2 at 2.8 GeV (4.7 GeV)]. This indicates that the ρ density-matrix parameters, with the present errors, are insensitive to the assumed form of the background.

Figure 16 and Table X show the density-matrix parameters evaluated in the Gottfried-Jackson,

helicity, and Adair systems as a function of t. Note that the ρ density-matrix elements can be expressed in terms of bilinear combinations of helicity or spin amplitudes and that, for example, ρ^0_{00} and ρ^1_{00} receive contributions only from ρ helicity-flip or spin-flip amplitudes [cf. Eq. (3), Appendix C, and Ref. 35].

We conclude the following from the behavior of the ρ^α_{ik}:

(1) The density-matrix parameters vary rapidly with t in the *Gottfried-Jackson* system. The t-channel helicity-flip amplitudes increase rapidly with increasing $|t|$. This behavior rules out t-channel helicity conservation.[10,11]

(2) The ρ^α_{ik} in the *Adair* system also vary significantly with t. This excludes the hypothesis of spin independence in the total c.m. system for ρ production.[37]

(3) In the *helicity* system the ρ helicity-flip contributions are zero within errors up to $|t| = 0.4$ GeV^2. In other words, the ρ production mechanism is consistent with the conservation of s-channel c.m. helicity for $|t| < 0.4$ GeV^2. More specifically, we have shown that there is no significant helicity flip at the $\gamma\rho$ vertex; in the absence of a measurement of the nucleon polarization we cannot determine whether the nucleon vertex conserves helicity. There are indications that s-channel helicity

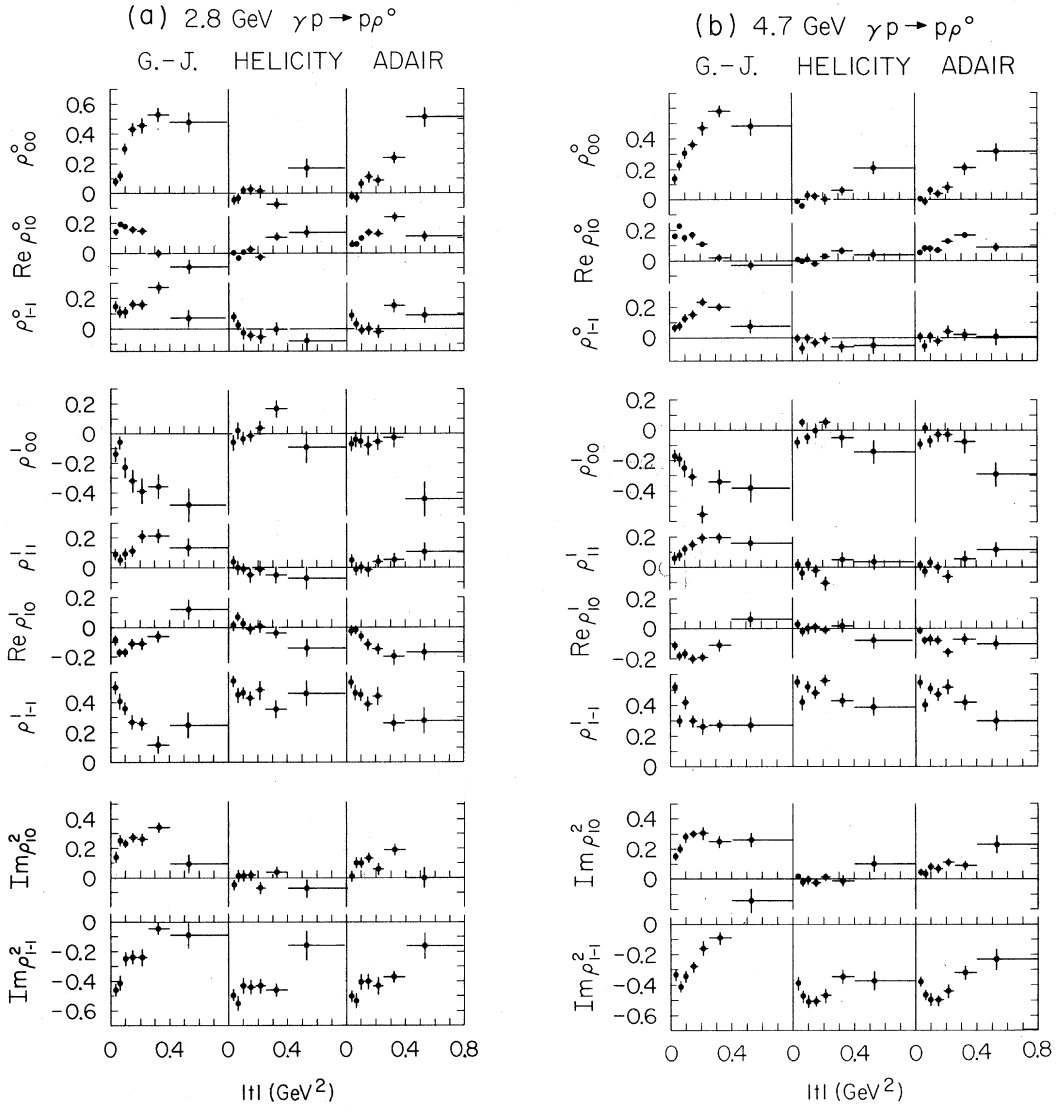

FIG. 16. Reaction $\gamma p \to p\rho^0$. The spin-density-matrix parameters as a function of t in the Gottfried-Jackson, helicity, and Adair systems.

is conserved in πp elastic scattering however[43]; factorization would then suggest that s-channel helicity conservation holds over-all for the reaction $\gamma p \to p\rho^0$. However, we must point out that while our data are consistent with helicity conservation at the $\gamma\rho$ vertex, within errors there is still room for an admixture of ρ^0 helicity-flip amplitudes.[44]

The fact that the helicity-flip contributions are at a minimum in the helicity system is further demonstrated in Fig. 17. A maximum-likelihood fit was made to determine the angle β through which a density matrix, corresponding to no helicity flip, must be rotated to give the best fit to the angular distribution in the helicity frame.[45] Figure 17 shows β, measured about the normal to the production plane, as a function of t together with lines indicating where the data points should fall if the flip terms were minimal in the Gottfried-Jackson (GJ), helicity (H), Adair system (A). For $|t| < 0.4$ GeV^2, the helicity system is clearly preferred; at larger $|t|$ some s-channel helicity-flip amplitudes seem to be present.

In Fig. 18 P_σ and Σ are shown as a function of t. We see that ρ production is completely dominated by natural parity exchange up to $t = 1$ GeV^2. Averaging P_σ over the range $|t| \leq 1$ GeV^2 we find the contribution from unnatural parity exchange to be $(3.1 \pm 3.1)\%$ at 2.8 GeV $[(-1.1 \pm 2.8)\%$ at 4.7 GeV]. Our values of Σ are in agreement with measurements made at DESY and Cornell.[40,41]

In summary, ρ photoproduction via $\gamma p \to p\rho^0$ proceeds almost completely through natural parity exchange and is consistent with helicity conservation in the s-channel c.m. system up to $|t| = 0.4$ GeV^2.

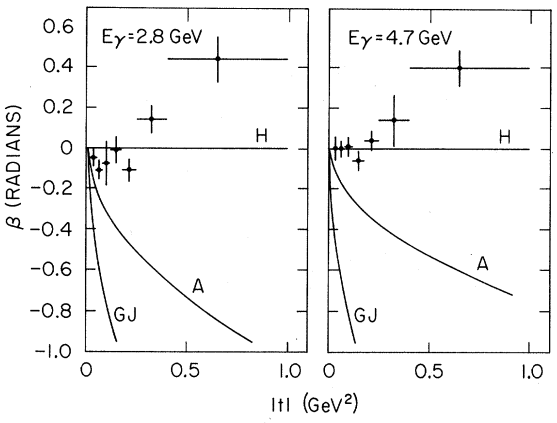

FIG. 17. Reaction $\gamma p \to p\rho^0$. The angle β for rotation about the normal to the production plane of the ρ density matrix from the helicity frame into the "minimum-flip" system as a function of t. The curves marked H, A, GJ show where the data points would lie if the minimum-flip system were the helicity, Adair, and Gottfried-Jackson frame, respectively.

Furthermore, t-channel helicity conservation and "spin independence" in the c.m. system are clearly ruled out.

6. *Cross Section for s-Channel Helicity-Conserving p-Wave Dipion States*

In order to obtain a cross section for p-wave dipion production in the ρ^0 mass region it is necessary either to determine directly the amount of p wave present from an analysis of the $\pi\pi$ angular distribution or, from a knowledge of the ρ^0 mass shape, to deduce which part of the $\pi\pi$ mass spectrum is ρ^0. The latter procedure requires the use of a model to describe the ρ^0 mass shape in photoproduction and is discussed in Sec. IV C. Here, we determine a *model-independent cross section* for p-wave $\pi\pi$ pairs. We make use of the result of Sec. IV B 5 that the production mechanism for p-wave $\pi\pi$ pairs conserves s-channel helicity at the $\gamma\pi\pi$ vertex for $|t| < 0.4$ GeV^2 and so yields pion pairs in a well-defined spin state. This implies (see Sec. IV B 3) that the decay angular distribution for p-wave pion pairs is given in the helicity system by

$$W(\theta,\Psi) = \frac{3}{8\pi}\left(\sin^2\theta + P_\gamma \sin^2\theta \cos 2\Psi\right),$$

which may be expressed in terms of spherical harmonics as

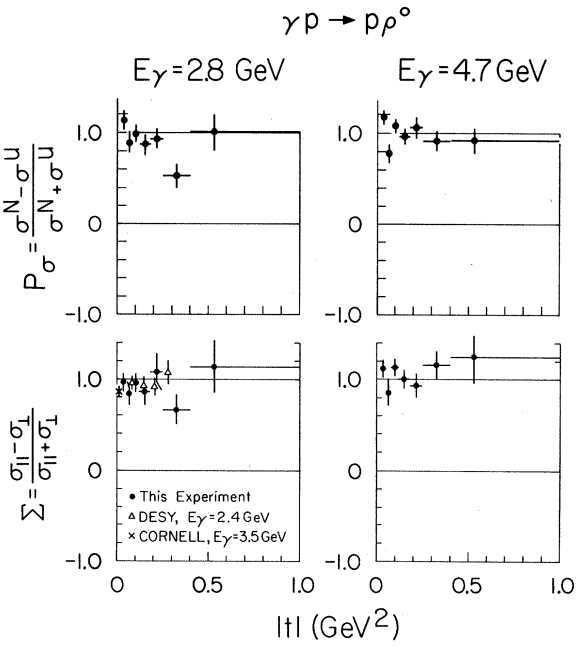

FIG. 18. Reaction $\gamma p \to p\rho^0$. The parity asymmetry, P_σ, and the asymmetry, Σ, as a function of t. The points labeled DESY and Cornell are from Refs. 40 and 41, respectively.

TABLE XI. Reaction $\gamma p \to p\pi^+\pi^-$. Dipion total cross sections, differential cross sections at $t=0$, and slope of differential cross sections (assuming the forms $d\sigma/dt|_{t=0}e^{At}$ and $d\sigma/dt|_{t=0}e^{At+Bt^2}$) from the intensity of the c.m. s-channel helicity-conserving p-wave state, II, from the parametrization technique, and from the Söding model. The values of $d\sigma/dt|_{t=0}$, A, and B were determined from fits to the differential cross section (see Table XII) for $|t|<0.4$ GeV^2. The errors for the Söding model do not include the systematic uncertainties in the model assumptions used.

	$E_\gamma = 2.8$ GeV			$E_\gamma = 4.7$ GeV		
	From II	From parametrization	From Söding model	From II	From parametrization	From Söding model
σ (μb)	18.6± 1.1	21.0± 1.0	18.6± 1.0	14.5± 1.0	16.2± 0.7	15.9± 0.7
			Using $\frac{d\sigma}{dt}=\frac{d\sigma}{dt}\Big\|_{t=0}e^{At}$			
$\frac{d\sigma}{dt}\Big\|_{t=0}$ (μb/GeV^2)	144 ±12	138 ± 8	104 ± 6	109 ± 8	114 ± 6	94 ± 6
A (GeV^{-2})	7.5± 0.6	6.6± 0.3	5.4± 0.3	7.6± 0.5	7.2± 0.3	5.9± 0.3
			Using $\frac{d\sigma}{dt}=\frac{d\sigma}{dt}\Big\|_{t=0}e^{At+Bt^2}$			
$\frac{d\sigma}{dt}\Big\|_{t=0}$ (μb/GeV^2)	154 ±20	153 ±15	98 ±10	104 ±14	128 ±12	91 ±10
A (GeV^{-2})	8.5± 1.9	8.2± 1.3	4.4± 1.3	6.8± 2.0	8.9± 1.2	5.5± 1.3
B (GeV^{-4})	3.1± 5.3	4.3± 3.4	−2.5± 3.4	−2.2± 5.5	4.4± 2.9	−1.2± 3.3

$$W(\theta,\Psi)=\frac{1}{(4\pi)^{1/2}}Y_0^0(\theta)-\frac{1}{(20\pi)^{1/2}}Y_2^0(\theta)$$
$$+2P_\gamma\left(\frac{3}{40\pi}\right)^{1/2}\mathrm{Re}Y_2^2(\theta,\Psi).$$

Y_2^2 is least affected by background due to its Ψ dependence. Consequently, we have determined II, the s-channel helicity-conserving p-wave cross section from

$$\mathrm{II}=\frac{1}{P_\gamma}\left(\frac{40\pi}{3}\right)^{1/2}\sum \mathrm{Re}Y_2^2=\frac{2.5}{P_\gamma}\sum \sin^2\theta\cos 2\Psi, \quad (7)$$

where the summation is over all events.

The dots marked on the histograms of Fig. 10(a) show II as a function of $M_{\pi\pi}$ for different t intervals. We notice that in the ρ^0 region II accounts for nearly all events and is zero within errors above $M_{\pi\pi}=1$ GeV. This shows that the background does not contribute to Y_2^2 and indicates the absence of high-mass helicity-conserving p-wave states. The total helicity-conserving p-wave cross section (corrected for the interval $|t|<0.02$ GeV^2) (Ref. 46) is given in Table XI; the differential II cross section is given in Table XII and Fig. 19.

TABLE XII. Reaction $\gamma p \to p\pi^+\pi^-$. Dipion differential cross sections, $d\sigma/dt$ (μb/GeV^2), determined from the intensity of the c.m. s-channel helicity-conserving p-wave state, II, the parametrization technique, and the Söding model.

	$E_\gamma = 2.8$ GeV			$E_\gamma = 4.7$ GeV		
$\|t\|$ (GeV^2)	From II	From parametrization	From Söding model	From II	From parametrization	From Söding model
0.02 −0.05	120 ±11	121 ±9	86 ±7	84 ±9	98 ±9	79 ±8
0.05 −0.075	88 ±10	92 ±8	73 ±7	66 ±7	75 ±5	63 ±5
0.075−0.10	67 ±10	74 ±7	64 ±7	53 ±6	56 ±5	54 ±5
0.10 −0.15	56 ± 6	55 ±4	51 ±4	44 ±4	45 ±3	45 ±3
0.15 −0.20	36 ± 5	43 ±4	47 ±4	36 ±4	35 ±3	36 ±3
0.20 −0.25	29 ± 4	33 ±3	29 ±4	16 ±3	19 ±2	22 ±2
0.25 −0.30	19 ± 4	21 ±3	24 ±3	13 ±3	18 ±2	21 ±2
0.30 −0.35	15 ± 4	17 ±2	19 ±3	9.0 ±2.2	11 ±1	14 ±2
0.35 −0.40	7.7± 3.0	12 ±2	13 ±2	6.7 ±1.8	8.4±1.0	9.4±1.5
0.40 −0.50	4.3± 1.5	5.6±1.1	6.7±1.4	5.5 ±1.1	5.7±0.6	6.4±0.9
0.50 −0.70	3.2± 0.8	2.6±0.6	2.8±0.8	0.6 ±0.5	2.2±0.3	2.6±0.5
0.70 −1.0	1.0± 0.6	2.2 ±0.4		0.9 ±0.3	0.77 ±0.16	
1.0 −1.5	0.7± 0.4	0.74±0.2		0.15 ±0.2	0.33 ±0.08	
1.5 −2.5	0.0± 0.17	0.0 ±0.09		0.20 ±0.09	0.07 ±0.03	
2.5 $-\|t\|_{max}$	0.0± 0.11	0.23±0.08		0.015±0.013	0.016±0.008	

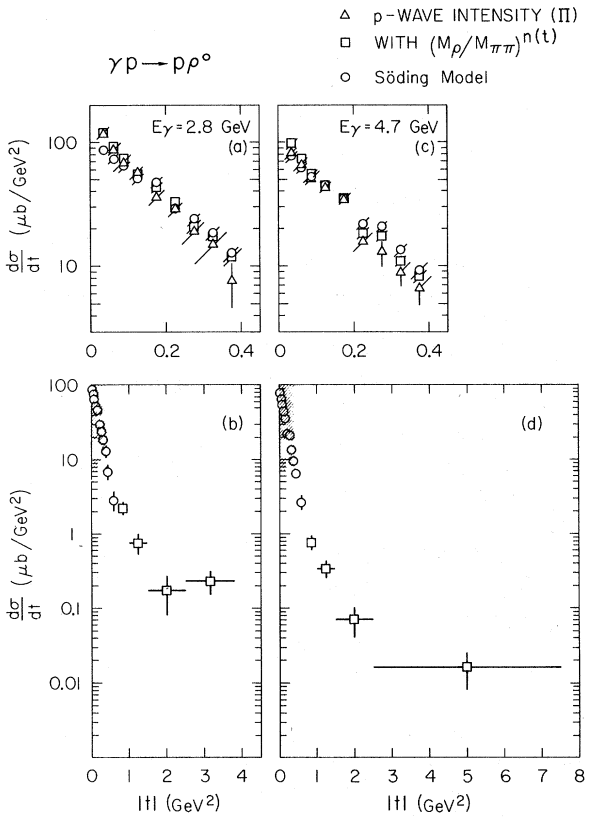

FIG. 19. Reaction $\gamma p \to p\rho^0$. Differential cross sections as a function of t for the helicity-conserving p-wave contribution $\Pi(\Delta)$, for ρ^0 production as obtained from fits with the Söding model (○) and from the parametrization $(M_\rho/M_{\pi\pi})^{n(t)}$ (□). The shaded regions are shown above on an expanded expanded scale.

We emphasize that Π is not necessarily a ρ^0 *cross section* since nonresonant, helicity conserving, p-wave $\pi\pi$ pairs may be present as a coherent background.

C. Determination of the ρ^0 Production Cross Section by the Use of Models

1. *The Ross-Stodolsky Model*

The Ross-Stodolsky model[47] suggests that the ρ^0 Breit-Wigner form should be multiplied by the factor $(M_\rho/M_{\pi\pi})^4$ to explain the mass shift for small $|t|$ (Sec. IV B 1). In order to test this we have made a maximum-likelihood fit (described in Appendix A) in which the ρ^0 Breit-Wigner form [Eq. (A2) of Appendix A] is multiplied by $(M_\rho/M_{\pi\pi})^n$. We have determined n for different t intervals using fitted values $M_\rho = 764$ MeV and $\Gamma_\rho = 143$ MeV.[17] These values for the ρ^0 mass and width were obtained by a fit to all events with $0.02 < |t| < 0.4$ GeV^2 allowing for a linear variation of n with t. Figure 20 shows n as a function of t. We find that $n \gtrsim 5$ for $t \simeq 0$ and reduces to zero for $|t| > 0.5$ GeV^2. From this we conclude that a t-independent Ross-Stodolsky factor multiplied into a p-wave Breit-Wigner form does not describe the data. However, as seen from Fig. 10, our parametrization with a t-dependent exponent does provide a good description of the mass spectrum. Consequently, we may use this parametrization to fit the $\gamma p \to p\pi^+\pi^-$ Dalitz plot and determine the amount of phase-space-like background and Δ production. We found the Δ cross sections listed in Table XIII and 5.7 ± 0.7 μb at 2.8 GeV (3.1 ± 0.3 μb at 4.7 GeV) for the phase-space-like background. By *assuming that the remaining part of the channel is* ρ^0 we can deduce a ρ^0 cross section which we refer to as the *parametrization cross section*. We have checked that the parametrization cross section is insensitive to the Breit-Wigner form used and to variations of n by ±1; in fact, a constant $n = 4$ gives essentially the same ρ^0 cross section. Consequently, the parametrization cross sections may be directly compared with previous track-chamber results.

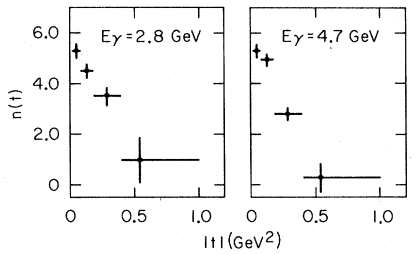

FIG. 20. Fitted values for $n(t)$ using the parametrization $(M_\rho/M_{\pi\pi})^{n(t)}$. (For details see Appendix A.)

The total[46] and differential parametrization cross sections are given in Tables XI and XII, respectively, and the differential cross section is plotted in Fig. 19.

2. *The Söding Model*

The Söding model explains the ρ^0 mass shift in terms of an interference between a diffractively produced ρ^0 and a Drell-type background.[48,49] The details of the model are given in Appendix B. In applying the model to our data we have made the following modifications to the original version of the model[49]:

(1) The direct ρ^0 production was made s-channel helicity-conserving in order to agree with our ex-

TABLE XIII. Cross sections for $\gamma p \to \Delta\pi$ and parity asymmetry, P_σ, for $\gamma p \to \Delta^{++}\pi^-$.

E_γ (GeV)	$\sigma_{\Delta^{++}\pi^-}$ (μb)	$\sigma_{\Delta^0\pi^+(\Delta^0\to p\pi^-)}$ (μb)	P_σ $\lvert t_\Delta\rvert < 0.5$ GeV^2
2.8	3.6 ± 0.4	0.5 ± 0.2	-0.27 ± 0.12
4.7	1.0 ± 0.1	0.16 ± 0.09	-0.53 ± 0.15

perimental observations.

(2) We added incoherently into the Drell term those πp scattering amplitudes that result in a spin flip of the proton.

(3) It has recently been pointed out that in adding the p-wave part of the Drell term to the ρ^0 "doubling counting" may occur. This can be avoided by adding a rescattering term to the Drell background which is equivalent to multiplying the Drell amplitude by $e^{i\delta}\cos\delta$, where δ is the phase shift for $I=1$, $l=1$ $\pi\pi$ scattering.[50,51] All Söding-model calculations in this paper use this correction. The addition of the rescattering term introduces an ambiguity into the definition of the ρ^0 cross section. The ρ^0 amplitude may be defined either as that resulting from the direct diffractive process [diagram (a) of Fig. 29], or, as the sum of this amplitude and the rescattering term [diagram (c) of Fig. 29]; this point is discussed in more detail in Appendix B. The cross sections given in the text originate from the first definition of the ρ^0 amplitude. For cross sections using the second definition see Appendix B.

(4) As will be discussed below, Δ^{++} production cannot be entirely accounted for by a simple one-pion-exchange (OPE) diagram like the Drell term; consequently, the Δ^{++} was taken out of the Drell term and was fitted incoherently.

(5) In calculating the Drell term, we tried different form factors for the π-p vertex, namely, the Ferrari-Selleri form factor,[52] the Benecke-Dürr form factor,[53] and no form factor. The ρ^0 masses, widths, and cross sections given in this section are from fits with the Ferrari-Selleri form factor. Results from the other fits are given in Appendix B.

In applying the model to the data we first determined the ρ^0 mass, M_ρ, its width, Γ_ρ, and the slope, A, of the momentum-transfer distribution in the interval $0.02 < |t| < 0.4$ GeV^2. In this fit we varied the amount of Söding amplitude, a_S [see Eq. (B1) of Appendix B], the ratio of the ρ^0 to Drell amplitudes, Y, and the amount of Δ^{++}. We found $M_\rho = 767 \pm 4$ MeV (770 ± 4 MeV), $\Gamma_\rho = 145 \pm 10$ MeV (155 ± 10 MeV), and $A_\rho = 6.0 \pm 0.3$ GeV^{-2}(6.3 ± 0.3 GeV^{-2}) at 2.8 GeV (4.7 GeV). In subsequent calculations in smaller momentum-transfer intervals, M_ρ, Γ_ρ, and A_ρ were held constant at the values given above and a_S, Y, and the amount of Δ^{++} were fitted. The fitted values of the ratio of ρ-to-Drell cross sections, σ_ρ/σ_D, derived from Y, are shown in Fig. 21 as a function of t. The curves give the t dependence of σ_ρ/σ_D calculated using the absolute prediction of the Drell intensity and the fitted total ρ^0 cross section, σ_ρ. The ratio σ_ρ/σ_D as given by the model is too small by a factor of 2 for the Ferrari-Selleri form factor used here, while it is approximately correct for the Benecke-Dürr form factor.

The Söding model describes well the $\pi^+\pi^-$ mass shapes and their variation with t [solid lines of Fig. 10(a)] and consequently the related dependence of the exponential slope of the t distribution on the $\pi^+\pi^-$ mass [solid lines of Figs. 11(c) and 11(d)]. The solid lines in Figs. 14 and 15 show the moments, and ρ_{ik} predicted by the model. The predicted moments agree well with the data. We note that the shape of the Y_4^0 moment is reproduced by the model indicating that the Drell term describes well both the 1^- and 3^- backgrounds in the ρ^0 region. Figure 15 shows that the model accounts for the variation of ρ_{ik} as a function of $\pi\pi$ mass; the behavior of the ρ_{ik} below (above) the ρ^0 peak is mainly determined by the Drell term (Δ^{++} reflection).

We have calculated the dipion density matrices for the Söding model in the region $|t| > 0.4$ GeV^2 and have found that the model does not account for the lack of helicity conservation in this region. In the framework of the model, therefore, we attribute the lack of helicity conservation of the dipion system at large $|t|$ to the ρ^0 production mechanism rather than to the influence of the Drell, Δ^{++}, and phase-space background terms.

The total[46] and differential ρ^0 cross sections obtained by fitting the Söding model to our data are given in Tables XI and XII, and in Fig. 19. The errors shown are statistical and do not reflect the uncertainties inherent in the model. These uncertainties are discussed in Sec. IV C 3. Two features should be noted, namely, that the differential cross section for ρ^0 production at $t=0$, and the slope of the momentum-transfer distribution, are both lower than those obtained from II or the parametrization method.

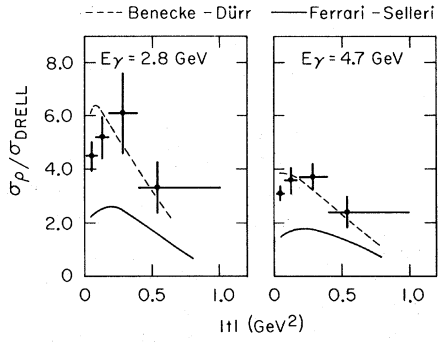

FIG. 21. The fitted ratio of the ρ^0 to Drell cross sections, $\sigma_\rho(t)/\sigma_{\text{Drell}}(t)$. The solid (dashed) curves show the predictions of the Söding model with the Ferrari-Selleri (Benecke-Dürr) form factor. Note that the Drell amplitude does not include Δ^{++} production.

3. *A Phenomenological Check of the Söding-Model Cross Sections*

The question now arises as to how much the Söding-model cross sections and slopes may be in error due to uncertainties in the Söding model. Some of these uncertainties are as follows: (a) lack of knowledge of the ρ^0 shape; (b) lack of knowledge of the πp form factor; (c) possible corrections to make the model gauge-invariant; (d) the possibility of exchanges other than one-pion exchange (as will be shown in Sec. IV E exchanges other than OPE are needed to explain Δ^{++} production). Point (b) was checked by repeating the fits with the Benecke-Dürr form factor[53] and with no form factor. Although this resulted in changes in the fitted ρ^0 width, the forward ρ^0 cross section and the ρ^0 mass remained the same within 1 standard deviation (see Appendix B). Uncertainties (c) and (d) imply that the Drell background may be unknown to a greater extent than allowed for by form-factor variation.

Uncertainties (a)–(d) lead us to an alternative, more phenomenological approach.[54] If the ρ^0 mass, M_ρ, and width, Γ_ρ, are taken from other experiments, the ρ^0 cross section may be deduced from the value of the double-differential cross section for dipion production at $M=M_\rho$, since the *rescattering correction [Fig. 29(c)] implies that the p-wave part of the Drell background should vanish at the* ρ *mass.*[50,51]

To determine the ρ^0 cross section at $t=0$ using this method: (a) We have fitted a smooth interpolation curve of the form Breit-Wigner $\times(M_\rho/M_{\pi\pi})^n$ to the dipion cross section $d^2\sigma/dtdM|_{t=0}$ of Table IX for dipion pairs in the region $0.6 < M_{\pi\pi} < 0.9$ GeV. In the fit we varied n and the mass and width of the ρ^0; as seen from Figs. 11(a) and 11(b), this gives a good fit to the data at both energies. (b) We have selected a mass and width for the ρ^0 and calculated[55] the ρ^0 forward differential cross section from

$$\frac{d\sigma}{dt}=\left(\frac{d^2\sigma}{dtdM}\right)^{M=M_\rho}\tfrac{1}{2}\pi\Gamma_\rho\,, \tag{8}$$

where we take $d^2\sigma/dtdM$ from the fitted curve obtained in step (a).

Figure 22 shows the ρ^0 forward cross section obtained by this method plotted as a function of the mass and width of the ρ.[56] These curves show that the ρ forward differential cross section can vary from 106 μb/GeV^2 to 155 μb/GeV^2 at 2.8 GeV (74 μb/GeV^2 to 118 μb/GeV^2 at 4.7 GeV) using the range of ρ^0 masses (775–755 MeV) and widths (110–147 MeV) found in the Review of Particle Properties.[57] With the values of M_ρ, Γ_ρ obtained in Sec. IV C 2, we find 148 ± 12 μb/GeV^2 at 2.8 GeV (109 ± 8 μb/GeV^2 at 4.7 GeV). These values are significantly larger than those resulting from our Söding-model fits (Table XI). Two effects are responsible for this. First, we have *not subtracted the background.* From the extrapolated cross section outside the ρ^0 region we estimate the background to be ~8% at 2.8 GeV (~2% at 4.7 GeV). Second, in the Söding-model fits the ρ cross section is obtained by integrating the ρ Breit-Wigner form over the available phase space; at low $|t|$ the area of the Breit-Wigner form is reduced relative to

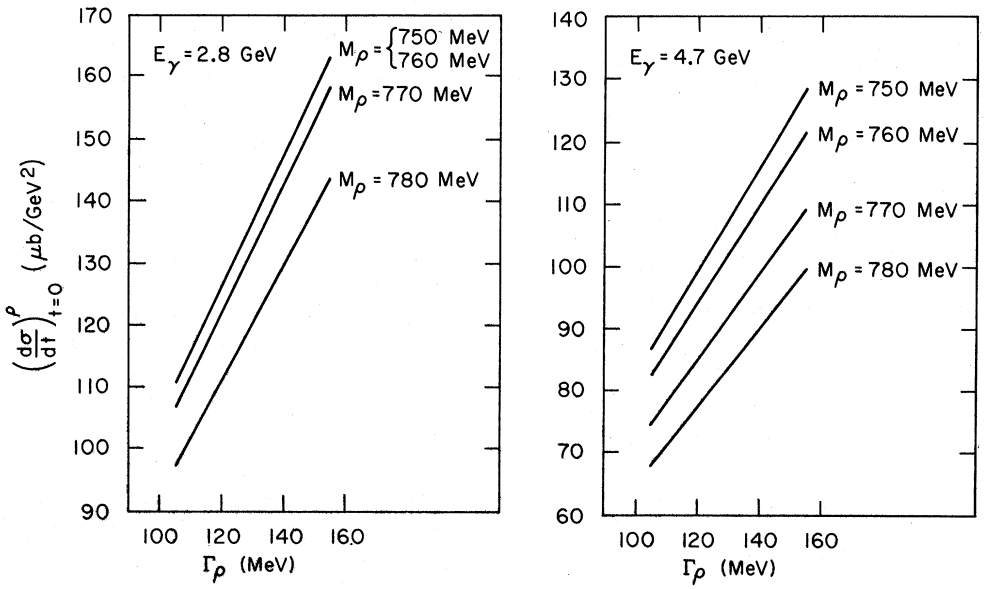

FIG. 22. The experimental forward differential ρ^0 cross section, $(d\sigma/dt)_{t=0}$, determined using a phenomenological Söding model (Sec. IV C 3), as a function of ρ^0 mass and width. Errors in $(d\sigma/dt)_{t=0}$ are discussed in Ref. 56.

that at large $|t|$, in contrast to the constant area implicit in Eq. (8). Consequently, Eq. (8) gives larger cross sections at low $|t|$ than do the Söding-model fits.

We have applied Eq. (8) to a series of t bins in the $0.02 < |t| < 0.5$ GeV^2 region (using, of course, t-independent M_ρ, Γ_ρ). The differential cross sections obtained with Γ_ρ set equal to the values found in the Söding-model fits, *viz.*, 145 MeV at 2.8 GeV (155 MeV at 4.7 GeV), and $M_\rho = 770$ MeV, are given in Table XIV. With the exception of the $|t|$ interval 0.02–0.075 GeV^2, where phase-space effects are important, the values of Table XIV agree well with those of Table XII. The cross sections of Table XIV are proportional to the assumed ρ width and show approximately the same dependence on the ρ^0 mass as is illustrated in Fig. 22. Figure 11 shows that the slope of the ρ^0 differential cross section obtained using Eq. (8) is independent of ρ^0 masses lying within the currently accepted range.[57]

We conclude that:

(1) The size of the Söding-model forward differential cross section as determined in this section depends on the mass and width of the ρ^0, being lowest for a high mass and a small width of the ρ^0.

(2) The lack of knowledge of the ρ mass and width, and of the form of the Drell background, implies that Söding-model cross sections as given in this and Sec. IV C 2 are uncertain to about ±20%.

We emphasize that the prodedure, outlined above, for checking the Söding model has determined ρ^0 cross sections from the ρ amplitude at $M = M_\rho$; these ρ^0 cross sections depend neither on the details of the ρ shape nor on the available phase space.

TABLE XIV. Reaction $\gamma p \to p\pi^+\pi^-$. Dipion differential cross sections, $d\sigma/dt$, differential cross sections at $t = 0$, $d\sigma/dt|_{t=0}$, and the slope of the differential cross section, A, from a fit of the form Be^{At}, for M_ρ, Γ_ρ equal to 770 MeV, 145 MeV at 2.8 GeV (770 MeV, 155 MeV at 4.7 GeV) determined using the technique described in Sec. IV C 3.

	$d\sigma/dt$ (μb/GeV^2)	
$\lvert t\rvert$ (GeV^2)	$E_\gamma = 2.8$ GeV	$E_\gamma = 4.7$ GeV
0.02 –0.05	130 ±14	94 ±9
0.05 –0.075	85 ±12	68 ±8
0.075–0.1	65 ± 9	59 ±7
0.1 –0.15	66 ± 8	53 ±6
0.15 –0.2	48 ± 6	37 ±4
0.2 –0.3	29 ± 3	22 ±3
0.3 –0.5	11 ± 1	10 ±1
$\left.\frac{d\sigma}{dt}\right\|_{t=0}$ (μb/GeV^2)	148 ±12	109 ±8
A (GeV^{-2})	6.3± 0.4	6.0±0.3

4. *Other Models*

Several models have been put forward recently to describe ρ^0 photoproduction; none, however, describes quantitatively all aspects of the data.

The dual-resonant model of Satz and Schilling[58] describes correctly the ρ^0 mass shape and its variation with momentum transfer, but predicts that the ρ^0 conserves t-channel helicity in contrast to the experimentally observed s-channel helicity conservation; also the Y_4^0 interference term predicted by the model has the wrong sign.

The model of Kramer and Quinn[59] calculates ρ^0 photoproduction using diagram (c) of Fig. 29. We have not made a detailed comparison with this model but we have compared our data in the $|t|$ interval 0.02–0.4 GeV^2 to an approximate form given by Kramer.[60] We find that in order to fit the mass spectrum we require a large width for the ρ^0 (170–180 MeV) and that the fit is poor (χ^2 of 145 for 48 degrees of freedom compared with a χ^2 of 65 for 48 degrees of freedom for the Söding model at 4.7 GeV). The model predicts that the ρ^0 conserves s-channel helicity and describes well the variation of the dipion density-matrix elements, ρ^0_{ik}, with mass.

ρ photoproduction has also been discussed using a Regge-pole model by Mannheim and Maor.[61] They suggest that the ρ^0 Breit-Wigner form should be multiplied by $(M_\rho/M_{\pi\pi})^4$ at $t = 0$ but do not predict a specific form for the variation of ρ^0 shape with momentum transfer.

Greenhut[62] has suggested that the ρ^0 mass skewing is due to an isoscalar s-wave dipion background; this is incompatible with the moments shown in Fig. 14.

In conclusion, the Söding model gives a good *quantitative* description for $|t| < 0.4$ GeV^2 of the ρ^0 mass shape and its variation with momentum transfer, the variation of the dipion density-matrix elements with dipion mass, and the moments of the dipion system. This model implies that not all p-wave dipion pairs are resonant since dipion pairs originate in part from the Drell term. The Kramer-Quinn model describes the features of ρ^0 photoproduction *qualitatively*. This model suggests that all p-wave dipion pairs should be interpreted as ρ^0; hence the ρ^0 cross sections would be given by II or by the parametrization cross section.

5. *Comparison with Other Experiments*

Previously published cross sections for ρ^0 photoproduction on hydrogen have been obtained using three different techniques:

(1) detection of symmetric $\pi^+\pi^-$ pairs with total energy near the maximum energy of a bremsstrahlung spectrum[63–65];

(2) detection of $p\pi^+\pi^-$ for $|t| > \sim 0.02$ GeV^2 using bubble[2,10,11,28] or streamer chambers[66];

(3) detection of the recoiling proton in a missing-mass spectrometer.[67]

We first compare our data to the double-differential cross section, $d^2\sigma/d\Omega dM$, for dipion production in the forward direction obtained by the DESY-MIT[65] group using the first technique.

In order to derive $d^2\sigma/d\Omega dM$ in the forward direction we have fitted our data to the form $B\exp(At)$ in the $|t|$ interval 0.02 to 0.4 GeV^2 in 40-MeV intervals of $\pi\pi$ mass. The quantity $B\exp(At_{\min})$ expressed in μb/sr MeV is plotted in Figs. 23(a) (2.8 GeV) and 23(b) (4.7 GeV) together with the data of the DESY-MIT group[65] at 2.9 GeV and 4.7 GeV. From the figure it may be seen that the DESY-MIT data yield a cross section which is higher, by about a factor 1.4, than the data of this experiment at the peak of the ρ^0. It is noteworthy that the shape of the data from the two experiments is similar in the ρ^0 region.

Apart from uncertainties in the normalization of the DESY-MIT experiment, which are ~10%, two effects could be responsible for the discrepancy:

(a) The data of the DESY-MIT group may contain a contribution from dipion pairs produced inelastically.

(b) The exponential extrapolation of our data to the forward direction may yield an incorrect estimate of the forward cross section if the slope changes at small $|t|$.

In order to illustrate the form of contamination that may occur in a counter experiment of the DESY-MIT type, we have selected $\pi^+\pi^-$ pairs from events other than $\gamma p \to p\pi^+\pi^-$ with the laboratory momentum Q of a $\pi^+\pi^-$ pair satisfying $|\overline{Q}-Q|/\overline{Q} < 0.18$, where $\overline{Q} = E_\gamma^{\max}/1.15$. We have chosen these limits to approximate the acceptance of the DESY-MIT experiment.[68] The mass spectra of pion pairs satisfying the criterion are shown in Figs. 24(a) and 24(b) for dipion transverse momentum squared $Q_T^2 < 0.05$ GeV^2. Inelastically produced ρ^0's occur at small Q_T^2 at 4.7 GeV; they persist to some extent at higher Q_T^2. At 2.8 GeV there is no strong evidence for inelastic ρ^0 production at small Q_T^2. A nonresonant background is present at both energies. The distribution of Q for elastic (i.e., from $\gamma p \to p\pi^+\pi^-$) and inelastic $\pi^+\pi^-$ pairs with $0.6 < M_{\pi\pi} < 0.9$ GeV is shown in Figs. 24(c) and 24(d). If we take our E_γ spectrum to be a line spectrum with energy $E_\gamma^{\max}$, we can estimate the background in the DESY-MIT experiment by assuming that the form of the $Q_{\text{inelastic}}$ distribution expressed as a function of $E_\gamma^{\max} - Q$ is independent of E_γ within the range of the DESY-MIT acceptance. We then weight the inelastic contributions with $1/E_\gamma$ (to approximate the bremsstrahlung spectrum of Ref. 65) and integrate over the acceptance region. The resulting background estimates are shown in Figs. 24(e) and 24(f); we see that the background is ~12% and is roughly independent of Q_T^2. This estimate will decrease slightly if differences in the decay angular distribution of elastic and inelastic dipion pairs are taken into account. We emphasize that the background estimate of Figs. 24(e) and 24(f) includes all inelastic dipion pairs within the interval $0.6 < M_{\pi\pi} < 0.9$ GeV. Appropriate fits to the counter data may subtract out the inelastic nonresonant but not the inelastic ρ^0 contribution to the background.

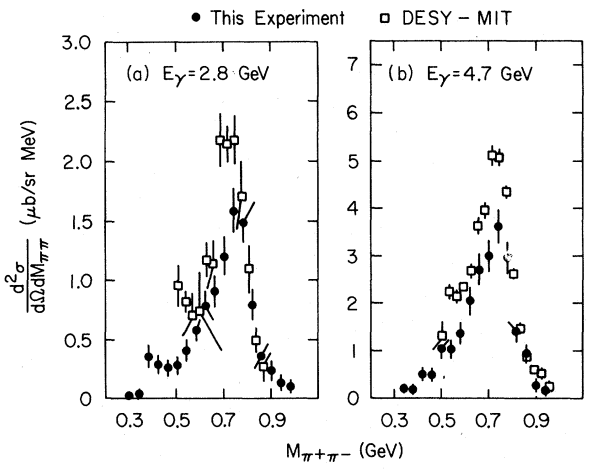

FIG. 23. Reaction $\gamma p \to p\pi^+\pi^-$. $d^2\sigma/d\Omega dM$ in the forward direction from this experiment compared with that from the DESY-MIT experiment (Ref. 65).

From this we conclude that the *forward ρ^0 cross section at 4.7 GeV* measured by the DESY-MIT group[65] could be overestimated by ~5% due to a background of inelastic ρ^0 production. A recent measurement by Berger *et al*[69] at Cornell indicates that the inelastic contamination in their experiment,[64] which has a similar acceptance to the DESY-MIT experiment, is ~(2 ± 5)% at 0° and for $E_\gamma \approx 8.5$ GeV. The contamination rises to 20–30% at $|t| = 0.4$ GeV^2.

A quadratic extrapolation to the forward direction (i.e., using the form e^{At+Bt^2}) increases our values of $d^2\sigma/d\Omega dM$ by about 12% (cf. Table XI); this together with an ~10% inelastic background (of which half is inelastic ρ^0) in the DESY-MIT data would reduce the discrepancy in $d^2\sigma/d\Omega dM$ between this and the DESY-MIT experiment to about 15%, a value which is close to the uncertainty of normalization of the DESY-MIT experiment.

We next compare $d\sigma/dt$ for $0.05 < |t| < 1$ GeV^2 with other experiments. In Fig. 25 we show our 4.7-GeV differential ρ^0 cross sections, determined by the parametrization method, together with similar-

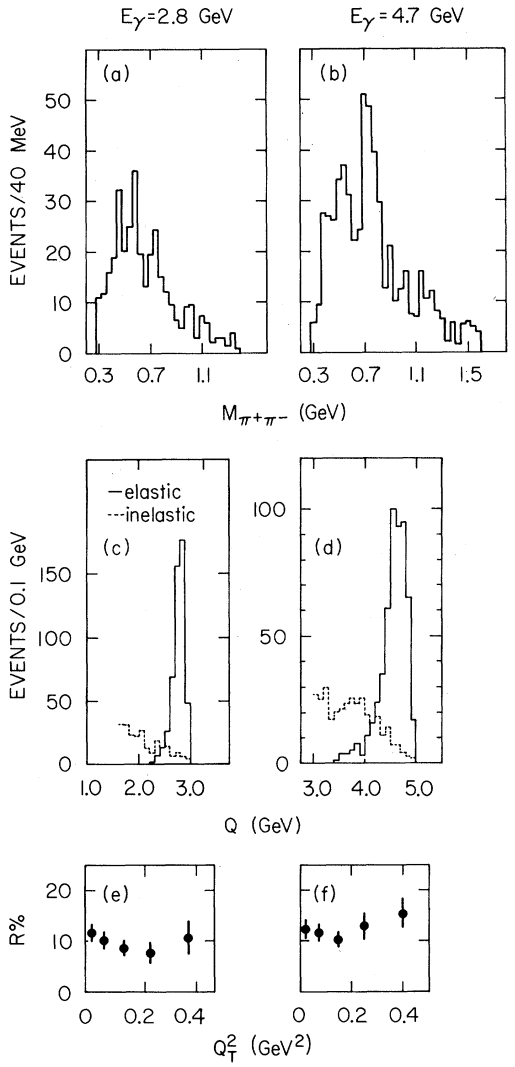

FIG. 24. (a) and (b) The mass distribution of inelastic $\pi^+\pi^-$ pairs for $Q_T^2<0.05$ GeV^2 (see text for the restrictions applied). (c) and (d) The distribution of the momentum, Q, of elastic (solid line) and inelastic (dashed line) $\pi^+\pi^-$ pairs for $0.6 < M_{\pi\pi} < 0.9$ GeV^2. (e) and (f) Contamination of $\pi^+\pi^-$ pairs from the reaction $\gamma p \to p\pi^+\pi^-$, $\pi\pi_{\text{elastic}}$, by inelastic $\pi^+\pi^-$ production, $\pi\pi_{\text{inelastic}}$, (i.e., from reactions other than $\gamma p \to p\pi^+\pi^-$). The $\pi\pi$ pairs are in the interval $0.6 < M_{\pi\pi} < 0.9$ GeV (for other restrictions see text) and the ratio $R = \pi\pi_{\text{elastic}}/(\pi\pi_{\text{elastic}} + \pi\pi_{\text{inelastic}})$ is plotted versus the square of the transverse momentum, Q_T^2.

ly determined cross sections from the DESY bubble chamber[11] ($4.5 < E_\gamma < 5.8$ GeV) and a SLAC counter experiment[67] ($E_\gamma \sim 6$ GeV). Within statistics the agreement between the three experiments is excellent. We remark that since the SLAC counter experiment detects the recoil proton in ρ^0 production there is no problem with contamination due to inelastic ρ^0 production. Our differential cross sections are also in agreement with those obtained

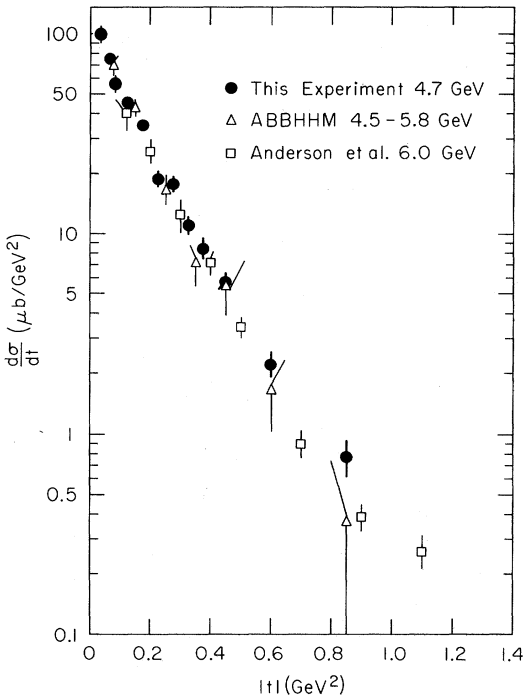

FIG. 25. The differential cross section for ρ^0 production: from this experiment (●) at 4.7 GeV using the parametrization technique; from the ABBHHM collaboration at 4.5–5.8 GeV (△) (Ref. 11); from Anderson *et al.*, (□) at 6 GeV (Ref. 67).

using a positron annihilation beam.[28]

The values obtained for the forward ρ^0 cross section in the SLAC counter experiment and ours differ due to the t range fitted and the form of curve used to extrapolate to $t=0$. Anderson *et al.*[67] used the shape of the experimental elastic πp scattering differential cross section, and from a fit in the $|t|$ interval 0.1 to 1.2 GeV^2 found $d\sigma/dt|_{t=0} = 152 \pm 15$ μb/GeV^2. A straight-line extrapolation of their data for $|t| < 0.7$ GeV^2 would actually fall below our value of 114 ± 6 μb/GeV^2; quadratic extrapolations give results in agreement with ours when fits are made in the $|t|$ range 0.02–1.0 GeV^2.

In conclusion, the results of this experiment agree well with other experiments in the t interval $0.05 < |t| < 1$ GeV^2. Our forward differential cross sections, $d\sigma/dt|_{t=0}$, are lower than those of Anderson *et al.*[67] due only to the form of extrapolation used. The dipion forward cross section $d^2\sigma/d\Omega dM$ at 4.7 GeV of the DESY-MIT group[65] is higher than that obtained in this experiment and we have demonstrated that this is partly due to an ~10% inelastic background. The remaining discrepancy, if not due to normalization problems in the counter experiment, may result from our procedure for extrapolating to $t=0$.

It must be emphasized that these conclusions

are based upon comparing our *parametrization cross section* and an extrapolation of our raw data with other experiments. Due to differences in the methods of analysis[70] we have not compared our Söding-model cross sections with those from other experiments.[11,64,65]

6. *Discussion of Cross Sections for ρ^0 Production*

In Table XI we have given six dipion forward cross sections for each energy using three techniques and two forms of extrapolation. Total cross sections are also given for each technique; they are insensitive to the form of extrapolation used. We here consider the problem of which dipion cross section gives the best measure of the ρ^0 cross section.

First, we consider the three techniques used to determine a dipion cross section. A problem arises because both the Kramer-Quinn model and the Söding model are compatible with our data. These two models lead to different definitions of ρ^0: The Kramer-Quinn model suggests that all p-wave dipion pairs should be considered as ρ^0 so that Π gives the cross section for s-channel helicity-conserving ρ^0 production and the parametrization cross section gives the total ρ^0 cross section. On the other hand, the Söding model suggests that there is a coherent p-wave background under the ρ^0 which should be subtracted out in order to determine a ρ^0 cross section. The two approaches lead to substantially different forward ρ^0 cross sections; since the Söding model gives the best quantitative fit to the data we are led to favor the Söding-model cross sections, but we do not rule out the possibility that the ρ^0 cross section should be determined from Π or by the parametrization technique. More generally, our Söding-model cross sections give the cross section for ρ^0 production when the ρ^0 cross section is defined as that obtained through the integration of a Breit-Wigner distribution which is normalized to the height of the dipion mass spectrum at the ρ^0 mass (with, of course, appropriate subtractions of Δ^{++} and "phase space"); to this extent the Söding-model cross sections can be considered model-independent.

We have used two fits (e^{At} and e^{At+Bt^2}) to obtain forward cross sections. Both these parametrizations of the differential cross section fit the data equally well and from Table XI it may be seen that B is zero within errors. However, differential cross sections are usually fitted with a B term (e.g., πp elastic scattering), so the forward ρ^0 cross sections and errors obtained using the e^{At+Bt^2} fit may be more realistic than those obtained with a linear extrapolation.

D. ρ^0-ω Interference

The combined data of the 2.8- and 4.7-GeV exposures show a 2.5-s.d. (standard deviation) effect in the $\pi^+\pi^-$ mass spectrum that may be attributed to ρ^0-ω interference (see Fig. 26). Our analysis of ρ^0-ω interference has recently been published.[6] Since the $\omega \to 2\pi$ decay rate is small and the interference effect is symmetric about a smooth curve through the ρ^0 mass spectrum, the effect of ρ-ω interference on our ρ^0 cross sections given above is negligible. In addition, fits using the parametrization technique with ρ^0-ω interference included, show that $n(t)$ (see Sec. IV C 1) is unaltered.

E. Δ Production

1. *Cross Sections and Decay Distributions*

In Fig. 10(b) we show the $\pi^\pm p$ mass spectra for the reaction $\gamma p \to p\pi^+\pi^-$. At both energies a clear Δ^{++} signal is found; some Δ^0 production may also be present. The shaded distributions are for events selected with $|t_\Delta| < 0.4$ GeV^2 (t_Δ is the square of the momentum transfer between the proton and the Δ) and $M_{\pi^+\pi^-} > 1.0$ GeV in order to remove most of the ρ^0 reflection and to minimize other backgrounds.

The solid curves in Fig. 10 were obtained from the Söding model fit with an incoherent Δ as described in Appendixes A and B. As can be seen from the figure this gives a reasonable fit to the mass spectrum in both the Δ region and in the

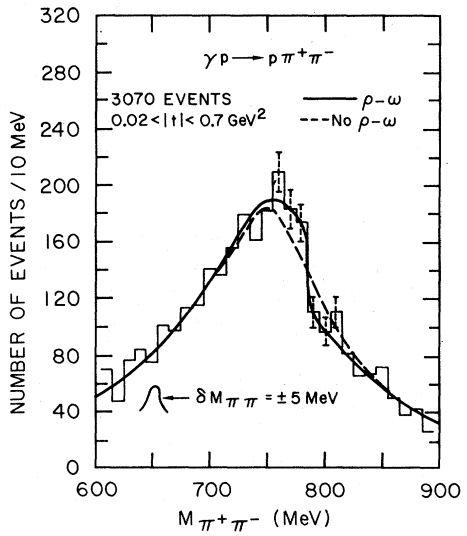

FIG. 26. Reaction $\gamma p \to p\pi^+\pi^-$. $\pi^+\pi^-$ mass distribution for the combined data at 2.8 and 4.7 GeV. The curves give the results of maximum-likelihood fits with (solid line) and without (dashed line) ρ^0-ω interference.

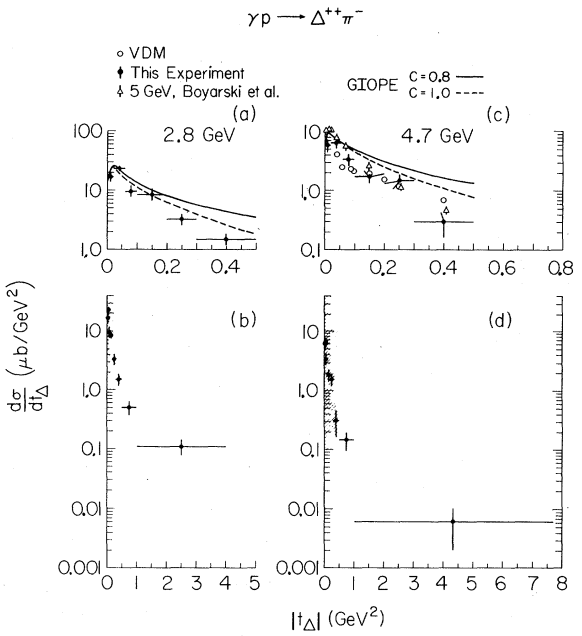

FIG. 27. Reaction $\gamma p \to \Delta^{++}\pi^-$. Differential cross sections $d\sigma/dt_\Delta$ from this experiment (●) and from Ref. 73 for $E_\gamma = 5$ GeV (Δ). The shaded regions in (b) and (d) are shown on an expanded scale in (a) and (c). The curves are the predictions of the gauge-invariant OPE model with absorption corrections for $C = 0.8$ (solid line) and $C = 1$ (dashed line). The points (○) are the VDM prediction of Ref. 82.

high-πp-mass region. We emphasize that in fitting the amount of Δ^{++} we have chosen a shape for the Δ which agrees with that expected from the (3, 3) πN phase shift, δ_{33}. The matrix element for Δ production, T_Δ, has the form

$$|T_\Delta|^2 \sim \frac{M}{q(M)} \frac{\sin^2\delta_{33}}{\Gamma(M)} \sim \frac{1}{\Gamma(M)} \frac{M}{q(M)} \frac{[M_\Delta \Gamma(M)]^2}{(M_\Delta^2 - M^2)^2 + [M_\Delta \Gamma(M)]^2}, \tag{9}$$

where $\Gamma(M)$ follows from $\tan\delta_{33} = M_\Delta \Gamma(M)/(M_\Delta^2 - M^2)$, $M_\Delta = 1.236$ GeV, M is the $\pi^+ p$ or $\pi^- p$ mass, and $q(M)$ is the momentum of the proton in the πp c.m. system. The values of δ_{33} have been taken from a phase-shift analysis.[71]

TABLE XV. Reaction $\gamma p \to \Delta^{++}\pi^-$, differential cross sections (μb/GeV^2).

$\lvert t_\Delta \rvert$ (GeV^2)	$E_\gamma = 2.8$ GeV	$E_\gamma = 4.7$ GeV
$\lvert t_\Delta \rvert_{min}$–0.02	17.1 ±3.5	5.9 ±1.5
0.02–0.06	23.6 ±2.6	6.4 ±1.2
0.06–0.10	9.7 ±1.9	3.4 ±0.9
0.10–0.20	8.4 ±1.0	1.8 ±0.6
0.20–0.30	3.3 ±0.7	1.5 ±0.3
0.30–0.50	1.5 ±0.3	0.31 ±0.13
0.50–1.0	0.51±0.13	0.14 ±0.05
1.0 –$\lvert t_\Delta \rvert_{max}$	0.11±0.03	0.006±0.004

In Table XIII the total cross sections for production of Δ^{++} and Δ^0 ($p\pi^-$ decay mode only) are given for the two energies. Figure 27 and Table XV show the differential cross sections $d\sigma/dt$ for Δ^{++} production obtained from an independent maximum-likelihood fit as described above for each t_Δ interval. Corrections for Δ^{++} production due to contamination from wide-angle electron-positron pair production and for scanning losses of events with short recoil-proton tracks (proton momenta <0.14 GeV/c) were found to be negligible from a Monte Carlo simulation.[30] If the second part of Eq. (9) is used together *with a conventional parametrization* for $\Gamma(M)$,[72] as was done by Boyarski *et al.*,[73] Δ *cross sections are found that are larger by ~20% than those given here.*

The Δ^{++} angular distributions have been analyzed in terms of the Δ spin density matrix in the Gottfried-Jackson frame. The z axis is taken as the direction of the incident proton in the Δ rest frame; the y axis is defined as the normal to the production plane ($\hat{y} \propto \hat{\gamma} \times \hat{\pi}^-$). The electric vector $\hat{\epsilon}$ of the photon makes an angle Φ with the production plane: $\cos\Phi = \hat{\gamma} \cdot (\hat{\epsilon} \times \hat{y})$, $\sin\Phi = \hat{y} \cdot \hat{\epsilon}$. The decay angles θ and ϕ are the polar and azimuthal angles of the outgoing proton in the Δ rest system: $\cos\theta = \hat{p} \cdot \hat{z}$, $\cos\phi = \hat{y} \cdot (\hat{z} \times \hat{p})/|\hat{z} \times \hat{p}|$, $\sin\phi = -(\hat{y} \times \hat{z}) \cdot (\hat{z} \times \hat{p})/|\hat{z} \times \hat{p}|$. The decay angular distribution is then given by[74]

$$W(\cos\theta, \phi, \Phi) = \frac{3}{4\pi}\Big[\rho^0_{33} \sin^2\theta + (\tfrac{1}{2} - \rho^0_{33})(\tfrac{1}{3} + \cos^2\theta) - \frac{2}{\sqrt{3}} \mathrm{Re}\rho^0_{31} \cos\phi \sin 2\theta - \frac{2}{\sqrt{3}} \mathrm{Re}\rho^0_{3-1} \cos 2\phi \sin^2\theta$$
$$- P_\gamma \cos 2\Phi \Big(\rho^1_{33} \sin^2\theta + \rho^1_{11} (\tfrac{1}{3} + \cos^2\theta) - \frac{2}{\sqrt{3}} \mathrm{Re}\rho^1_{31} \cos\phi \sin 2\theta - \frac{2}{\sqrt{3}} \mathrm{Re}\rho^1_{3-1} \cos 2\phi \sin^2\theta \Big)$$
$$- P_\gamma \sin 2\Phi \Big(\frac{2}{\sqrt{3}} \mathrm{Im}\rho^2_{31} \sin\phi \sin 2\theta + \frac{2}{\sqrt{3}} \mathrm{Im}\rho^2_{3-1} \sin 2\phi \sin^2\theta \Big) \Big], \tag{10}$$

where P_γ is the degree of linear polarization. We define the parity asymmetry, P_σ, in terms of the cross sections for natural and unnatural parity exchange in the t channel, σ^N and σ^U:

$$P_\sigma = \frac{\sigma^N - \sigma^U}{\sigma^N + \sigma^U} . \quad (11)$$

Since a meson of spin 0 is produced at the photon vertex, we can find P_σ from the azimuthal distribution of the production normal with respect to the plane of polarization of the photon. At high energies we have

$$W(\Phi) = 1 - P_\sigma P_\gamma \cos 2\Phi . \quad (12)$$

In terms of density-matrix elements,[75]

$$P_\sigma = \mathrm{Tr}\rho^1 = 2(\rho^1_{33} + \rho^1_{11}) . \quad (13)$$

Counter experiments detecting the π^- only measure the polarization asymmetry A,

$$A = \frac{\sigma_\perp - \sigma_\parallel}{\sigma_\perp + \sigma_\parallel} = P_\sigma P_\gamma . \quad (14)$$

To obtain the nine measurable density-matrix parameters and P_σ, events were selected with $M_{p\pi^+} < 1.32$ GeV and the method of moments was used with the Eberhard-Pripstein procedure[76] to remove the ρ^0 reflection. Only events with $-1.0 < \cos\theta_H < 0.3$ at 2.8 GeV ($\cos\theta_H < 0.7$ at 4.7 GeV) were used, where θ_H is the angle in the Δ rest frame between the decay proton and the Δ line of flight in the total c.m. system. Figure 28 and Table XVI show the ρ^α_{ik} and P_σ obtained this way. The values of P_σ averaged over $|t| < 0.5$ GeV^2 are given in Table XIII. It is clear that OPE alone (i.e., the Söding model) cannot explain the data since it would require $P_\sigma = -1$ [$\rho^1_{11} = -\frac{1}{2}$ and all other ρ^α_{ik} in Eq. (10) equal zero]. Qualitatively the same result was obtained in an experiment done at low energy.[77]

2. *Comparison with Theory*

The values of P_σ show that Δ^{++} production does not occur through one-pion exchange alone. At lower energies it was found[11] that the minimal gauge-invariant extension of one-pion exchange (GIOPE) of Stichel and Scholz[78] including absorption corrections in the final state[79] gives a fair description of Δ^{++} production for $|t_\Delta| < 0.3$ GeV^2. At high energies and very small momentum transfers [$(|t_\Delta|)^{1/2} < 0.15$ GeV] it was observed that the GIOPE in the Born approximation reproduces well the differential cross section.[73] Following the idea of vector dominance we calculated the predictions of GIOPE applying absorption corrections both in the initial and final state.[80] This was done by multiplying the helicity amplitudes for spin J by the factor[81]

$$\left[1 - C_{\mathrm{in}} \exp\left(-\frac{(J-\frac{1}{2})^2}{2A_{\mathrm{in}} q_{\mathrm{in}}^2}\right)\right]^{1/2} \times \left[1 - C_{\mathrm{out}} \exp\left(-\frac{(J-\frac{1}{2})^2}{2A_{\mathrm{out}} q_{\mathrm{out}}^2}\right)\right]^{1/2} ,$$

where q is the c.m. momentum, A the slope pa-

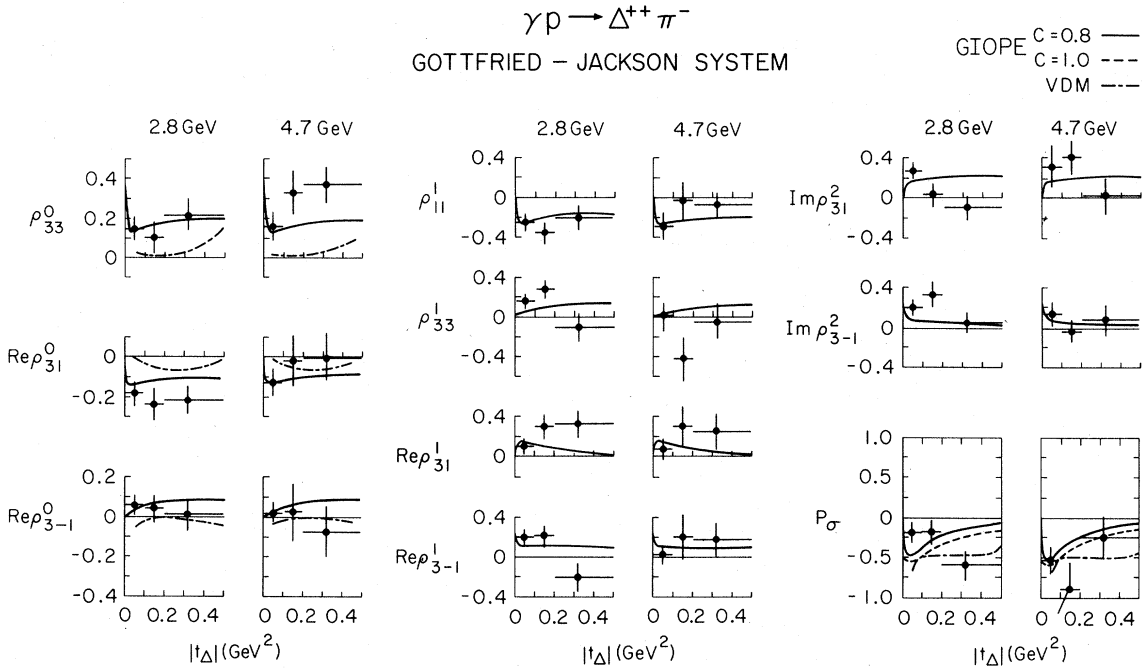

FIG. 28. Reaction $\gamma p \to \Delta^{++}\pi^-$. Density-matrix parameters and parity asymmetry P_σ. The solid curves are the predictions of the gauge-invariant OPE model with absorption corrections for $C = 0.8$. The dashed-dotted curves show the VDM predictions (Ref. 82).

rameter, C the absorption parameter ($C=\sigma_T/4\pi A$, σ_T the total cross section for scattering of either the initial- or final-state particles), and the indices "in," "out" refer to the initial and final states, respectively. The slope parameters were assumed to be the same as measured for Compton scattering and elastic πp scattering, respectively, i.e., $A_{\text{in}}=6$ GeV^{-2}, $A_{\text{out}}=8$ GeV^{-2}. For the absorption parameters C_{in}, C_{out} several sets of values between zero and unity were tried (see below). The finite width of the Δ was taken into account by integrating over the π^+p mass range using the (3, 3) elastic scattering cross section.

The solid curves in Fig. 27 show the predictions of GIOPE for $d\sigma/dt_\Delta(\gamma p\to\Delta^{++}\pi^-)$ for $C_{\text{in}}=C_{\text{out}}=C=0.8$. For comparison we also give the predictions for $C=1$ (dashed curves). The curves for $C=1$ agree approximately with the data for $|t_\Delta|<0.3$ GeV^2; at larger $|t_\Delta|$ too much Δ^{++} is predicted. It is interesting to note that, for $|t_\Delta|>0.02$ GeV^2, the OPE graph alone leads to approximately the same $d\sigma/dt_\Delta$.

In Fig. 28 we compare the measured density-matrix parameters and P_σ with the predictions of GIOPE. It can be seen that the diagrams necessary to give gauge invariance simulate some natural-parity-exchange contributions in the t channel. Although there is agreement for $|t_\Delta|\lesssim 0.1$ GeV^2 in an average sense, we cannot test the strong variations predicted by GIOPE for $|t_\Delta|\lesssim 0.1$ GeV^2. For $|t_\Delta|>0.1$ GeV^2 some of the ρ^α_{ik} and P_σ are not reproduced well.

The vector-dominance model (VDM) relates the reaction $\gamma p\to\pi^-\Delta^{++}$ to the reactions $\pi p\to\Delta V^0$, where V^0 is ρ^0, ω, or ϕ. Boyarski *et al.*,[73] whose $\gamma p\to\pi^-\Delta^{++}$ data agree with ours, found that the comparison disagreed by a factor 2–5. Gotsman[82] has fitted the π-induced reactions to a sum of Regge exchange amplitudes in order to perform the line reversal needed for the comparison (not done by Boyarski *et al.*[83]). With $\gamma_\rho^2/4\pi=0.5$ (γ_ρ describes the γ-ρ coupling strength), his predictions for 5 GeV are in fair agreement with our $d\sigma/dt$ for $|t|>0.1$ GeV^2. While the predictions for some of the ρ^α_{ik} and for P_σ (see dot-dashed curve in Fig. 28) are in qualitative agreement, the prediction $\rho^0_{33}\simeq 0$ is not supported by the data.

In *conclusion,* the density-matrix parameters, the parity asymmetry, and the differential cross section indicate the presence of processes other than OPE in Δ^{++} production. We are thus left with the result that whereas ρ^0 production in the $p\pi^+\pi^-$ channel can be explained well by the Söding model, Δ^{++} production cannot. There is not necessarily any conflict in this because there is little overlap between the ρ^0 and Δ^{++}. The ρ^0 mass asymmetry is due to interference with $\pi^+\pi^-$ pairs corresponding mainly to higher πp masses which are assumed to originate from OPE in the framework of the Söding model. However, the scarcity of events other than the phase-space-like background outside the ρ^0 and Δ^{++} bands (see Figs. 8 and 30) prevents us from testing this assumption by analyzing the angular distributions in this region.

F. Search for High-Mass Vector-Meson Production

The $\pi^+\pi^-$ mass distributions in the channel $\gamma p\to p\pi^+\pi^-$ have been examined for the production of higher-mass vector mesons, in particular, the vector mesons ρ' and ρ'', with masses of ~1.3 and 1.7 GeV predicted by the Veneziano model.[84]

TABLE XVI. Reaction $\gamma p\to\Delta^{++}\pi^-$. Δ^{++} density-matrix elements in Gottfried-Jackson frame and P_σ.

	$E_\gamma=2.8$ GeV			$E_\gamma=4.7$ GeV		
$\lvert t_\Delta\rvert$ (GeV^2)	$\lvert t_\Delta\rvert_{\min}$–0.1	0.1–0.2	0.2–0.5	$\lvert t_\Delta\rvert_{\min}$–0.1	0.1–0.2	0.2–0.5
ρ^0_{33}	0.14±0.06	0.10±0.08	0.22±0.08	0.16±0.06	0.33±0.11	0.37±0.09
$\mathrm{Re}\rho^0_{31}$	−0.18±0.06	−0.24±0.08	−0.22±0.07	−0.13±0.07	−0.02±0.13	−0.01±0.12
$\mathrm{Re}\rho^0_{3-1}$	0.06±0.05	0.04±0.06	0.01±0.08	0.02±0.06	0.03±0.14	−0.07±0.13
ρ^1_{11}	−0.26±0.10	−0.36±0.12	−0.20±0.12	−0.29±0.13	−0.03±0.18	−0.07±0.12
ρ^1_{33}	0.16±0.08	0.28±0.09	−0.10±0.14	0.02±0.14	−0.42±0.22	−0.05±0.16
$\mathrm{Re}\rho^1_{31}$	0.10±0.08	0.30±0.13	0.33±0.14	0.07±0.10	0.30±0.21	0.25±0.19
$\mathrm{Re}\rho^1_{3-1}$	0.20±0.09	0.22±0.10	−0.20±0.14	0.02±0.10	0.21±0.23	0.18±0.17
$\mathrm{Im}\rho^2_{31}$	0.27±0.08	0.04±0.13	−0.10±0.13	0.31±0.21	0.41±0.17	0.01±0.17
$\mathrm{Im}\rho^2_{3-1}$	0.20±0.10	0.34±0.13	0.06±0.10	0.14±0.12	−0.03±0.11	0.09±0.16
P_σ	−0.18±0.14	−0.17±0.15	−0.58±0.17	−0.52±0.15	−0.89±0.32	−0.23±0.26

We used the technique described in Appendix A, plus an additional Breit-Wigner distribution corresponding to the ρ' or ρ'', to fit the Dalitz plot. The fitted cross section for the vector meson is approximately proportional to Γ/R, where Γ is the width of the resonance and R is the fraction of decay to a dipion state. With $\Gamma = 200$ MeV, $R = 1$, and the masses given above, we find upper limits (1 s.d.) at 4.7 GeV of 0.5 μb and 0.3 μb for the ρ' and ρ'', respectively.

G. Summary of the Channel $\gamma p \to p\pi^+\pi^-$

The channel has been shown to be dominated by ρ^0 and Δ^{++} production. We summarize the characteristics of ρ^0 production in Secs. IV G 1–IV G 4 and of Δ^{++} production in Sec. IV G 5.

1. *Dipion Mass Distribution*

In common with other photoproduction experiments we find that the ρ^0 produced in the channel $\gamma p \to p\pi^+\pi^-$ is shifted to lower masses than found in πp interactions and that the ρ^0 shape is skewed with respect to a p-wave Breit-Wigner distribution. We have shown, in addition, that the ρ^0 mass shape changes as a function of the momentum transfer.

2. *Dipion Angular Distribution*

The dipion angular distribution was studied by the method of moments and by a density-matrix analysis.

We conclude:

(a) The dipion pairs in the ρ^0 region are in a predominantly p-wave state and it is the p-wave part of the mass spectrum that shows the skewing.

(b) p-wave dipion production occurs predominantly through natural parity exchange in the t channel.

(c) The p-wave pion pairs are produced by a mechanism that, within errors, conserves s-channel c.m. helicity at the $\gamma\pi\pi$ vertex for $|t| < 0.4$ GeV^2.

3. *Comparison of Dipion Production with Models*

We find that a modified Söding model describes well the following:

(a) the shape of the dipion mass spectrum and its change with momentum transfer;

(b) the variation of the dipion density-matrix elements with dipion mass;

(c) the moments corresponding to dipion states with spin greater than unity.

Other models do not describe well at least one of the above features of the data.

4. *Dipion Cross Sections*

By using the dipion angular distribution and the dipion mass spectrum we have determined two dipion cross sections, namely, the s-channel helicity-conserving p-wave cross section, Π, and the parametrization cross section. We emphasize that neither Π nor the parametrization cross section are necessarily ρ cross sections. Both Π and the parametrization cross sections agree well with other experiments for $|t| > 0.05$ GeV^2. The *extrapolation* of our cross sections to $t = 0$ is compatible with other experiments. Discrepancies in the published forward cross sections can be understood as the result of inelastic backgrounds in other experiments and/or the extrapolation procedures used.

We deduce a ρ cross section using the Söding model. Our Söding-model analysis shows that the ρ cross section is uncertain to ~20%, due to theoretical uncertainties in the model and lack of knowledge of the ρ mass and width.

5. Δ^{++} *Production*

A density-matrix analysis shows that the Δ^{++} is produced by a mixture of natural and unnatural parity exchange in the t channel. Neither the vector-dominance model of Gotsman[82] nor the modified GIOPE model describes both the Δ^{++} differential cross sections and density-matrix elements.

ACKNOWLEDGMENTS

We wish to thank the SLAC operations crew of the accelerator and R. Watt and the 82-in. bubble-chamber operation group. We thank P. Klein and W. Graves for help in the early stages of the experiment. We acknowledge the diligent work of the scanners at SLAC and Berkeley and in particular the help in data reduction by D. Blohm, K. Eymann, W. Hendricks, M. Tartar, and A. Wang. We thank Professor D. Yennie, Professor F. Gilman, Professor J. Pumplin, and Dr. A. Schwimmer for many useful discussions and suggestions.

APPENDIX A: FITTING PROCEDURE FOR THE PARAMETRIZATION CROSS SECTIONS AND THE ρ^0 DENSITY-MATRIX ELEMENTS

The probability, dP, for producing a given event of the reaction $\gamma p \to p\pi^+\pi^-$ with $\pi\pi$ mass $M_{\pi\pi}$, $\pi^+ p$ mass $M_{\pi^+ p}$, and with $\pi^+\pi^-$ angles θ, ϕ, and Φ (defined in Ref. 36) was taken to be

$$dP = |M|^2 d(\text{phase space}),$$

where

$$|M|^2 = a_\rho f_{BW\rho}(M_{\pi\pi})\left(\frac{M_\rho}{M_{\pi\pi}}\right)^{n(t_\rho)} W(\theta,\phi,\Phi)\frac{e^{A_\rho t_\rho}}{N_\rho}$$

$$+ a_\Delta f_{BW\Delta}(M_{\pi^+p})\frac{F(t_\Delta)}{N_\Delta} + \frac{a_{ps}}{N_{ps}}\,. \qquad \text{(A1)}$$

Here, a_ρ, a_Δ, and a_{ps} are the fractions of ρ, Δ^{++}, and phase space, respectively ($a_\rho + a_\Delta + a_{ps} = 1$). $f_{BW\rho}$ is a relativistic Breit-Wigner distribution with an energy-dependent width suggested by Jackson,[72]

$$f_{BW\rho}(M_{\pi\pi}) = \frac{M_{\pi\pi}}{q(M_{\pi\pi})}\,\frac{M_\rho\Gamma(M_{\pi\pi})}{(M_{\pi\pi}^2 - M_\rho^2)^2 + M_\rho^2\Gamma^2(M_{\pi\pi})}\,, \qquad \text{(A2)}$$

where $q(M_{\pi\pi})$ is the momentum of a pion in the dipion rest frame and

$$\Gamma(M_{\pi\pi}) = \Gamma_\rho\left(\frac{q(M_{\pi\pi})}{q(M_\rho)}\right)^3\left(\frac{2}{1+[q(M_{\pi\pi})/q(M_\rho)]^2}\right). \qquad \text{(A3)}$$

The Δ^{++} shape used is

$$f_{BW\Delta}(M_{\pi^+p}) = \frac{M_{\pi^+p}}{q(M_{\pi^+p})}\,\frac{\sin^2\delta_{33}}{M_\Delta\Gamma(M_{\pi^+p})} \qquad \text{(A4)}$$

with δ_{33} taken from a phase-shift analysis[71] and

$$\Gamma(M_{\pi^+p}) = \tan\delta_{33}(M_\Delta^2 - M_{\pi^+p}^2)/M_\Delta\,, \qquad \text{(A5)}$$

with $M_\Delta = 1.236$ GeV, and $q(M_{\pi^+p})$ is the momentum of the proton in the π^+p rest frame. Here $W(\theta,\phi,\Phi)$ describes the ρ-decay angular distribution for the appropriate frame and is given in Eq. (2) of Sec. IV B 3; t_ρ is the square of the momentum transfer from γ to ρ and A_ρ is the slope of the momentum-transfer distribution of the ρ; $F(t_\Delta)$ is a description of our observed momentum-transfer distribution of the Δ. The decay of the Δ^{++} is nearly isotropic and it was therefore not necessary to include a detailed decay distribution. N_ρ, N_Δ, and N_{ps} are normalization factors which ensure that the ρ, Δ, and phase-space terms integrate to unity over the Dalitz plot.

The likelihood function was written as $\sum_i \ln dP_i$ and was maximized in the fits by varying parameters in the combinations appropriate to the fits as discussed below. For the maximization we used the programs MURTLEBERT and OPTIME.[85]

1. *Parametrization-Cross-Section Fits*

In these fits to the Dalitz plot the $\pi^+\pi^-$ angular distribution, $W(\theta,\phi,\Phi)$, was set equal to $\frac{3}{4}\sin^2\theta_H$, and M_ρ, Γ_ρ, and A_ρ were determined from an overall fit in the region $0.02 < |t_\rho| < 0.4$ GeV^2 with an approximate linear $n(t)$ dependence (see Fig. 20 and Ref. 17). With M_ρ, Γ_ρ, and A_ρ fixed at these values, the quantities a_ρ, a_Δ, and the final value of $n(t)$ were fitted for different t_ρ intervals.

2. *ρ Density-Matrix-Element Fits*

In these fits using all the independent variables except t, $W(\theta,\phi,\Phi)$ was expressed in terms of the nine independent density-matrix elements [Eq. (2)]; M_ρ, Γ_ρ, A_ρ, $n(t)$, a_ρ, and a_Δ were set at the values determined above and the nine density-matrix elements were fitted. No constraints were applied to the density-matrix elements.

APPENDIX B: THE SÖDING MODEL

We have calculated the predictions of the Söding model[49] using a modified version of a computer program written by Söding. The matrix element used to describe the reaction $\gamma p \to p\pi^+\pi^-$ is the sum of helicity-conserving ρ production [diagram (a) of Fig. 29], two Drell diagrams [Fig. 29 (b)], a rescattering term [Fig. 29 (c)], and incoherently, Δ^{++} production and a phase-space term.

A ρ production amplitude may be defined in one of two ways, namely, (1) as diagram (a) in Fig. 29 or (2) as the sum of diagrams (a) and (c) in Fig. 29. We choose the first definition since, for $\Gamma_\rho \to 0$ (i.e., the limit of a stable ρ^0), diagram (c), which depends on Γ_ρ^2, vanishes with respect to diagram (a). This definition is also in keeping with the vector-dominance picture of photon interactions (see the discussion of Bauer[51]), and with the intuitive view that (c) is a correction to the Drell terms (b). The analysis presented in the text uses definition (1). At the end of this Appendix we discuss briefly an argument for, and the results of using, definition (2).

We write the matrix element as

$$|M|^2 = a_S|F_\rho\hat{\epsilon}_\rho\cdot\vec{q}(M_{\pi\pi}) + Y(F_{\pi^-} + F_{\pi^+})|^2/N_S$$
$$+ a_\Delta f_{BW\Delta}F_\Delta(t_\Delta)/N_\Delta + (1 - a_S - a_\Delta)/N_{ps}\,, \qquad \text{(B1)}$$

where a_S and a_Δ are the fractions of dipion production described by the Söding model and Δ^{++} pro-

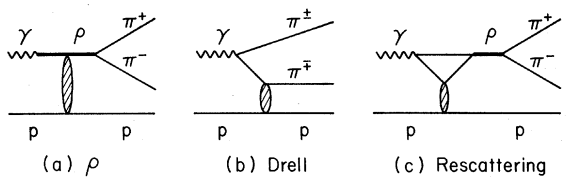

FIG. 29. Diagrams for the reaction $\gamma p \to p\pi^+\pi^-$ corresponding to the Söding model: (a) diffractive ρ production, (b) Drell diagrams, (c) rescattering correction to the Drell diagrams.

duction, respectively; N_S, N_Δ, and N_{ps} normalize the three terms to unity when integrated over phase space. The relative amounts of the ρ^0 and Drell terms are given by Y.

F_ρ is the ρ amplitude with

$$F_\rho = ie^{A_\rho t/2}(\sigma_\rho A_\rho e^{-A_\rho t_{\min}})^{1/2} \times E_{\text{c.m.}} k_{\text{c.m.}}/(M^2 - M_{\pi\pi}{}^2 - iM_\rho\Gamma), \quad \text{(B2)}$$

where t is the square of the momentum transfer to the ρ and A_ρ is the slope of the exponential distribution in t; M_ρ is the ρ mass; Γ is the ρ width with

$$\Gamma = \Gamma_\rho\left(\frac{q(M_{\pi\pi})}{q(M_\rho)}\right)^3 M_\rho/M_{\pi\pi} \quad \text{(B3)}$$

and $q(M_{\pi\pi})$, $q(M_\rho)$ are the pion momenta in the $\pi\pi$ rest frame for $\pi\pi$ masses, $M_{\pi\pi}$, M_ρ, respectively. The ρ^0 production cross section, σ_ρ, was set to a nominal value (15 μb); $t_{\min}$ is the square of the minimum momentum transfer necessary to produce the ρ^0. $E_{\text{c.m.}}$ and $k_{\text{c.m.}}$ are the total energy and the γ momentum in the γp c.m. system. Assuming s-channel helicity conservation for ρ^0 production, $\hat{\epsilon}_\rho$ is calculated by rotating $\hat{\epsilon}_\gamma$, the photon polarization vector in the c.m. system, through the ρ^0 c.m. production angle around the production normal.

For the Drell amplitudes we use

$$F_{\pi^\pm} = \mp(\hat{\epsilon}_\gamma \cdot \vec{q}_{\pi^\pm})T(\pi^\mp p)G(t_{\pi^\pm})/(m_\pi{}^2 - t_{\pi^\pm}), \quad \text{(B4)}$$

where $t_{\pi^\pm}$ is the square of the momentum transfer between the photon and $\pi^\pm$; $q_{\pi^\pm}$ is the momentum of the $\pi^\pm$ in the γp c.m. system, and $G(t_{\pi^\pm})$ is the form factor for off-shell $\pi^\pm p$ scattering. We used the form factor of Ferrari-Selleri,[52]

$$G(t_{\pi^\pm}) = \frac{1}{1 + (m_\pi{}^2 - t_{\pi^\pm})/65m_\pi{}^2}. \quad \text{(B5)}$$

Because of the Ward identity there should be no form factor for the $\gamma\pi\pi$ vertex.[86]

With the form factor $G(t_{\pi^\pm})$ factored out, the off-shell elastic πp scattering amplitude is set equal to the on-shell πp scattering amplitude:

$$T_1(\pi p) = \sum_{l=0}^{3}[(l+1)A_l^+ + lA_l^-]P_l(\cos\theta)M_{\pi p},$$
$$T_2(\pi p) = \sum_{l=0}^{3}\left(\sin\theta(A_l^+ - A_l^-)\frac{d}{d(\cos\theta)}P_l(\cos\theta)\right)M_{\pi p}, \quad \text{(B6)}$$

where T_1, T_2 are the spin-nonflip and spin-flip amplitudes, respectively; θ is the πp center-of-mass scattering angle, $M_{\pi p}$ is the πp mass, and $P_l(\cos\theta)$ are the Legendre polynomials. The elastic πp partial-wave amplitudes which are defined, in the usual notation, by[87]

$$A_l^\pm = (\eta_l^\pm e^{2i\delta_l^\pm} - 1)/2ik_{\pi p}, \quad \text{(B7)}$$

where $k_{\pi p}$ is the π momentum in the πp rest frame, correspond to $J = l \pm \frac{1}{2}$. For $\pi^- p$ the appropriate isospin sum is used for the $A_l^\pm$. For πp masses greater than 1.74 GeV we take $T(\pi^+ p)$ to be purely imaginary with an exponential t dependence.

The T_1 term is multiplied by

$$(M_\rho{}^2 - M_{\pi\pi}{}^2)/(M_\rho{}^2 - M_{\pi\pi}{}^2 - iM_\rho\Gamma_\rho)$$

which is an approximation to the rescattering correction[50] corresponding to the inclusion of diagram (c) of Fig. 29. The use of the rescattering correction in this form is justified by the fact that the Drell term produces predominantly p-wave $\pi\pi$ pairs.[50] In order to test this approximation we have calculated the model both with and without the rescattering correction and have found that the correction does not significantly alter the predicted form of the dipion moments (in particular, Y_4^0) or the density-matrix elements. The spin-flip terms T_2 are assumed not to interfere with the ρ^0 so no rescattering correction was used on them; the T_2 terms were added incoherently to the ρ^0 and spin-nonflip Drell terms. This is an approximation to the fact that a helicity-conserving ρ^0 amplitude does not interfere with the helicity-flip Drell amplitude.

The remaining terms in (B1), corresponding to incoherent Δ^{++} and phase space, are described in Appendix A. In fitting the model the parameters a_S, Y, a_Δ, M_ρ, and Γ_ρ were varied as described in Sec. IV C 2.

The relative importance, and t dependence, of the terms in the Söding amplitude is illustrated in Fig. 30. For this figure we used the Ferrari-Selleri form factor, (B5), for $G(t_{\pi^\pm})$.

Below we examine the sensitivity of the model to (a) the form factor in the Drell term, (b) the coherence of the Δ^{++} production amplitude, (c) the phase shifts, and (d) the phase of the ρ production amplitude.

(a) We have tried the Ferrari-Selleri[52] and Benecke-Dürr[53] form factors and a constant for $G(t_{\pi^\pm})$. Table XVII shows that the ρ^0 mass and width, the ρ^0 forward cross section, and A_ρ do not depend significantly on the form factor.

(b) The results presented in this paper are calculated with $\eta_{33} = 1.0$, $\delta_{33} = 0.0$ in $T(\pi^+ p)$ (i.e., no Δ in the Drell term), and the Δ^{++} term is added incoherently. We have also fitted the model with the Δ^{++} as predicted by the Drell amplitude plus an incoherent Δ^{++} and have found that all fitted values for the ρ agree within 1 standard deviation.

(c) To check the importance of the accuracy of the phase shifts we have made the approximation $T_{1,2} = i|T_{1,2}|$ and have refitted the model. The results changed by less then 1 standard deviation.

(d) When F_ρ is multiplied by $e^{-0.2i}$ (~20% real

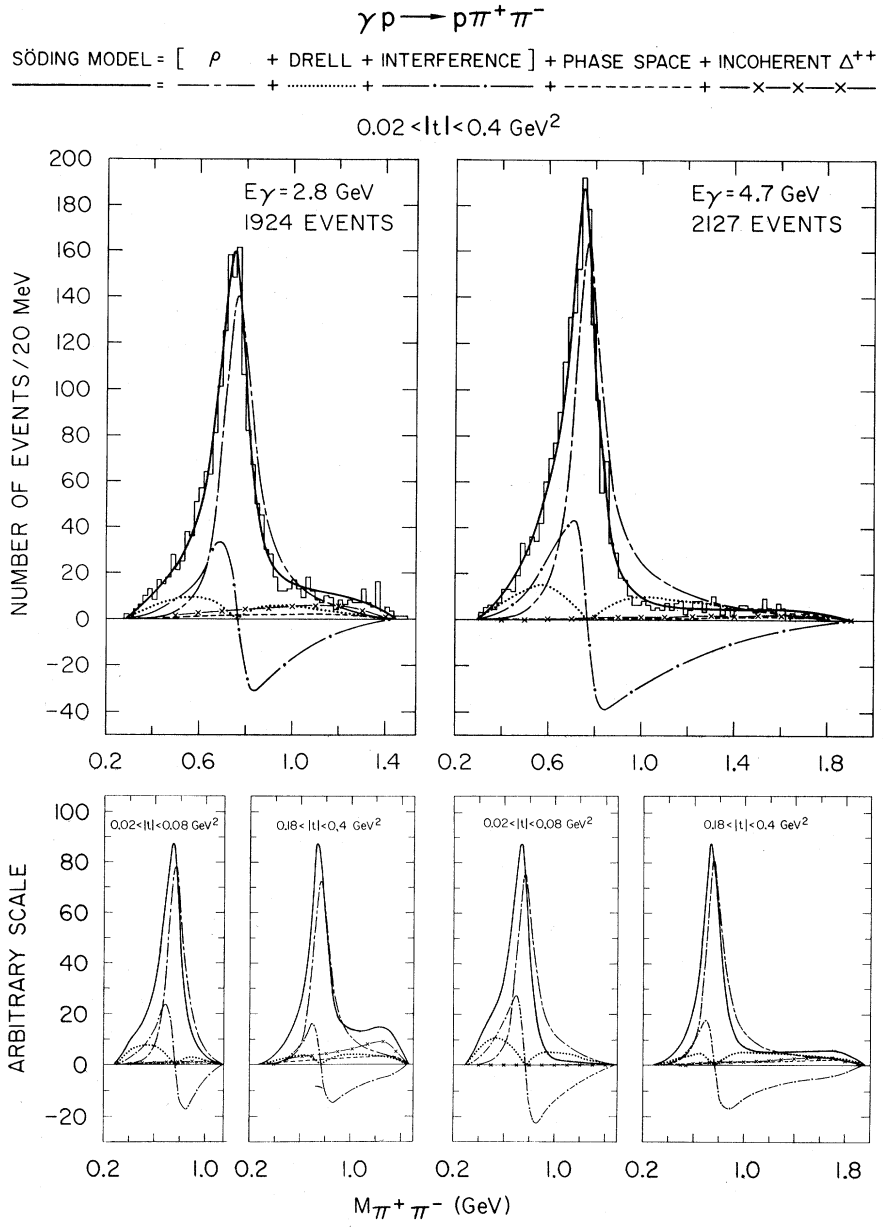

FIG. 30. The contributions of ρ, Drell, interference terms, phase space, and Δ^{++} to the $\pi^+\pi^-$ mass spectrum from a Söding-model fit to the channel $\gamma p \to p\pi^+\pi^-$ in the region $0.02 < |t| < 0.4$ GeV^2. The lower diagrams give the contributions in the intervals $0.02 < |t| < .08$ GeV^2 and $0.18 < |t| < 0.4$ GeV^2.

part) the results are unchanged to within 1 standard deviation.

We conclude that our results are insensitive to a variation of the form of the Drell term within the limits allowed for by changes in the form factor, the coherence of Δ^{++} production, or changes in phases. However, corrections to make the model gauge-invariant could change the Drell term beyond these limits.[86]

We now consider the calculation of the ρ^0 cross section when the ρ^0 *is defined as the sum of diagrams (a) and (c) of Fig. 29.* The physical idea behind this separation[88] is to define the ρ^0 amplitude as those parts of the amplitudes of Fig. 29 which vary rapidly with $M_{\pi\pi}$ in the region of the ρ^0 and to define as background that part which is smooth in the neighborhood of M_ρ. Clearly the fitting procedure is unchanged and, to the extent that the Drell term, D, is imaginary, the ρ^0 cross section defined above is increased by a term proportional to $D^2 \sin^2\delta$, where δ is the $l=1$, $I=1$, $\pi\pi$ phase shift. We obtain values for the ρ cross sec-

TABLE XVII. ρ mass and width, the slope, A, of the ρ differential cross section [from $d\sigma/dt = (d\sigma/dt)_{t=0} e^{At}$], and the forward differential cross section found from Söding-model fits with different form factors.

Form factor	M_ρ (MeV)	Γ_ρ (MeV)	A (GeV^{-2})	$(d\sigma/dt)_{t=0}$ (μb/GeV^2)	E_γ (GeV)
Ferrari-Selleri	767±5	145±10	5.4±0.3	104±6	2.8
Benecke-Dürr	773±5	155±10	5.3±0.3	102±6	2.8
No form factor	772±5	153±10	5.3±0.3	101±6	2.8
Ferrari-Selleri	770±5	155±10	5.9±0.3	94±6	4.7
Benecke-Dürr	770±5	164±10	6.0±0.3	97±6	4.7
No form factor	767±5	167±10	5.9±0.3	98±6	4.7

tion of 20.4±1 μb at 2.8 GeV (16.9±0.7 μb at 4.7 GeV). The ρ^0 forward cross section increased to 109±6 μb/GeV^2 at 2.8 GeV (102±6 μb/GeV^2 at 4.7 GeV) which are 5–10% higher than the values in Table XI. The slope of the ρ^0 momentum-transfer distribution is increased by about 1 standard deviation at both energies.

APPENDIX C: HELICITY AMPLITUDES AND DENSITY MATRICES OF PHOTOPRODUCED ρ^0 MESONS

In this appendix we present the relation between the density matrices ρ^α_{ik} measured in this experiment and the helicity amplitudes describing ρ^0 photoproduction. (We use the notation of Ref. 35.)

We write the helicity amplitudes, which are functions of s and t, as

$$T_{\lambda_\rho \lambda_{N'}, \lambda_\gamma \lambda_N},$$

where λ_ρ, λ_γ, $\lambda_{N'}$, λ_N are ρ-meson, photon, final- and initial-proton helicities. Parity conservation gives the following relation between helicity amplitudes[89]:

$$T_{\lambda_\rho \lambda_{N'}, \lambda_\gamma \lambda_N} = (-1)^{(\lambda_\rho - \lambda_\gamma) - (\lambda_{N'} - \lambda_N)} T_{-\lambda_\rho - \lambda_{N'}, -\lambda_\gamma - \lambda_N}.$$

Consequently,

$$\sum_{\lambda_{N'} \lambda_N} (T_{\lambda_\rho \lambda_{N'}, \lambda_\gamma \lambda_N} T^*_{\lambda'_\rho \lambda_{N'}, \lambda'_\gamma \lambda_N}) = (-1)^{(\lambda_\rho - \lambda'_\rho) - (\lambda_\gamma - \lambda'_\gamma)} \sum_{\lambda_{N'} \lambda_N} (T_{-\lambda_\rho \lambda_{N'}, -\lambda_\gamma \lambda_N} T^*_{-\lambda'_\rho \lambda_{N'}, -\lambda'_\gamma \lambda_N}). \quad \text{(C1)}$$

If only natural [$P = (-1)^J$] or only unnatural parity [$P = -(-1)^J$] exchanges contribute in the t channel, we have to leading order in the energy of the incoming photon the additional symmetry[39]

$$T_{\lambda_\rho \lambda_{N'}, \lambda_\gamma \lambda_N} = \pm (-1)^{\lambda_\rho - \lambda_\gamma} T_{-\lambda_\rho \lambda_{N'}, -\lambda_\gamma \lambda_N}, \quad \text{(C2)}$$

where the upper (lower) sign applies to natural (unnatural) parity exchanges. We define the density-matrix elements by

$$\rho^0_{ik} = \frac{1}{A} \sum_{\lambda_\gamma \lambda_{N'} \lambda_N} T_{\lambda_{\rho i} \lambda_{N'}, \lambda_\gamma \lambda_N} T^*_{\lambda_{\rho k} \lambda_{N'}, \lambda_\gamma \lambda_N},$$

$$\rho^1_{ik} = \frac{1}{A} \sum_{\lambda_\gamma \lambda_{N'} \lambda_N} T_{\lambda_{\rho i} \lambda_{N'}, -\lambda_\gamma \lambda_N} T^*_{\lambda_{\rho k} \lambda_{N'}, \lambda_\gamma \lambda_N},$$

$$\rho^2_{ik} = \frac{i}{A} \sum_{\lambda_\gamma \lambda_{N'} \lambda_N} \lambda_\gamma T_{\lambda_{\rho i} \lambda_{N'}, -\lambda_\gamma \lambda_N} T^*_{\lambda_{\rho k} \lambda_{N'}, \lambda_\gamma \lambda_N}, \quad \text{(C3)}$$

$$\rho^3_{ik} = \frac{1}{A} \sum_{\lambda_\gamma \lambda_{N'} \lambda_N} \lambda_\gamma T_{\lambda_{\rho i} \lambda_{N'}, \lambda_\gamma \lambda_N} T^*_{\lambda_{\rho k} \lambda_{N'}, \lambda_\gamma \lambda_N},$$

with

$$A = \sum_{\lambda_{\rho i} \lambda_\gamma \lambda_{N'} \lambda_N} T_{\lambda_{\rho i} \lambda_{N'}, \lambda_\gamma \lambda_N} T^*_{\lambda_{\rho i} \lambda_{N'}, \lambda_\gamma \lambda_N},$$

where ρ_{ik} stands for $\rho_{\lambda_{\rho i} \lambda_{\rho k}}$. If we use linearly polarized photons ρ^0, ρ^1, and ρ^2 can be measured; for circularly polarized photons ρ^0 and ρ^3 are measurable.

Using (C1), and with an implied summation over nucleon spins, we obtain the following expressions for the density-matrix elements in terms of helicity amplitudes $T_{\lambda_\rho \lambda_\gamma}$:

$$\rho^0_{00} = \frac{1}{A}(T_{0+} T^*_{0+} + T_{0-} T^*_{0-}),$$

$$\rho^0_{11} = \frac{1}{A}(T_{++} T^*_{++} + T_{+-} T^*_{+-}),$$

$$\mathrm{Re}\rho^0_{10} = \frac{1}{A} \mathrm{Re}(T_{++} T^*_{0+} + T_{+-} T^*_{0-}),$$

$$\rho^0_{1-1} = \frac{1}{A}(T_{++} T^*_{-+} + T_{+-} T^*_{--}),$$

$$\rho^1_{00} = \frac{1}{A}(T_{0+} T^*_{0-} + T_{0-} T^*_{0+}) = \frac{1}{A} 2\,\mathrm{Re}(T_{0+} T^*_{0-}),$$

$$\rho^1_{11} = \frac{1}{A}(T_{++} T^*_{+-} + T_{+-} T^*_{++}) = \frac{1}{A} 2\,\mathrm{Re}(T_{++} T^*_{+-}),$$

$$\mathrm{Re}\rho^1_{10} = \frac{1}{A}\,\mathrm{Re}(T_{++}T^*_{0-} + T_{+-}T^*_{0+}), \qquad \text{(C4)}$$

$$\rho^1_{1\,-1} = \frac{1}{A}(T_{++}T^*_{--} + T_{+-}T^*_{-+}),$$

$$\mathrm{Im}\rho^2_{10} = \frac{1}{A}\,\mathrm{Re}(T_{+-}T^*_{0+} - T_{++}T^*_{0-}),$$

$$\mathrm{Im}\rho^2_{1\,-1} = \frac{1}{A}(T_{+-}T^*_{-+} - T_{++}T^*_{--}),$$

$$\mathrm{Im}\rho^3_{10} = \frac{1}{A}\,\mathrm{Im}(T_{++}T^*_{0+} - T_{+-}T^*_{0-}),$$

$$\mathrm{Im}\rho^3_{1\,-1} = -\frac{i}{A}(T_{++}T^*_{-+} - T_{+-}T^*_{--}).$$

From the 11 independent density-matrix elements ($\rho^0_{00} + 2\rho^0_{11} = 1$) and the cross section

$$\frac{d\sigma}{d\Omega} = \left(\frac{2\pi}{E_{\gamma\,\mathrm{c.m.}}}\right)^2 \frac{A}{4},$$

we get 10 bilinear combinations of helicity amplitudes:

$$T_{++}T^*_{++} + T_{+-}T^*_{+-} = A\rho^0_{11} = T_{--}T^*_{--} + T_{-+}T^*_{-+}, \qquad \text{(C5)}$$

$$T_{0+}T^*_{0+} + T_{0-}T^*_{0-} = A\rho^0_{00}, \qquad \text{(C6)}$$

$$\mathrm{Re}(T_{++}T^*_{+-}) = \tfrac{1}{2}A\rho^1_{11} = \mathrm{Re}(T_{--}T^*_{-+}), \qquad \text{(C7)}$$

$$\mathrm{Re}(T_{0+}T^*_{0-}) = \tfrac{1}{2}A\rho^1_{00} = \mathrm{Re}(T_{0-}T^*_{0+}), \qquad \text{(C8)}$$

$$T_{++}T^*_{--} = \tfrac{1}{2}A(\rho^1_{1\,-1} - \mathrm{Im}\rho^2_{1\,-1}) = T_{--}T^*_{++}, \qquad \text{(C9)}$$

$$T_{+-}T^*_{-+} = \tfrac{1}{2}A(\rho^1_{1\,-1} + \mathrm{Im}\rho^2_{1\,-1}) = T_{-+}T^*_{+-}, \qquad \text{(C10)}$$

$$\mathrm{Re}(T_{++}T^*_{0-}) = \tfrac{1}{2}A(\mathrm{Re}\rho^1_{10} - \mathrm{Im}\rho^2_{10}) = \mathrm{Re}(T_{--}T^*_{0+}), \qquad \text{(C11)}$$

$$\mathrm{Re}(T_{+-}T^*_{0+}) = \tfrac{1}{2}A(\mathrm{Re}\rho^1_{10} + \mathrm{Im}\rho^2_{10}) = \mathrm{Re}(T_{-+}T^*_{0-}), \qquad \text{(C12)}$$

$$T_{++}T^*_{-+} = \tfrac{1}{2}A(\rho^0_{1\,-1} + i\,\mathrm{Im}\rho^3_{1\,-1}) = T_{--}T^*_{+-}, \qquad \text{(C13)}$$

$$T_{+-}T^*_{--} = \tfrac{1}{2}A(\rho^0_{1\,-1} - i\,\mathrm{Im}\rho^3_{1\,-1}) = T_{-+}T^*_{++}. \qquad \text{(C14)}$$

A derived quantity is the parity asymmetry P_σ,

$$P_\sigma = 2\rho^1_{1\,-1} - \rho^1_{00}.$$

When $P_\sigma = \pm 1$ we get the following additional relation (inserting helicity amplitudes in $2\rho^1_{1\,-1} - \rho^1_{00} = \pm 1$):

$$|T_{++} \mp T_{--}|^2 + |T_{+-} \mp T_{-+}|^2 + |T_{0+} \pm T_{0-}|^2 = 0. \qquad \text{(C15)}$$

For $P_\sigma = \pm 1$ we have, therefore,

$$T_{++} = \pm T_{--},$$

$$T_{+-} = \pm T_{-+},$$

$$T_{0+} = \mp T_{0-}.$$

This is the t-channel parity relation (C2).

Some counter experiments measure the quantity Σ,

$$\Sigma = \frac{\rho^1_{11} + \rho^1_{1\,-1}}{\rho^0_{11} + \rho^1_{1\,-1}},$$

which is *not related unambiguously* to natural and unnatural parity exchange. We get from $\Sigma = \pm 1$

$$(T_{++} \mp T_{+-})(T^*_{-+} \mp T^*_{+-}) + (T_{++} \mp T_{+-})(T^*_{++} \mp T^*_{--}) = 0.$$

For pure natural (unnatural) parity exchange Σ is $+1(-1)$, but this would also happen for $T_{++} = \pm T_{+-}$ which has no relation to t-channel exchanges. *From $\Sigma = \pm 1$ the parity of the t-channel exchange can be deduced only when either the nonflip or the double-flip amplitudes are zero.*

A measurement of the angular distribution $W(\Phi)$ of the production plane (i.e., of the azimuthal distribution of the outgoing proton) with respect to the photon polarization vector gives

$$W(\Phi) = 1 - \cos 2\Phi\ \mathrm{Tr}\rho^1.$$

The quantity

$$\mathrm{Tr}\rho^1 = 2\rho^1_{11} + \rho^1_{00} = \frac{1}{A}[\mathrm{Re}(T_{0+}T^*_{0-}) + 2\,\mathrm{Re}(T_{++}T^*_{+-})]$$

has no direct relation to the parity of the t-channel exchange. For helicity conservation $\mathrm{Tr}\rho^1 = 0$ and $W(\Phi)$ must be isotropic.

Experimental results. In our experiment with linearly polarized photons we find:

$$P_\sigma \approx +1.0,$$

$$\rho^0_{11} \approx 0.5,$$

$$\rho^1_{1\,-1} \approx 0.5,$$

$$\mathrm{Im}\rho^2_{1\,-1} \approx -0.5$$

(all other measurable elements are ~ zero).

(a) From (C6) we conclude that helicity flips $\lambda_\gamma = \pm 1$ to $\lambda_\rho = 0$ vanish.

(b) From (C15) and (C10) we conclude that helicity flips $\lambda_\gamma = \pm 1$ to $\lambda_\rho = \mp 1$ vanish.

(c) From (C15) we find $T_{++} = T_{--}$.

Point (a) was known from unpolarized experiments. We have established (b) and (c) by using linearly polarized photons and by measuring the full angular distribution. Points (a), (b), and (c) together establish helicity conservation at the $\gamma\rho$ vertex.

In the forward direction T_{+-}, T_{-+}, go to zero[90] because angular momentum conservation does not allow $|\Delta\lambda| = 2$. If these double-flip amplitudes were large, a dip in the forward ρ^0 cross section would be expected. From an experiment using unpolarized photons which found no dip in the differential cross section at small t, and a vanishing ρ^0_{00}, it could be concluded that helicity-flip terms are small in the forward direction, but nothing could be deduced about the parity of the exchanged particle.

†Work supported in part by the U. S. Atomic Energy Commission and the National Science Foundation.

*Present address: Stanford University, High Energy Physics Laboratory, Stanford, Calif. 94305.

‡On leave from Max-Planck-Institut für Physik und Astrophysik, München, Germany.

§On leave from University of Hamburg, Hamburg, Germany.

‖Present address: DESY, Hamburg, Germany.

**Present address: Stanford Linear Accelerator Center, Stanford University, Stanford, Calif. 94305.

††Present address: Laboratoire Interuniversitaire des Hautes Energies, Bruxelles, Belgium.

[1]J. Ballam, G. B. Chadwick, R. Gearhart, Z. G. T. Guiragossián, P. R. Klein, A. Levy, M. Menke, J. J. Murray, P. Seyboth, G. Wolf, C. K. Sinclair, H. H. Bingham, W. B. Fretter, K. C. Moffeit, W. J. Podolsky, M. S. Rabin, A. H. Rosenfeld, and R. Windmolders, Phys. Rev. Letters 23, 498 (1969); 23, 817(E) (1969).

[2]H. H. Bingham, W. B. Fretter, K. C. Moffeit, W. J. Podolsky, M. S. Rabin, A. H. Rosenfeld, R. Windmolders, J. Ballam, G. B. Chadwick, R. Gearhart, Z. G. T. Guiragossián, M. Menke, J. J. Murray, P. Seyboth, A. Shapira, C. K. Sinclair, I. O. Skillicorn, G. Wolf, and R. H. Milburn, Phys. Rev. Letters 24, 955 (1970).

[3]J. Ballam, G. B. Chadwick, R. Gearhart, Z. G. T. Guiragossián, M. Menke, J. J. Murray, P. Seyboth, A. Shapira, C. K. Sinclair, I. O. Skillicorn, G. Wolf, R. H. Milburn, H. H. Bingham, W. B. Fretter, K. C. Moffeit, W. J. Podolsky, M. S. Rabin, A. H. Rosenfeld, and R. Windmolders, Phys. Rev. Letters 24, 960 (1970); 24, 1467(E) (1970).

[4]J. Ballam, G. B. Chadwick, R. Gearhart, Z. G. T. Guiragossián, M. Menke, J. J. Murray, P. Seyboth, A. Shapira, C. K. Sinclair, I. O. Skillicorn, G. Wolf, R. H. Milburn, H. H. Bingham, W. B. Fretter, K. C. Moffeit, W. J. Podolsky, M. S. Rabin, A. H. Rosenfeld, and R. Windmolders, Phys. Rev. Letters 24, 1364 (1970); 26, 155(E) (1971).

[5]H. H. Bingham, W. B. Fretter, K. C. Moffeit, W. J. Podolsky, M. S. Rabin, A. H. Rosenfeld, R. Windmolders, J. Ballam, G. B. Chadwick, R. Gearhart, Z. G. T. Guiragossián, M. Menke, J. J. Murray, P. Seyboth, A. Shapira, C. K. Sinclair, I. O. Skillicorn, G. Wolf, and R. H. Milburn, Phys. Rev. Letters 25, 1223 (1970).

[6]K. C. Moffeit, H. H. Bingham, W. B. Fretter, W. J. Podolsky, M. S. Rabin, A. H. Rosenfeld, R. Windmolders, J. Ballam, G. B. Chadwick, R. Gearhart, Z. G. T. Guiragossián, M. Menke, J. J. Murray, P. Seyboth, A. Shapira, C. K. Sinclair, I. O. Skillicorn, G. Wolf, and R. H. Milburn, Nucl. Phys. B29, 349 (1971).

[7]J. J. Murray and P. R. Klein, SLAC Report No. SLAC-TN-67-19, 1967 (unpublished).

[8]C. K. Sinclair, J. J. Murray, P. R. Klein, and M. Rabin, IEEE Trans. Nucl. Sci. 16, 1065 (1969).

[9]R. A. Gearhart, P. R. Klein, J. J. Murray, W. J. Podolsky, M. S. Rabin, and C. K. Sinclair, Nucl. Instr. Methods 75, 220 (1969).

[10]Cambridge Bubble Chamber Group, Phys. Rev. 146, 994 (1966).

[11]Aachen-Berlin-Bonn-Hamburg-Heidelberg-München Collaboration, Phys. Rev. 175, 1669 (1968).

[12]L. J. Lanzerotti, R. B. Blumenthal, D. C. Ehn, W. L. Faissler, P. M. Joseph, F. M. Pipkin, J. K. Randolph, J. J. Russell, D. G. Stairs, and J. Tenenbaum, Phys. Rev. 166, 1365 (1968).

[13]R. H. Milburn, Phys. Rev. Letters 10, 75 (1963).

[14]F. R. Arutyunian, I. I. Goldman, and V. A. Tumanian, Zh. Eksperim. i Teor. Fiz. 45, 312 (1963) [Soviet Phys. JETP 18, 218 (1964)]; F. R. Arutyunian and V. A. Tumanian, Phys. Letters 4, 176 (1963).

[15]W. J. Podolsky, LRL Report No. UCRL-20198, 1971 (unpublished).

[16]F. T. Solmitz, A. D. Johnson, and T. B. Day, Alvarez Group (UCRL) Programming Note No. P-117, 1966 (unpublished); O. I. Dahl, T. B. Day, F. T. Solmitz, and N. L. Gould, Alvarez Group (UCRL) Programming Note No. P-126, 1968 (unpublished).

[17]K. C. Moffeit, LRL Report No. UCRL-19890, 1970 (unpublished).

[18]T. M. Knasel, DESY Report No. 70/3, 1970 (unpublished).

[19]H. Meyer, B. Naroska, J. H. Weber, M. Wong, V. Heynen, E. Mandelkow, and D. Notz, Phys. Letters 33B, 189 (1970).

[20]This correction, which was not applied in our earlier publications, was determined by a careful re-scan of part of our 4.7-GeV film. The corrections to $d\sigma/dt(\gamma p \to p\pi^+\pi^-)$ at 4.7 GeV are $(15\pm6)\%$, $(5\pm4)\%$, and $(5\pm5)\%$ for the $|t|$ intervals 0.02–0.05 GeV^2, 0.05–0.075 GeV^2, and 0.075–0.1 GeV^2, respectively.

[21]J. Ballam, G. B. Chadwick, Z. G. T. Guiragossián, P. Klein, A. Levy, M. Menke, E. Pickup, P. Seyboth, T. H. Tan, and G. Wolf, Phys. Rev. Letters 21, 1544 (1968).

[22]D. O. Caldwell, V. B. Elings, W. P. Hesse, R. J. Morrison, F. V. Murphy, and B. W. Worster, Phys. Rev. Letters 25, 609 (1970).

[23]E. D. Bloom, R. L. Cottrell, D. H. Coward, H. DeStaebler Jr., J. Drees, G. Miller, L. W. Mo, R. E. Taylor, J. I. Friedman, G. C. Hartman, and H. W. Kendall, SLAC Report No. SLAC-PUB-653, 1969 (unpublished).

[24]We have checked the pK^+K^- and $pK^+K^-\pi^+\pi^-$ samples for possible contamination. The shape and position of the E_γ and χ^2 distributions are as expected for 3C fits, with 100% (90%) of the events inside the E_γ limits 2.4–3.3 GeV (4.1–5.3 GeV). For pK^+K^- fits simulated by $p\pi^+\pi^-\pi^0$ or $n\pi^+\pi^+\pi^-$ events one expects a flat χ^2 distribution and energies below the E_γ limits, which is in contrast to our observation. From this and Monte Carlo studies we estimate the contamination to be less than 5% at 2.8 GeV (10% at 4.7 GeV). This uncertainty is included in the errors of the cross sections.

[25]Four of the nine events fitting $\gamma p \to pp\bar{p}$ had two baryon tracks which could be identified by ionization. All nine events had fitted photon energies in the range $4.2 < E_\gamma < 5.0$ GeV and kinematic $\chi^2 < 8.0$ with an average χ^2 of 3.2. These are the values expected for real events $\gamma p \to pp\bar{p}$ giving a 3C fit. For background events simulating this channel smaller E_γ and larger χ^2 would be expected. We therefore conclude that our sample contains no sizeable background contamination.

[26]Aachen-Berlin-Bonn-Hamburg-Heidelberg-München Collaboration, Phys. Rev. 188, 2060 (1969); H. Spitzer, DESY Internal Report No. DESY-F1-71/4, 1971 (unpublished).

[27]The cross sections at $E_\gamma = 1.44$ GeV were obtained from a small film sample taken in conjunction with the 2.8- and 4.7-GeV exposures. A total cross-section

measurement at 1.44 GeV has been reported in Ref. 1. We use the same event sample and corrections as described in this reference.

[28]Y. Eisenberg *et al.*, Phys. Rev. D 5, 15 (1972); see also Y. Eisenberg *et al.*, Phys. Rev. Letters 22, 669 (1969); J. Ballam *et al.*, *ibid.* 21, 1541 (1968); Phys. Letters 30B, 421 (1969).

[29]H. Spitzer, DESY Internal Report No. DESY-F1/4, 1967 (unpublished).

[30]We used the event simulation program PHONY: E. Burns and D. Drijard, Trilling-Goldhaber Group (UCRL) Technical Note No. 143, 1968 (unpublished).

[31]A comparison of the channels $\gamma p \to n\pi^+\pi^+\pi^-$ and $\gamma n \to p\pi^+\pi^-\pi^-$ is made in Ref. 15. [See also G. Alexander *et al.*, Phys. Rev. Letters 26, 340 (1971)].

[32]Cross sections for the channel $\gamma p \to p\pi^+\pi^-$ are corrected for the region $|t|<0.02$ GeV^2 and for the loss of events with $|t|>0.02$ GeV^2. These corrections are not applied to histograms of mass distributions.

[33]D. McLeod, S. Richert, and A. Silverman, Phys. Rev. Letters 7, 383 (1961).

[34]R. L. Thews, Phys. Rev. 175, 1749 (1968).

[35]K. Schilling, P. Seyboth, and G. Wolf, Nucl. Phys. B15, 397 (1970); B18, 332(E) (1970).

[36]The y axis is the normal to the production plane, defined by the cross product $\hat{k}\times\hat{\rho}$ of the directions of the photon and the vector meson. The x axis is given by $\hat{x}=\hat{y}\times\hat{z}$. The angle Φ between the electric vector of the photon, $\hat{\epsilon}$, and the production plane in the total c.m. system is defined by $\sin\Phi=\hat{y}\cdot\hat{\epsilon}$ with the sign ambiguity defined by $\cos\Phi=\hat{\epsilon}\cdot(\hat{y}\times\hat{k})$. The decay angles θ, ϕ are the polar and azimuthal angles of the direction of flight, $\hat{\pi}$, of the π^+ in the ρ rest system:

$$\cos\theta=\hat{\pi}\cdot\hat{z},$$

$$\cos\phi=\hat{y}\cdot(\hat{z}\times\hat{\pi})/|\hat{z}\times\hat{\pi}|,$$

$$\sin\phi=-\hat{x}\cdot(\hat{z}\times\hat{\pi})/|\hat{z}\times\hat{\pi}|.$$

[37]Y. Eisenberg, E. E. Ronat, A. Brandstetter, A. Levy, and E. Gotsman, Phys. Letters 22, 223 (1966); G. Kramer, DESY Report No. DESY-67/32, 1967 (unpublished).

[38]F. Cooper, Phys. Rev. 167, 1314 (1968).

[39]G. Cohen-Tannoudji, A. Morel, and Ph. Salin, Nuovo Cimento 55A, 412 (1968).

[40]L. Criegee, G. Franke, G. Löffler, K. P. Schüler, U. Timm, W. Zimmermann, H. Werner, and P. W. Dougan, Phys. Rev. Letters 25, 1306 (1970).

[41]G. Diambrini-Palazzi, G. McClellan, N. Mistry, P. Mostek, H. Ogren, J. Swartz, and R. Talman, Phys. Rev. Letters 25, 478 (1970).

[42]We have checked the reliability of the errors on the ρ_{ik} obtained from the maximum-likelihood analysis. To this end 1000 experiments with 100 s-channel helicity-conserving ρ^0 events were generated. In a maximum-likelihood analysis the ρ_{ik} were determined separately for each experiment. The width of the distribution of the ρ_{ik} fitted for each experiment was found to be consistent with the error on ρ_{ik} as given by the maximum-likelihood analysis.

[43]F. J. Gilman, J. Pumplin, A. Schwimmer, and L. Stodolsky, Phys. Letters 31B, 387 (1970).

[44]M. Hontebeyrie *et al.*, in a discussion of helicity conservation, have proposed a certain parametrization of the helicity amplitudes [M. Hontebeyrie, C. Meyers, J. Procureur, and Ph. Salin, University of Bordeaux preprint Report No. PTB-40, 1971 (unpublished)]. Using their parametrization and fitting the resulting density matrix to our 4.7-GeV data in the range $0.02\le|t|\le0.4$ GeV^2, we find ρ^0 helicity-flip contributions to the cross sections of 6% for $|t|=0.2$ GeV^2 (30% for $|t|=0.4$ GeV^2). The helicity flip occurs almost entirely in the "double-flip" terms d and f of Hontebeyrie *et al.*

[45]The density-matrix elements used in this fit are given by

$$\rho_{ik}=d^1_{im}(\beta)\tilde{\rho}_{mn}d^1_{nk}(-\beta)$$

with $\tilde{\rho}^0_{11}=\tilde{\rho}_{-1-1}=\frac{1}{2}$, $\tilde{\rho}^1_{1-1}=\tilde{\rho}^1_{-11}=\frac{1}{2}$, $\tilde{\rho}^2_{1-1}=-\tilde{\rho}^2_{-11}=-\frac{1}{2}i$. Other $\tilde{\rho}_{mn}$ are zero. The rotation matrices $d^1(\beta)$ describe a rotation through the angle β about the normal to the production plane. The ρ_{ik} were inserted in $W(\cos\theta,\phi,\Phi)$ of Eq. (2) above and β was fitted using Eq. (A1) of Appendix A.

[46]All total cross sections for ρ^0 production given in this paper are corrected for the interval $|t|<0.02$ GeV^2. We fit the differential distribution to the form Be^{At}; the cross-section correction is then given by $\int_{t_{\min}}^{0.02\ \mathrm{GeV}^2} Be^{At}dt$, where $t_{\min}$ is the square of the minimum momentum transfer required to produce the ρ^0. Differential cross sections have been fitted to the forms e^{At} and e^{At+Bt^2}; both forms give equally good fits to the data. We give forward cross sections determined from both fits to indicate the dependence of the forward cross section on the type of extrapolation used.

[47]M. Ross and L. Stodolsky, Phys. Rev. 149, 1172 (1966).

[48]S. D. Drell, Rev. Mod. Phys. 33, 458 (1961).

[49]P. Söding, Phys. Letters 19, 702 (1965); see also A. S. Krass, Phys. Rev. 159, 1496 (1967).

[50]J. Pumplin, Phys. Rev. D 2, 1859 (1970).

[51]T. Bauer, Phys. Rev. Letters 25, 485 (1970); D. Yennie (private communication).

[52]E. Ferrari and F. Selleri, Phys. Rev. Letters 7, 387 (1961).

[53]J. Benecke and H. P. Dürr, Nuovo Cimento 56A, 269 (1968); see also G. Wolf, Phys. Rev. 182, 1538 (1969).

[54]This approach was suggested to us by D. Yennie (private communication).

[55]This follows from using a ρ Breit-Wigner term of the form

$$\frac{M_\rho\Gamma_\rho/\pi}{(M^2-M_\rho^2)^2+M_\rho^2\Gamma_\rho^2}$$

whose integral is normalized to unity for $M_\rho\Gamma_\rho\to0$.

[56]Owing to the uncertainty in the determination of $d^2\sigma/dtdM$ a forward cross section estimated for a given M_ρ, Γ_ρ is uncertain to about $\pm10\%$. The relative positions of the lines for different M_ρ are determined by the form of the curve used to fit $d^2\sigma/dtdM$ so this figure gives only a qualitative indication of the dependence of $d\sigma/dt$ on M_ρ.

[57]Particle Data Group, Phys. Letters 33B, 1 (1970).

[58]H. Satz and K. Schilling, Nuovo Cimento 67A, 511 (1970). The dual model has recently been reformulated to conserve s-channel helicity at the $\gamma\rho$ vertex [P. Dewey and B. Humpert, Lett. Nuovo Cimento 1, 651 (1971)]. We find that this helicity-conserving dual model fits the 4.7-GeV data well with a fitted ρ^0 mass and width of 761 MeV and 130 MeV, respectively. The moments and density-matrix elements agree well with the data. The predicted cross section for $\gamma p\to p\pi^+\pi^-$ (Δ^{++} excluded) is about 20% higher than that observed experimentally.

[59]G. Kramer and J. L. Uretsky, Phys. Rev. 181, 1918

(1969); G. Kramer and H. R. Quinn, Nucl. Phys. B27, 77 (1971).

[60]G. Kramer, in Proceedings of the Daresbury Study Weekend, 1970, edited by A. Donnachie and E. Gabathuler, DNPL Report No. DNPL/R7 (unpublished).

[61]P. D. Mannheim and U. Maor, Phys. Rev. D 2, 2105 (1970).

[62]G. K. Greenhut, Phys. Rev. D 3, 1152 (1971).

[63]G. McClellan, N. Mistry, P. Mostek, H. Ogren, A. Silverman, J. Swartz, R. Talman, K. Gottfried, and A. I. Lebedev, Phys. Rev. Letters 22, 374 (1969).

[64]G. McClellan, N. Mistry, P. Mostek, H. Ogren, A. Silverman, J. Swartz, and R. Talman, Cornell Report No. CLNS-154, 1970 (unpublished).

[65]H. Alvensleben, U. Becker, William K. Bertram, M. Chen, K. J. Cohen, T. M. Knasel, R. Marshall, D. J. Quinn, M. Rohde, G. H. Sanders, H. Schubel, and Samuel C. C. Ting, Phys. Rev. Letters 23, 1058 (1969).

[66]M. Davier, I. Derado, D. Drickey, D. Fries, R. Mozley, A. Odian, F. Villa, and D. Yount, Phys. Rev. D 1, 790 (1970).

[67]R. Anderson, D. Gustavson, J. Johnson, D. Ritson, B. H. Wiik, W. G. Jones, D. Kreinick, F. Murphy, and R. Weinstein, Phys. Rev. D 1, 27 (1970).

[68]Their acceptance is $|\bar{Q}-Q|/\bar{Q}<0.18$, $\bar{Q}=E_\gamma^{\max}/1.15$. For reasons of statistics we accepted all $\pi^+\pi^-$ decay angles, whereas the DESY-MIT group measured only a small fraction of the decay distribution around $\theta_H=90°$. They then assumed a $\sin^2\theta_H$ distribution to obtain cross sections integrated over the decay angles. The experimentally observed $\cos\theta_H$ distribution of the inelastic $\pi^+\pi^-$ pairs in the ρ^0 region is roughly constant.

[69]C. Berger *et al.*, Cornell Report No. CLNS-168, 1971 (unpublished).

[70]G. McClellan *et al.* (Ref. 64) use a different ρ^0 mass and width from that used by us. Also they allow the phase of the ρ^0 and Drell terms to vary in order to fit the experimental mass distribution and do not take account of the t dependence of the Drell terms. The Söding model of Alvensleben *et al.* (Ref. 65) takes into account neither the $\pi\pi$ mass and momentum dependence of the Drell terms, nor the contribution from the Drell terms alone; neither do they use a rescattering correction. The ABBHHM collaboration (Ref. 11) determined only the total ρ^0 cross sections with the Söding model; in this determination no rescattering corrections were applied. In view of these differences published Söding-model cross sections are not directly comparable. However, we may compare ρ^0 cross sections determined using the technique of Sec. IV C 3. We have compared the 4.7-GeV cross sections of Table XIV with those of the Cornell group at 5.5 GeV as given by H. O. Ogren [Ph.D thesis, Cornell University, 1970 (unpublished)]. We have scaled the Cornell cross sections to the same ρ^0 width as used by us and have reduced their cross sections by 10% [see Fig. 24(f)] to take account of inelastic background; the resulting cross sections agree within errors with those of Table XIV in the interval $0.02<|t|<0.3$ GeV^2 while their cross sections at smaller $|t|$ are higher than would be expected from a linear extrapolation of our data.

[71]A. Donnachie, R. G. Kirsopp, and C. Lovelace, CERN Report No. CERN-TH-838, 1967 (unpublished). We set $\delta_{33}=0$ for $M>1.8$ GeV.

[72]J. D. Jackson, Nuovo Cimento 34, 1644 (1964).

[73]A. M. Boyarski, R. Diebold, S. D. Ecklund, G. E. Fischer, Y. Murata, B. Richter, and W. S. C. Williams, Phys. Rev. Letters 22, 148 (1969).

[74]D. S. Beder and P. Söding, UCRL Report No. UCRL-17867, 1967 (unpublished).

[75]P. Stichel, Z. Physik 180, 170 (1964).

[76]P. Eberhard and M. Pripstein, Phys. Rev. Letters 10, 351 (1963).

[77]R. W. Morrison, D. J. Drickey, and R. F. Mozley, Nuovo Cimento 56A, 409 (1968).

[78]P. Stichel and M. Scholz, Nuovo Cimento 34, 1381 (1964).

[79]M. P. Locher and W. Sandhas, Z. Physik 195, 461 (1966).

[80]G. Kramer, K. Schilling, and L. Stodolsky, Nucl. Phys. B5, 317 (1968).

[81]K. Gottfried and J. D. Jackson, Nuovo Cimento 34, 735 (1966).

[82]E. Gotsman, Phys. Rev. 186, 1543 (1969) and private communication.

[83]These authors have estimated that the line-reversal correction will not change their conclusion [R. Diebold (private communication)].

[84]J. A. Shapiro, Phys. Rev. 179, 1345 (1969).

[85]J. Friedman, Alvarez Programming Group (UCRL) Note No. P-156, 1966 (unpublished); P. H. Eberhard and W. O. Koellner, LRL Report No. UCRL-20160 (OPTIME), 1971 (unpublished).

[86]D. Yennie (private communication).

[87]P. Bareyre, C. Brickman, A. V. Stirling, and G. Villet, Phys. Letters 18, 342 (1965).

[88]F. Gutbrod (private communication).

[89]M. Jacob and G. C. Wick, Ann. Phys. (N.Y.) 7, 404 (1959).

[90]Ling-Lie Chau Wang, Phys. Rev. 142, 1187 (1966).